

Controlled Release Tetracycline Derivative-Lipid-Complex Extrudates for the Treatment of Periodontitis

Dissertation

zur Erlangung des

Doktorgrades der Naturwissenschaften (Dr. rer. nat.)

der

Naturwissenschaftlichen Fakultät I

Biowissenschaften

der Martin-Luther-Universität

Halle-Wittenberg,

vorgelegt

von Herrn Apotheker Martin Kirchberg

geb. am 29. Juni 1990 in Bernburg (Saale)

Gutachter:

1. Prof Dr. Karsten Mäder
2. Prof Dr. Jürgen Siepmann
3. Prof. Dr. Thomas Groth

Datum der öffentlichen Verteidigung: 24.02.2021

Learning never exhausts the mind.

Leonardo da Vinci (1452 – 1519)

TABLE OF CONTENT

Table of Content	I
Abbreviations and Symbols	V
1 Introduction	1
1.1 Periodontal Disease.....	1
1.1.1 Biofilm Formation and Pathogenesis.....	1
1.1.2 Diagnosis of Gingivitis and Periodontitis.....	4
1.1.3 Risk Factors.....	5
1.1.4 Relation to Systemic Health Issues.....	7
1.2 Traditional Treatment – Mechanical Debridement.....	8
1.3 Local Antibiotic and Antiseptic Adjuvants.....	8
1.3.1 Commercial Drug Delivery Systems.....	9
1.3.2 Experimental Drug Delivery Systems.....	11
1.4 Aims and Objectives.....	11
2 Materials	13
2.1 Tetracyclines.....	13
2.2 Fatty Acid Salts – Magnesium Stearate and Calcium Stearate.....	14
2.3 PLGA and PEG-PLGA.....	15
2.4 Additional Excipients for Incorporation Into the Drug Delivery System.....	16
2.5 Further Excipients and Materials.....	17
3 Methods	19
3.1 Chelation of the Tetracycline Derivatives.....	19
3.2 Complex Characterization.....	19
3.2.1 UV/Vis-Spectroscopy.....	19
3.2.2 Attenuated Total Reflection Infrared Spectroscopy (ATR-FTIR).....	20
3.2.3 Disc Diffusion Tests.....	20
3.2.4 Microscopy.....	20
3.2.5 Stability Studies.....	20

3.3	Production	21
3.3.1	Cryomilling	21
3.3.2	Hot Melt Extrusion.....	21
3.4	Extrudate Characterization	23
3.4.1	Texturure Analysis	23
3.4.2	Differential Scanning Calorimetry.....	23
3.4.3	X-ray Powder Diffraction	24
3.4.4	<i>In Vitro</i> Release	24
3.4.4.1	Prerelease: Drug Extraction	24
3.4.4.2	Sample Preparation and Release Parameters for the <i>In Vitro</i> Release.....	25
3.4.4.3	Drug Quantification via HPLC coupled to a UV/Vis-Detector	25
3.4.4.4	Quantification via HPLC coupled to a Tandem Mass Spectrometry Detector (LC-/MS/MS).....	26
3.4.5	Multispectral Fluorescence Imaging.....	27
3.5	Antimicrobial <i>In Vitro</i> Evaluation	27
3.5.1	Microoganisms.....	28
3.5.2	Minimal Inhibitory Concentration (MIC) Determination	28
3.5.3	Activity against Biofilm Formation.....	29
3.5.4	Activity on Prefomed Biofilms.....	29
3.5.5	<i>In vitro</i> Simulation of Gingival Flow and Release Kinetics	30
4	Results and Discussion	31
4.1	Chelation of the Tetracycline Derivatives	31
4.2	Complex Characterization	32
4.2.1	UV/Vis-Spectroscopy	32
4.2.2	Attenuated Total Reflection Infrared Spectroscopy	35
4.2.3	Microscopy.....	38
4.2.4	Disc Diffusion Tests	40
4.3	First Prototypes	41

4.3.1	Cryomilling and Extrusion of the Minocycline Lipid Complex in Combination with PLGA	41
4.4	Characterization of the First Prototypes	44
4.4.1	Texture Analysis	44
4.4.2	<i>In vitro</i> release	45
4.4.3	Stability studies	47
4.4.4	Multispectral Fluorescence Imaging monitored Water Penetration	48
4.5	Antimicrobial <i>In Vitro</i> Performance of the First Prototypes	50
4.5.1	Antimicrobial Performance against Planktonic Bacteria.....	51
4.5.2	Antimicrobial Activity on the Formation of Biofilms	51
4.5.3	Antimicrobial Activity on Preformed Biofilms	53
4.5.4	Antimicrobial Activity of Eluates obtained from the Gingival Flow Simulation	54
4.6	Second Generation Prototypes	59
4.6.1	Cryomilling and Hot-Melt Extrusion with PEG-PLGA	60
4.7	Characterization of the Second Generation Prototypes	61
4.7.1	Texture Analysis	61
4.7.2	X-ray Powder Diffraction	63
4.7.3	Differential Scanning Calorimetry	66
4.7.4	<i>In Vitro</i> Release	69
4.8	Antimicrobial <i>In Vitro</i> Performance of the Second Generation Prototypes.....	72
4.8.1	Antimicrobial Activity on the formation of Biofilms	73
4.8.2	Antimicrobial Activity on Preformed Biofilms	74
4.8.3	Antimicrobial Activity of the Eluates obtained from the Gingival Flow Simulation.....	76
4.9	An Approach to further Improvement through the Implementation of PVM/MA	78
5	Summary and Perspectives	87
	References.....	VIII
	Deutsche Zusammenfassung.....	XXI

Danksagung	XXV
Lebenslauf	XXVII
Publikationsliste und Auszeichnungen	XXVIII
Selbstständigkeitserklärung	XXX

ABBREVIATIONS AND SYMBOLS

API	Active pharmaceutical ingredient
arbU	Arbitrary Unit
ATR-FTIR	Attenuated total reflectance – Fourier transform infrared
CAL	Clinical attachment level
cfu	Colony forming units
δ	Deformation vibration
DSC	Differential scanning calorimetry
EUCAST	European Committee on Antimicrobial Susceptibility Testing
HPLC	High Performance Liquid Chromatography
IR	Infrared
Log P	Logarithm of the octanol/water participation coefficient
LPS	Lipopolysaccharide
MIC	Minimal inhibitory concentration
MLC	Minocycline lipid complex
M_w	Molecular weight
NMP	N-methylpyrrolidone
PBS	Phosphate buffered saline

PEG	Polyethylene glycol
PEG-PLGA	Polyethylene - Poly(lactic-co-glycolic acid)
PEG-PLGA _{6P}	PEG-PLGA - Expansorb DLG 50 - 6P
PEG-PLGA _{7P}	PEG-PLGA - Expansorb DLG 50 - 7P
PGA	Poly(glycolic acid)
pH	Negative decimal logarithm of the proton concentration (power of hydrogen)
PGA	Poly(glycolic acid)
PLA	Poly(lactic acid)
PLGA	Poly(lactic-co-glycolic acid) polymer
PLGA ₅₀₂	Poly(lactic-co-glycolic acid) - Resomer 502
PLGA ₅₀₃	Poly(lactic-co-glycolic acid) - Resomer 503
PPD	Pocket probing depth
PVM/MA	Poly(vinyl methyl/maleic anhydride) copolymer
RANK	Receptor Activator of NF- κ B
RNA	Ribonucleic acid
ROI	Region of interest
SRP	Scaling and root planning
ssp	Species pluralis

TFA	Trifluoroacetic acid
T_G	Glass transition temperature
TLR	Toll-like receptors
UV/Vis	Ultraviolet / Visible
ν	Valence vibration
ν_{as}	Asymmetric valence vibration
XRPD	X-ray powder diffraction

1 INTRODUCTION

1.1 PERIODONTAL DISEASE

The terminus periodontal disease covers any inherited or acquired disorder affecting the teeth surrounding and supporting tissue (periodontium) (1). Mainly, periodontal disease refers to bacterial inflammations of the periodontium, which are accompanied by a progressing degeneration of the gingival tissue and the alveolar bone (2). This condition is widely spread among all age groups, starting at adolescent age, of developing as well as of modern countries (3). The progression of periodontal disease can be differentiated depending on the severity. The mildest form of periodontal disease is called gingivitis, which can evolve into the more critical periodontitis.

1.1.1 BIOFILM FORMATION AND PATHOGENESIS

In a healthy patient, the gingiva is pale, closely attached to the teeth and free of plaque. Also, the oral cavity serves as a microbiome for several hundred bacterial species (4). Commensal bacteria contribute to the oral health through the colonization of the whole oral cavity, which reduces the availability of binding sites for pathogens (5). Prevalently induced through poor oral hygiene, this desirable condition starts to falter. With neglecting the oral hygiene, bacteria begin to adhere to the salivary pellicles, which can be assessed as the first step to the colonization, and the subsequent biofilm formation (5,6). Gram-positive oral *Streptococci* are regarded as pioneers among these bacteria (e.g. *S. gordonii*, *S. sanguinis*). With a variety of cell-surface polypeptides, like streptococcal antigens (Agl/II), they possess an extensive ability to attach to bacterial and human receptors (7). After successful adherence to the gingival soft and hard tissue, these *Streptococci* offer binding sites for planktonic bacteria, which could otherwise not adhere to oral surfaces by themselves. Through this mechanism, known as co-aggregation, multiple bacterial species are gathered in the newly established biofilm. Co-aggregation is an essential process in the progression of biofilm growth, and therefore contributes to periodontal disease. Especially the obligate anaerobic *Fusobacterium nucleatum* is crucial for the co-aggregation. This bacterium was found to act as a “bridge” between the gram-positive, less harmful early colonizers and the more pathogenic, gram-negative late colonizers (6,8).

During the growth of the biofilm, adherent bacteria secrete larger molecules, which can form an extracellular scaffold, if left undisturbed. This emerging biofilm matrix strengthens the adhesion to the surface and the cohesion within the biofilm (6).

Another major consequence of these biofilm matrices is the decreased susceptibility to external antimicrobial agents (9).

Within these biofilms, interspecies interactions take place in various ways. One way of interaction is the formation of mutual relationships. For instance, *Veillonella* species utilize lactic acid provided by different *Streptococci* as carbon source for promoted growth (10). Also, bacteria are able to communicate through unilateral or bilateral alteration in gene expression, caused by the sole presence of another bacterial species (6). Besides these cooperative forms of interaction, some bacteria are also able to express antimicrobial substances, which can lead to competition between different bacteria. Therefore well-known is again the group of oral *Streptococci*. They produce hydrogen peroxide, which is a highly oxidative substance. This substance can penetrate into other bacterial cells and unfold fatal effects on intracellular macromolecules, while the *Streptococci* remain unaffected (11). This oxidative agent can also inhibit the proliferation of commensal and pathogenic bacteria. It has been observed, that during the development of periodontal disease certain *Streptococci* (e.g. *S. sanguinis*), which might had an initial protective effect, become less frequent within the biofilm (12).

The presence of these commensal bacteria constantly stimulates the innate immune system of the host on a low level, creating a healthy homeostasis. This ongoing challenge is discussed to contribute to the protection of the gingival tissue through the onset of a complex cascade of immunologic reactions (13). Exemplarily, Toll-like-receptors (TLR), which identify pathogens and commensal bacteria, as well as lipopolysaccharide-binding protein are present in the gingival epithelium (13–15). The TLRs induce an immunologic response through the expression of mediators like interleukin-8, which leads to an increased recruitment of neutrophils, or like antimicrobial β -defensins, to keep the bacteria at bay.

So, how does the growth of the biofilm lead to inflammatory and degenerative disease? The shift from an initially harmless biofilm to a microbial threat is induced through a change in the biofilm's microbial composition. Commensal bacteria get replaced by gram-negative and anaerobic bacteria with an association to periodontal disease. Due to the complexity of the biofilm composition, it is nearly impossible to isolate single bacteria as the responsible pathogens (2). Nevertheless, certain bacterial species are considered as keystone pathogens for the progression of the disease. Among them are *Porphyromonas gingivalis* and *Tannerella forsythia*, which were found to be more prevalent in individuals with diagnosed periodontitis (16). Together with *T. denticola*, they form the so called "red complex" (17), which refers to a group of bacteria infamous

for being present in periodontal sites and modulating the host defense mechanisms. Especially the influence of *P. gingivalis* on the host immune response is well examined (13,18).

P. gingivalis is able to secrete the serine phosphatase SerB. Subsequently, SerB enables the infiltration of *P. gingivalis* into gingival epithelial cells, and eventually dephosphorylates multiple intracellular molecules. One effect thereof is the suppression of further interleukin-8 expression, resulting in a delay of neutrophil transition to the compromised tissue. Furthermore, *P. gingivalis* negatively impacts the expression of E-selectin, a cell adhesion molecule responsible for the recruitment of leukocytes. Another tool in possession of *P. gingivalis* are lipopolysaccharides (LPS) on the bacterium's surface. A part of these LPS is lipid A, which can act as an antagonist on TLR4-receptors, resulting in an impediment of the intracellular killing ability in macrophages. In contrast, regular LPS of gram-negative bacteria act as agonists on these receptors (13,18). Also, the bacterium can set crosstalk in motion between TLR2 and complement receptors (C5aR) with different signaling pathways (19). In macrophages, these signaling cascades also result in an impediment of their killing activity, similar to TLR4-antagonism (18). Additionally, *P. gingivalis* can collect the circulating binding protein (C4b) on its surface, enabling a downregulation of inflammatory marker expression (20). These mechanisms, which can be summarized as "local chemokine paralysis", evade and manipulate effectively the innate immunologic surveillance, and enable the further microbial colonization.

The alteration of the immune response during this shift to dysbiosis benefits the whole biofilm community. As the biofilm grows, the integrity of the gingival tissue gets compromised. The homeostasis within the gingival tissue is heavily disrupted, which results in a rebound of the immunologic response (18). However, the innate and adapted immune responses are insufficient to contain and oppose the already established biofilm at this stage. The now properly working TLR-signaling cascades lead to high cytokine levels, which directly affect bone remodeling processes. These inflammatory cytokines cause an imbalance in the homeostasis between bone loss inducing RANK-ligands and osteoprotegerin, a decoy receptor for RANK-ligands (13,21). Consequently, these RANK-ligands activate osteoclasts, which start to resorb alveolar bone tissue. Without intervention, the bone resorption will culminate in the loss of teeth. Hence, the inflammatory immune response with associated bone loss is consequence and symptom of the bacterial infestation in progressed periodontal disease.

The pathogenesis of periodontitis according to Page and Kornman (22) is illustrated in Figure 1.

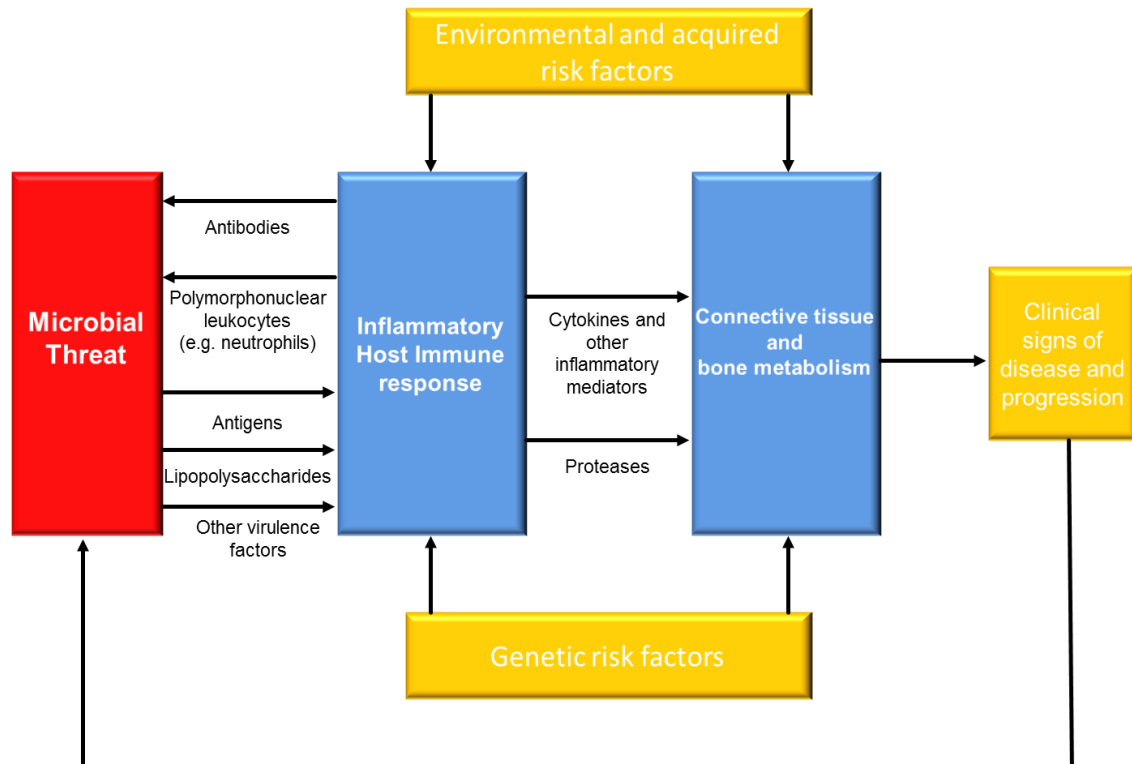


Figure 1: Pathogenesis of periodontitis according to Page & Kornman 1997 (modified)

1.1.2 DIAGNOSIS OF GINGIVITIS AND PERIODONTITIS

As already mentioned, periodontal disease can be differentiated, depending on the progress of the just described processes. In gingivitis, the mildest form of the periodontal disease, mainly the visible part of the gum is affected: the gingival margin and the entrance of the gingival sulcus (23). Within hours, early-colonizers lay the foundation for the formation of the biofilm, also referred to as plaque. If left undisturbed, initial lesions become visible within the first 2 to 4 days. They are recognizable by dilated blood vessels, caused by inflammatory reactions in the gingival epithelial region, with a release of crevicular fluid. Patients often do not perceive the threat of the disease during this stage, because they do not feel any pain yet. These painless symptoms are the gingival erythema, possible bleeding under mechanical stress, visible plaque and malodor. However, if the biofilm is not removed, these lesions advance, and lead to a regression of the gingiva with associated attachment loss. Within two weeks, the gingival pockets are deepened enough to enable progressing biofilm growth. This stadium represents the transition from gingivitis to periodontitis with the subsequent tissue degeneration induced by the anaerobic late-colonizers.

The state of periodontitis is characterized through an aggravation of the existing clinical picture. Tissue degradation and recession leads to intensified gingival bleeding and exposure of the sensitive cervix. This exposure is a visible sign of the gingival atrophy, and the formation of even deeper gingival pockets, which are accompanied by alveolar

bone-, attachment- and eventually tooth loss. Hence the main difference between gingivitis and periodontitis is the limitation of gingivitis the gingival margin, while periodontitis affects severely the complete periodontium. Figure 2 illustrates the influence of periodontitis on the periodontium.

The already mentioned pocket depth is an important clinical value for the diagnosis as well as for the evaluation of therapy success. Dentists can access the gingival pocket with graduated periodontal probes, to define the pocket probing depth (PPD) (24). Depending on the deployed definition of periodontitis, the diagnosis can vary. Commonly, pocket depths of 1-3 mm, preferably 1-2 mm are considered as healthy. 4-5 mm represents the beginning of periodontitis, while depths above 5 mm are regarded as manifested periodontitis, which requires professional treatment. The diagnosis can also be confirmed with a dental X-ray examination. Another therapy-related value is the clinical attachment level (CAL) (25), which is defined as the distance between cemento-enamel junction (Figure 2) of the tooth and the most apical probing depth. Depending on how quick the disease progresses, periodontitis can also be separated in a rapid, aggressive form and in a slower progressing chronic form.

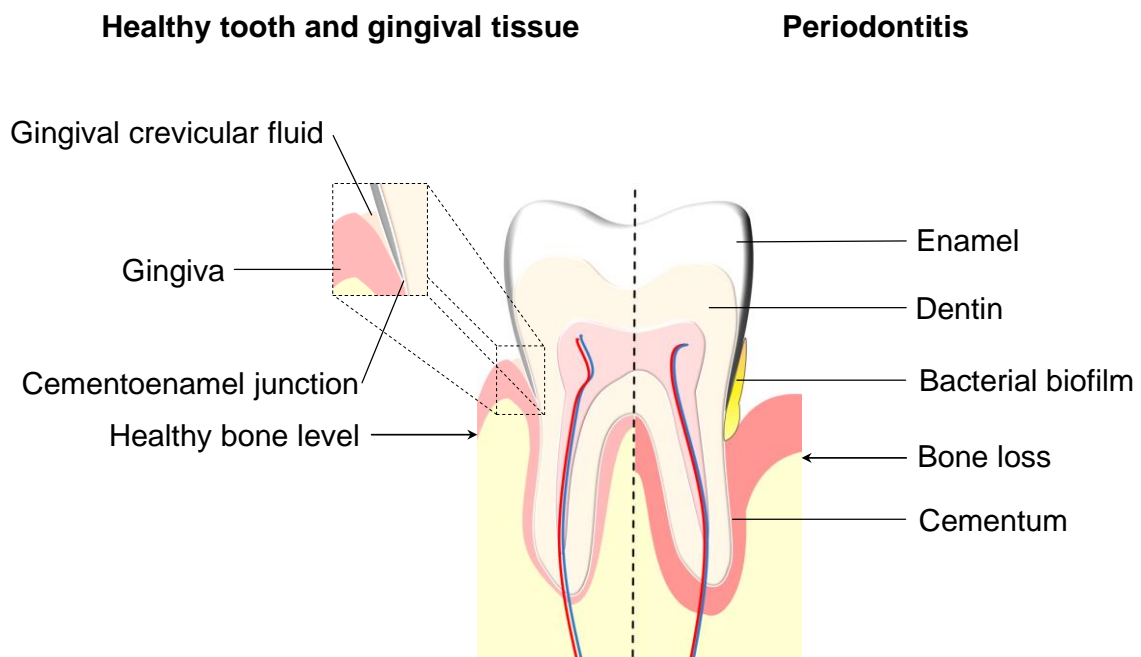


Figure 2: Schematic representation of a tooth in health (left) and affected by periodontitis (right)

1.1.3 RISK FACTORS

The recognized risks for the development of periodontal disease can be distinguished in risk factors, which are either modifiable or unmodifiable by the patients habits (3,26).

As described in 1.1.1, neglecting oral health measurements is an important and modifiable risk factor for the development of biofilms and periodontal disease (27).

Hence, proper oral hygiene measurements paired with periodical professional cleaning can prevent the occurrence of periodontal disease. The second major risk factor is tobacco use and smoking. Many studies demonstrated, that smoking increases drastically the occurrence of periodontal diseases (28,29). More than 4000 toxic substances within tobacco smoke have been reported, which negatively affect the gingival microbiome, the gingival blood flow and the immune response as well as the periodontal wound healing. But the acquired risk decreases to almost non-smoker-levels with the number of years passed after leaving the habit behind. Also, the consumption of alcohol can be considered as a modifiable risk for periodontal disease, due to disturbance of the immune response (30). Patients suffering from diabetes are as well at higher risk for developing periodontitis (31). The mechanisms between periodontitis and diabetes are not completely elucidated, but anew an interfering with the host immune response is supposed to be involved. Another risk factor is certain salvia flow reducing medication, which also promotes periodontal disease. For instance, substances derived from the groups of tricyclic antidepressants, antihistamines or sympathomimetic drugs can lead to such a reduced gingival flow (3). Last but not least, psychological stress is a modifiable risk factor (32). Stress can negatively affect the immune response, and result in increased salivary stress markers (e.g. cortisol). Equally, stress can contribute indirectly to periodontal disease, through induction of behavioral reactions, like increased tobacco consume, ingestion of unhealthy nutrition or neglecting oral hygiene.

Regarding the gender, males are more often diagnosed with periodontal disease. It is discussed, that this is not a genetic cause, but an outcome of their lifestyle (26). However, women are also endangered, due the strong systemic impact of hormonal changes on the female body as on the periodontium (33). For instance, a pregnancy can increase the risk of gingival inflammation. Also, with begin of the menopause, the prevalence of osteoporosis rises, which can be linked to alveolar bone loss as well (26,34). But these risk factors are considered as modifiable, as they can be treated by the dental surveillance of pregnant women and supplementing menopausal women with calcium and vitamin D to impede general osteoporosis.

As unmodifiable risk factor, genetics play a key role in the development and familial accumulation of periodontal disease, like in so many other diseases (3,26,35). Especially in combination with environmental and demographic influences, this risk factor can be more or less pronounced. Finally, age is the last to be mentioned unmodifiable risk factor. Periodontitis is more prevalent in the elder population (36), but

it is not clear, if periodontitis is more aggressive at higher age, or if the higher prevalence is the result of cumulative effects over time (35).

1.1.4 RELATION TO SYSTEMIC HEALTH ISSUES

Besides a possible tooth loss, and the connected loss of life quality, periodontitis possesses far more pathogenic potential. Periodontitis is associated to systemic health issues, which arise from bacteria infiltrating the human body through the inflamed gingival tissue. The inflamed gingival sulci offer a surface of approximately 8 to 20 cm² (37), from where the bacteria can easily enter the systemic circulation, promoting inflammatory processes in distant tissues.

For instance, a strong association to the occurrence of severe cardiovascular diseases has been found (38–41). The consensual main cause therefore is the chronically elevated, systemic inflammatory burden. Higher levels of inflammatory cytokines result in the formation of vascular arethomas by the host immune response. The general inflammatory situation also sets the environment for the development of rheumatoid arthritis (42). Furthermore, periodontal pathogens, among them again *P. gingivalis*, directly contribute to inflammations within the joints, and are considered triggers for auto-immune reactions. Thus, it was observed, that periodontitis often precedes the development of rheumatoid arthritis.

In 1.1.3, diabetes was listed as a risk factor for the development of periodontal disease. But the depiction of the relationship between periodontitis and diabetes as bilateral is more accurate (31,43,44), as the inflammatory conditions negatively affect the glycaemic control. Graziani et al. concluded periodontitis as significantly impactful on diabetes control, incidence and the occurrence of complications (43).

There is also evidence for a connection to Alzheimer's disease (45,46). Alzheimer patients demonstrated higher levels of serum antibodies to periodontal pathogens, and Alzheimer patients with diagnosed periodontitis exhibited an increased cognitive decline in a six month observational cohort study. Again, the systemic inflammation is discussed as potential cause for the unfolding of degenerative processes.

The linkage of periodontitis to a variety of severe, systemic health issues highlights the gravity of this disease. According to recent data, periodontitis was diagnosed in about 50% of adults in a randomized population sample aged 10-79 years in Norway (47). Similar values (45%) have been described for the USA (48). This high prevalence and the described pathogenesis make periodontitis a menace, which should not be

underestimated. Thus, these circumstances underline the need for effective treatment concepts.

1.2 TRADITIONAL TREATMENT – MECHANICAL DEBRIDEMENT

The regular treatment of periodontitis basically involves mechanical debridement, and the deployment of improved oral health measures (49,50). During the mechanical debridement, calculus and plaque on subgingival levels are removed with hand instruments by a dentist. This procedure effectively disrupts the attached biofilms, and can take several sessions. The treatment is continued by scaling and root planning (SRP). During scaling, calcified accretions are removed, while root planning involves the removal of corrupted cementum. These procedures are considered as gold standard in periodontal therapy, and positively affect the clinical periodontal parameters. PPD as well as bleeding on probing can be reduced, while CAL gains are achieved.

In parallel, the implementation of improved oral health measures ensures a lasting therapy success. This includes the guidance in cleaning technique and the encouragement to use dental floss and interdental brushes. If properly applied, these measures can control the formation of plaque and prevent gingival inflammation. Also, the periodically assistance by professional mechanical plaque removal is advised, but the benefits are controversially discussed. If oral cleaning techniques are repeatedly instructed, the additional professional cleaning did not offer benefits towards plaque reduction and gingival bleeding (50,51). Also, no conclusions concerning the CAL are obtained during the professional cleaning. However, the professional cleaning can help the patients to stick to their oral hygiene protocol and recall appointments, but it will not replace thorough oral health measurements.

For the aftercare, patients are usually recalled within 6 to 8 weeks for re-evaluation of their therapy progress (52,53). From there on, the recall intervals are individually customized depending on the severity of their periodontitis.

1.3 LOCAL ANTIBIOTIC AND ANTISEPTIC ADJUVANTS

For the treatment of gingivitis and slight cases of periodontitis, the mechanical debridement can be sufficient to restore gingival health. But in cases of progressed, severe periodontitis with persistent and recurrent localized deep sites, the application of a local antibiotic as an additional treatment step is indicated (50,54). In these cases, additional clinical improvements can be observed, compared to mechanical

debridement alone. Local delivery of antibiotics also offers several advantages compared to systemic treatments.

A much lower dose is sufficient, which results in a reduction of adverse side effects (e.g. in the gastrointestinal tract). The active pharmaceutical ingredient (API) is directly available at the desired application site, and an improved compliance can also be expected, as patients are unlikely to miss an application.

However, the gingival pocket is a challenge for such local antibiotic formulations with a desired release period of several weeks. Within the gingival crevice, a constant flow of gingival fluid ensures a morefold turnover per hour (55), which leads to a rapid and undesired removal of the drug from the periodontal pocket. A rational approach to overcome this problem is the development of controlled release formulations. Furthermore, the space within the gingival sulcus is limited, and reoccurring mechanical stress can also put strain on the drug delivery system. Hence, potential drug delivery systems need to offer mechanical stability and a reliable release pattern. These traits should ideally be completed by biodegradability, ease of application, a simple and robust production process and focus on the stability of the API. Of course, several commercial and experimental drug delivery systems aimed to fulfill these requirements and will be discussed in the following sections.

1.3.1 COMMERCIAL DRUG DELIVERY SYSTEMS

Most commercial drug delivery systems for local periodontitis treatment incorporated a tetracycline derivative as API, such as tetracycline, minocycline or doxycycline. For instance, tetracycline containing Actisite® fibers were one of the first approaches. They consisted of an ethylene and vinyl acetate copolymer and provided a controlled release of about 10 days. However, the non-biodegradability of the polymer was a serious disadvantage. The fibers had to be removed from the application site after the treatment period. In addition, their application required a certain degree of dexterity (56).

Then, doxycycline hyclate containing in situ forming depot Atridox® was introduced. It provides effective concentrations in the periodontal pocket over a time period of 21 days. The formulation was degradable, but with the drawback of the organic solvent N-methylpyrrolidone (NMP) (57,58) NMP, like many other organic solvents, can cause irritations and high doses can act hepatotoxic (59). Another doxycycline containing composition is Ligosan®. The mixture of PGA (poly(glycolic acid)) and high- and low-viscosity PEG-PLGA-polymers (polyethylene glycol-poly(lactic-co-glycolic acid)) forms a gel, that delivers the antimicrobial in concentrations, that might exert antibacterial

activity up to 11 days. It can solely be applied with a special application system, which can complicate the handling (60–62).

Another tetracycline derivative is minocycline. Minocycline loaded PLGA microspheres are available as Arestin® in the U.S. (63). They are biodegradable, but comparable to Ligosan®, a special syringe is necessary for the application (64).

As a further semisolid preparation, the Elyzol® dental gel was available. In this case, metronidazole benzoate is suspended in a glycerolmonooleate and triglyceride matrix, which forms a cubic phase after administration. Unfortunately, the API levels of this composition diminish within a short period of only 36 h (65).

Also, Periochip®, an antiseptic formulation, is still in practical use. It contains the antiseptic drug chlorhexidine gluconate and is able to reduce the microbial load over 7 to 11 days (66,67). As well, two different chlorhexidine salts act as API in the ChloSite®. The API is incorporated in a xanthan matrix, which offers a release of up to 3 weeks (68). Table 1 gives an overview about these systems and their state of use.

Table 1: Overview of common commercial systems for the treatment of periodontitis (antiseptic formulations are marked with a grey background) ¹ – available in the U.S. ² – available in Germany (2020)

Product	API	Auxiliary Excipients	Dosage Form	Estimated Release Period	Remark
Actisite®	Tetracycline	Ethylene-vinyl acetate copolymer	Fiber	~ 10 days	Not biodegradable
Arestin®¹	Minocycline hydrochloride	PLGA	Micro particles	Several weeks	Requires special equipment
Atridox®¹	Doxycycline hyclate	PLA NMP	In-situ forming depot	7 days	Two-syringe system with NMP
Elyzol®	Metronidazole benzoate	Glycerol monooleate Sesame oil Water for injection	Gel	36 hours	Requires special equipment
Ligosan®^{1,2}	Doxycycline	PGA PEG-PLGA	Gel	11 days	Requires special equipment
ChloSite®²	Chlorhexidine digluconate/dihydrochloride	Xanthan gum	Gel	2-3 weeks	Antiseptic API
Periochip®^{1,2}	Chlorhexidine gluconate	Hydrolyzed gelatin Glycerol Purified water	Preformed insert	7 – 11 days	Antiseptic API

1.3.2 EXPERIMENTAL DRUG DELIVERY SYSTEMS

Research efforts have been undertaken to overcome the disadvantages of the current systems. Thereby, several alternative approaches for the improved treatment of periodontitis have been described *in vitro* or in *preclinical models*.

For instance, nanoparticles with diverse polymeric or inorganic matrices have been investigated as local drug delivery systems. Dinarvand et al. (69) manufactured PLGA nanoparticles with incorporated minocycline, offering a release period of up to 5 days. Besides PLGA, the polysaccharide Chitosan was utilized to encapsulate several APIs as nanoparticulate application form (70). Also, silver and zinc oxide nanoparticles exhibited antimicrobial potential, especially against endodontic pathogens (71) (Endodontics refers to studies of the inner tooth).

As observable in Table 1, semisolid dosage forms like gels were quite popular among the commercial periodontal treatment options. Hence, it does not surprise, that such systems were in the focus of further research. The chitosan gel with incorporated metronidazole (72) tested in a clinical trial, or an as well clinically tested minocycline ointment (73) can be listed as examples thereof.

Another innovative approach was the development of *in-situ* forming PLGA-implants, with doxycycline, metronidazole or chlorhexidine as API (74,75). Implant formation occurs via solvent exchange and a release period of 7 days has been achieved. Furthermore, their mechanical properties were tailored with additional excipients like acetyltributyl citrate as plasticizer and hydroxypropyl methylcellulose as adhesive polymer.

Recently, minocycline was also successfully incorporated in electrospun membranes, which offered a prolonged release of several weeks (76). Despite the challenging production process with the necessary use of chloroform, they offered a convincing *in vitro* performance.

1.4 AIMS AND OBJECTIVES

As initially described, the association of systemic diseases elevates periodontitis to a threat to the general well-being. Paired with the high prevalence, periodontal disease can be considered a serious public health concern. Thus, there is an undeniable need for effective therapies. A few potent therapeutic options already exist, as well as experimental formulations with high potential. But they all offer opportunities for improvement. Some of them lack biodegradability or require potentially toxic organic

solvents for the production. Others only offer a short time of antibiotic activity, are laborious to produce or difficult to handle and apply. Hence, an ideal drug delivery system for the treatment of periodontitis should offer several properties, as already implied in 1.3:

- Stabilization of the API
- Controlled release over a period of at least 42 days (Recall interval during aftercare)
- Biodegradability
- A robust, eco-friendly and inexpensive production process (including absence of toxic solvents)
- Mechanical stability
- Easy handling and effortless application

This thesis attempts to develop a dosage form, which is able to meet all criteria. Therefore, tetracycline derivatives as antibiotic API and their possible alteration and stabilization will be explored. Furthermore, the production and characterization of hot-melt extrudates as solid monolithic dosage form will be major subjects of the following chapters.

2 MATERIALS

2.1 TETRACYCLINES

First discovered as products of different *Streptomyces* species in the mid of the 20th century, chlortetracycline and oxytetracycline were the first identified substances of this family of antibiotics. Subsequently, other natural derivatives were isolated, including tetracycline, which gave the name for this antibiotic group (77). "Tetracyclines" refers to their chemical structure, which consists of a linear fused nucleus of four rings (A-D) (Figure 3). Soon after, the natural occurring substances were chemically modified, leading to the class of semi-synthetic tetracyclines. Through the addition of functional groups, several new derivatives were generated. Two of them, minocycline and doxycycline, are in frequent use against various diseases up to this day.

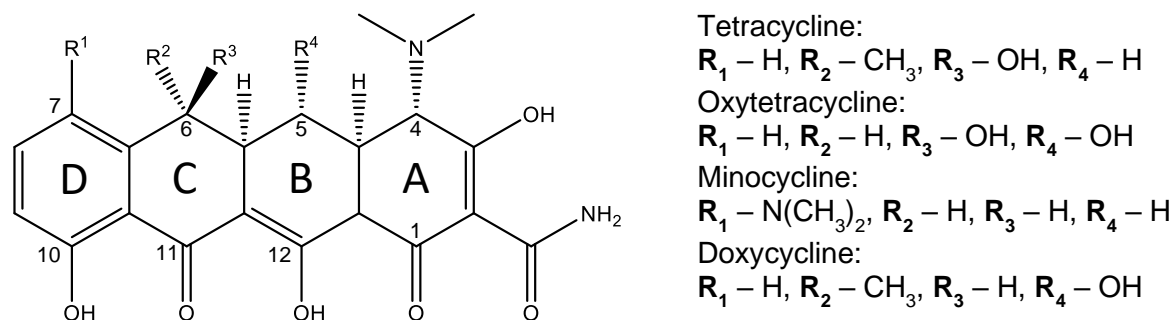


Figure 3: Chemical structure of tetracyclines

Important functional groups for their pharmacodynamic properties are already found in the core structure (78). The fused tetracycle, with the natural stereochemical configuration at 4a, 12a and the dimethylamino group at C4, as well as the keto-enol system at C 11, 12 and 12a were identified as essential. The diketone system (C11 and 12), the enol (C1 and 3) and the carboxamide group (C2) cause the strong chelating tendency of the tetracyclines, which can also affect their antimicrobial activity (78).

Tetracyclines appear as yellow colored powders, and they all possess a broad spectrum of activity against gram-positive and gram-negative bacteria. Their bacteriostatic mode of action targets the bacterial protein synthesis (78,79). Thereby, their capability to chelate divalent cations is likely to play a key role in the penetration of bacterial cell walls (80). Tetracyclines convert to positively charged complexes (probably with magnesium) to cross gram-negative cell walls through porin channels. In gram-positive bacteria, the uncharged, lipophilic form is transported into the cells. However, within the bacterial cells, tetracyclines target the ribosomal 30S-subunit,

which prevents the binding of aminoacyl-tRNA to the messenger RNA – ribosome complex.

Besides their antimicrobial properties, tetracyclines, especially minocycline and doxycycline, possess several other beneficial effects (77). For instance, they inhibit matrix metalloproteinases, which is useful in conditions where these metalloproteinases induce tissue damage (e.g. heart remodeling and inflammatory processes). Furthermore, they hinder reactive oxygen species from inflicting cellular damage. Also, there is evidence for anti-apoptotic and anti-inflammatory properties of doxycycline and specially minocycline (77,81).

Regarding the pharmacokinetics of tetracyclines, the older tetracycline derivatives (tetracycline and oxytetracycline) tend to be more reliant on food intake compared to the newer ones (minocycline and doxycycline) (82). Hence, the oral bioavailability is higher for the newer derivatives, but the presence of polyvalent cations negatively affects the uptake of all tetracycline derivatives. For the intended local administration of these drugs, the food effect will be of lesser importance. Concerning their stability, it should be noted, that in aqueous media at 37 °C, minocycline demonstrated earlier signs of decomposition (83). The excretion of the tetracyclines takes place via renal and biliary pathways with slightly higher excretion via feces.

The utilized tetracycline derivatives are listed in Table 2.

Table 2: Utilized tetracycline derivatives and their origin

Tetracycline derivative	Source	Remark
Oxytetracycline dihydrate	Sigma Aldrich, Germany	Purity > 95%
Doxycycline	Ontario Chemicals, Canada	Purity 99%
Minocycline	Ontario Chemicals, Canada	Purity 98%
Minocycline Hydrochloride	TCI Europe, Belgium	Purity >98%

2.2 FATTY ACID SALTS – MAGNESIUM STEARATE AND CALCIUM STEARATE

Magnesium and calcium stearate are salts of vegetable- or animal derived organic acids blends, mainly consisting of stearic and palmitic acid. They appear as white, soft, crystalline or amorphous powder. They are not toxic (peroral) and insoluble in ethanol, ether, water, and hardly soluble in hot ethanol. Primarily they are in use as lubricant for tableting and capsule production (84,85).

The utilized magnesium stearates Magnesia 4263 and Magnesia 4264 (vegetable), and calcium stearate Magnesia 4273 (vegetable) were kindly gifted by Magnesia Germany (Müllheim, Germany). In case of magnesium stearate, both products were equally suitable for the intended application, but most experiments were carried out with Magnesia 4263.

2.3 PLGA AND PEG-PLGA

In the past decades, PLGA copolymers (Figure 4) have been in use in a variety of drug delivery systems for controlled release purposes. The reason therefore is their biocompatibility, biodegradability and the adjustability of their release properties (86). Depending on the molecular weight, the proportion of lactic and glycolic acid, and the modification of the endcaps (e.g. esterified PEG), the release pattern can be tailored to the desired purpose.

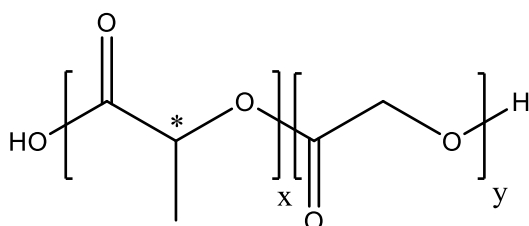


Figure 4: Chemical structure of PLGA copolymer (x – Lactic acid chain; y – Glycolic acid chain)

The polyester PLGA consists of poly(lactic acid) (PLA) and poly(glycolic acid) (PGA). The α -carbon of lactic acid is asymmetric, resulting in two different enantiomers. The L- and D -form of the polyester demonstrate crystalline properties, while poly D, L-lactic acid is amorphous. PLGA generally refers to the poly D,L-lactic-co-glycolic acid, where both enantiomers are present in an equal ratio. In contrast, PGA is highly crystalline and does not possess an asymmetric carbon atom. The biodegradability of PLGA is complex and influenced by many factors (87). The basic mechanism of the polymer degradation is the hydrolysis of the ester bonds in aqueous surrounding, resulting in the formation of oligomers and monomers. The emerging monomers of lactic and glycolic acid, in turn, contribute to further polymer degradation by reducing the local pH, promoting hydrolysis. This autocatalysis causes heterogeneous polymer degradation inside the PLGA matrix. As the polymer degradation progresses, smaller chain segments can dissolve, which can lead to polymer erosion. However, the monomers can be metabolized to CO_2 and H_2O , and they are also excretable via renal pathways.

As initially mentioned, the drug release can be modified. The proportion of lactic and glycolic acid offers the basis for the aspired release period from several weeks to

months or years (86). Higher PGA content in PLGA-polymers leads to shorter degradation times, due to an increase in hydrophilicity. Also, the release period is reliant on the molecular weight and the endcaps of the polymer chains. Acid groups lead to faster degradation than ester groups, due to promoted hydrolysis.

Another possibility is the PEGylation of PLGA. PEGylated PLGA copolymers exhibit a slower degradation and, in contrast to PLGA, erosion starts at the very beginning of the release period. (88). PLGA matrices begin to erode, as soon as the molecular weight (M_w) drops to 7000 – 8000 g/mole. But as soon as the PLGA erosion starts, the process unfolds more drastically, which results in faster decrease of final polymer mass. The slower degradation of PEG-PLGA derives from a higher water penetration generated by PEG. Eventually, this leads to an accelerated diffusion of the acidic oligomers and monomers, which decreases autocatalysis and therefore hydrolysis.

The PLGA polymers utilized in this work were Resomer[®] 502 (M_w 7 – 17 kDa) and Resomer[®] 503 (M_w 24 – 38 kDa), which were a gift from Evonik (Darmstadt, Germany). Both PLGA polymers have esterified endcaps with an estimated degradation time frame < 3 months. As PEG-PLGA polymers served Expansorb[®] DLG 50 – 6P (M_w 30 – 60 kDa, 10% PEG) and Expansorb[®] DLG 50 – 7P (M_w 60 - 85 kDa, 5% PEG). These polymers were kindly provided by Merck KGaA (Darmstadt, Germany).

2.4 ADDITIONAL EXCIPIENTS FOR INCORPORATION INTO THE DRUG DELIVERY SYSTEM

Table 3: Additional excipients for the incorporation into the drug delivery system

Substance/Trade name	Source	Purpose
Nile Red	Sigma Aldrich, Germany	Fluorescence dye
PEG 1500	Thermo Fisher Scientific GmbH, Germany	Plasticizer
PVM/MA	Sigma Aldrich, Germany	Mucoadhesive supplement
Tegin 4100 Pellets	Evonik, Germany	Plasticizer

2.5 FURTHER EXCIPIENTS AND MATERIALS

Table 4: Further excipients and materials

Substance/Trade name	Source	Purity / Remark
Acetone	Carl Roth, Germany	Synthesis and analytical grade
Acetonitrile	VWR Chemicals, Germany	HPLC grade
Aqua bidistilled	Institute of Pharmacy, Martin Luther University Halle-Wittenberg, Germany	Produced by bidestillation
Aqua demineralized	Institute of Pharmacy, Martin Luther University Halle-Wittenberg, Germany	Produced by ion exchange and reverse osmosis
Brown Glass Vials	Infochroma AG, Switzerland	Used for sample preparation and release experiments
Centrifuge tubes	VWR Chemicals, Germany	
Di-Sodium hydrogen phosphate dihydrate	Grüssing, Germany	Purity 99%
Ethanol (non-denatured)	Chemical Distribution , Institute of Pharmacy, Martin Luther University Halle-Wittenberg, Germany	Purity 99.5%
Falcon tubes (opaque)	VWR Chemicals, Germany	Storage
Formic acid	Carl Roth, Germany	LC/MS grade
Hydrochloric acid	Carl Roth, Germany	Purity > 25%
Methanol	Carl Roth, Germany	HPLC grade
Parafilm® M PM-922	Pechiney Plastic Packaging Inc., United States of America	Sealing
Potassium dihydrogen phosphate	Carl Roth, Germany	Purity > 98%
Phosphoric acid	Carl Roth, Germany	Purity 85%
Syringes (varying volume)	B. Braun, Germany	
Teflon syringe filter (0.45 µm)	Sigma Aldrich, Germany	
Teflon foil	W+B Datentechnik GmbH, Germany	Cover
Trifluoroacetic acid	Merck Schuchardt oHG, Germany	Purity > 99%

Table 5: Microorganisms and excipients for the antimicrobial activity testing in Bern

	Microorganism	Source	Remark
Microorganisms	<i>Actinomyces naeslundii</i> ATCC 12104		
	<i>Fusobacterium nucleatum</i> ATCC 25586		
	<i>Parvimonas micra</i> ATCC 33270	Laboratory of oral Microbiology, Department of Periodontology, School of Dental Medicine, University of Bern, Switzerland	Part of six species biofilm
	<i>Porphyromonas gingivalis</i> ATCC 33277		
	<i>Streptococcus gordonii</i> ATCC 10558		
	<i>Tannerella forsythia</i> ATCC 43037		
	Substance/Material	Source	Remark
Reagents and Materials	Acetic acid	Laboratory of oral Microbiology, Bern	Used in biofilm quantification
	Arestin® microspheres	OraPharma, Bridgewater, NJ, USA	Used as positive control
	Bovine serum albumin	Laboratory of oral Microbiology, Bern	For cultivation
	Crystal violet solution	Laboratory of oral Microbiology, Bern	Used for staining of biofilms
	Microtiter plates	Laboratory of oral Microbiology, Bern	Used in the assays
	Resazurin	Merck KGaA, Germany	Used as redox indicator
	Tryptic soy agar plates	Oxoid, Great Britain	For cultivation
	Wilkins Chalgren broth	Oxoid, Great Britain	For cultivation
	β-NAD	Merck KGaA, Germany	For cultivation

3 METHODS

3.1 CHELATION OF THE TETRACYCLINE DERIVATIVES

The formation of lipophilic chelate complexes between tetracycline derivatives and fatty acid salts was proposed as a potential pathway to increase the drug stability and extend the release period of these drugs. The tetracycline derivatives minocycline, doxycycline and oxytetracycline were chosen as active pharmaceutical ingredients (API), to be paired with magnesium- or respectively calcium stearate, to investigate their capability of forming such complexes.

Therefore, these components were tested in molar ratios of 1:1, 2:1 and 1:2 (API : Fatty acid salt). Thus, corresponding quantities were weighed into flasks (e.g. 10 mg of minocycline and 25.48 mg of magnesium stearate for a molar ratio of 1:2) and suspended in pure ethanol. Subsequently, these suspensions were heated in a water bath at 70 °C for at least 1 minute.

For the further analysis, besides these ethanolic complex solutions, the dried complex was utilized. Either retrieved from solvent evaporation (glass like films) or drying in a compartment dryer (powder form). To receive the dried powder, the complex solution was spread on Teflon foil covered petri dishes in form of droplets. Subsequently, the petri dishes were stored in a vacuum drying oven for at least 12 hours at 25 °C. Finally, the complex powder was collected from the petri dishes and if necessary stored at -20 °C. Alternatively, the solutions were dried in a rotary evaporator, or a heated in an orbital shaker to create glass-like films within the flasks.

3.2 COMPLEX CHARACTERIZATION

3.2.1 UV/VIS-SPECTROSCOPY

Absorption spectra of the pure tetracycline derivatives and their complexes were investigated with a Shimadzu UV-1800 spectrophotometer (Shimadzu, Duisburg, Germany). Therefore, 10 µl of freshly prepared 5 mg/ml stock solutions were diluted with 3 ml ethanol. Subsequently, these solutions were transferred in a quartz cuvette and absorption spectra were recorded in the range from 230 or respectively 250 to 450 nm in 1 nm steps. For the data evaluation, the UVProbe-software 2.61 was utilized.

3.2.2 ATTENUATED TOTAL REFLECTION INFRARED SPECTROSCOPY (ATR-FTIR)

Infrared spectra were recorded on a Bruker IFS 28 equipped with a Sensir ATR unit (Bruker, Billerica, United States) operating from 4000 to 680 cm^{-1} at room temperature. Samples were prepared by producing homogeneous compacts of the desired sample and zinc selenide. The data was analyzed with the OPUS4.2 software.

3.2.3 DISC DIFFUSION TESTS

The tetracycline derivative complexes required the proof of their antibacterial activity. Disc diffusion tests are a standard method for such a susceptibility testing (89), and they were carried out according to the recommendations of the EUCAST (90). Test substances were minocycline, doxycycline and oxytetracycline complexes containing each 10 mg/ml dissolved in ethanol. Due to the use of the dihydrate salt of oxytetracycline, 10.782 mg were necessary to obtain a solution, which resembled 10 mg/ml of pure oxytetracycline. As control served the pure tetracycline derivatives dissolved in ethanol, and also pure ethanol. The solutions were diluted in a ratio of 3:7 with ethanol and immediately thereafter, unloaded antibiotic test discs with a diameter of 6 mm (BD, Allschwil, Switzerland) were loaded with 10 μl of the respective solution. Thus, each disc contained 30 μg of API. An overnight culture of *Staphylococcus aureus* ATCC 29213 was suspended to McFarland 0.5, and subsequently 100 μl were spread on Mueller-Hinton-agar plates (Oxoid, Basingstoke, Great Britain). As soon as the solvent evaporated from the test discs, they were placed on the agar plates. After incubation at 35 °C for 18 h, the diameters of the inhibition zones were measured.

3.2.4 MICROSCOPY

10 mg of the respective tetracycline derivate were weighed into 4 ml glass vials together with accordingly 0.5, 1 or 2 mole of magnesium stearate or calcium stearate. 2 ml of ethanol were added to suspend the powder mixture. The suspensions were placed in an orbital shaker (Torrey Pines Scientific Inc., Carlsbad, CA, USA) and heated at 75 °C to evaporate the ethanol at moderate shaking. Subsequently, the mixture solidified on the inner glass vial surface. The nature of the formed glass like films depended on the molar ratio. Samples were scraped from the inner surface and examined with a light microscope (Carl Zeiss Microscopy, Jena, Germany).

3.2.5 STABILITY STUDIES

In case of the minocycline complex, stability studies were carried out. 10 mg of pure minocycline and 20 mg of the dried minocycline complex were weighed into 4 ml glass vials. One of each vial was incubated with PBS pH 7.0 and an additional one was

exposed to phosphate buffer, which has been acidified with hydrochloric acid towards pH 2.3. Samples were taken daily until the 9th day, without a replacement of buffer. Ongoing, the sample taking intervals were stretched to 3 to 4 days.

Chromatograms were recorded on an Agilent 1200 Series system with a XTerra RP18 5 μ m 3.9x150 column (Waters). 10 μ l sample volume was injected at a flow rate of 1.0 ml/min. A gradient program was applied to the mobile phase (Table 6). The retention time was 4.8 minutes and for the evaluation of the chromatograms, the Chem32 software was utilized.

Table 6: Mobile phase gradient program for the stability studies

Time [min]	Flowrate [μ l/min]	Water + 0.1% TFA [%]	Methanol + 0.1% TFA [%]
0.00	1000	95.0	5.0
7.00	1000	0.0	100.0
10.0	1000	0.0	100.0
11.0	1000	95.0	5.0

3.3 PRODUCTION

3.3.1 CRYOMILLING

To achieve a sufficient filling of the extrusion chamber, batch sizes of at least 1 g were necessary. Hence, it was mandatory to produce larger amounts of the in 3.1 described dried MLC powder. 1 g of the extrusion precursor contains 412.3 mg MLC with 115 mg minocycline. The remaining 587.7 mg consist of the desired PLGA- or PEG-PLGA-polymer, and additional excipients like plasticizers, if desired. These blends were filled into the grinding chamber with two 10 mm steel spheres and adjusted in the Retsch CryoMill (Retsch, Haan, Germany). The milling program included an automatic pre-cooling phase, followed by 5 milling cycles at 30 Hz for 150 s. Between each milling cycle, a 30 s lasting cooling phase at 5 Hz reassured low process temperatures within the grinding chamber. These settings were applied to all produced extrudates.

3.3.2 HOT MELT EXTRUSION

Extrudates were produced with a twin-screw extruder ZE 5 Eco (Three-Tec, Seon, Switzerland) with an integrated SK 500 E frequency converter (Figure 5). 300 and 600 μ m dies were utilized together with screws with a length/diameter ratio of 21.25. The applied temperatures for each heating zone were dependent on the extrudate composition and empirically adjusted. The temperatures are listed below in Table 7: Extrusion temperatures for each extrudate composition. The screw speed was set to

800 rpm according to the frequency converter, which transfers to manually counted, actual 140 rpm. At these settings, the extrusion precursor was carefully filled with a laboratory spatula into the therefore scheduled opening by hand. Microscopic slides were placed on the sides of the die opening with an additional slide on top of them, to avoid an upcoiling of the extruded material. Finally, the extrudates were cut into pieces of approximately 10 cm with a scalpel and stored within opaque falcon tubes at 5 to 8 °C, until they were required for further examination.

Table 7: Extrusion temperatures for each extrudate composition

Extrusion material	Temperature	Heating Zone 1	Heating Zone 2	Heating Zone 3
		1	2	3
Pure MLC		49 °C	52 °C	55 °C
MLC + PLGA ₅₀₂		49 °C	49 °C	53 °C
MLC + PLGA ₅₀₃		49 °C	49 °C	53 °C
PLGA ₅₀₂ / PLGA ₅₀₃ (50:50)		49 °C	51 °C	53 °C
MLC + PLGA ₅₀₂ / PLGA ₅₀₃ (50:50) + 10% GMS		49 °C	51 °C	53 °C
MLC + PEG-PLGA _{6P}		49 °C	52 °C	54 °C
MLC + PEG-PLGA _{6P} + 5% PEG		49 °C	51 °C	53 °C
MLC + PEG-PLGA _{6P} + 10% PEG (300/ 600 µm diameter)		48 °C	49 °C	52 °C
MLC + PEG-PLGA _{6P} + 10% PEG + 5% PVM/MA (300/ 600 µm diameter)		49 °C	51 °C	53 °C
MLC + PEG-PLGA _{7P}		49 °C	55 °C	51 °C

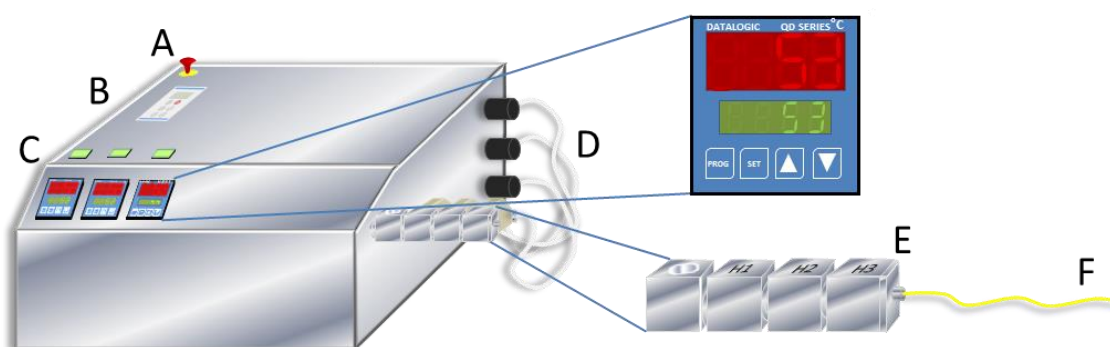


Figure 5: Schematic representation of the twin screw extruder ZE 5 Eco. A – Emergency power switch; B – Control panel of the SK 500 E frequency converter; C – Temperature control panel with set and actual temperature display; D – Heating system with heating plugs and connection to the control console; E – Extrusion chamber with opening on top of the left block, three separate heating zones (H1-H3) and a changeable extrusion die at the backside of H3; F – Emerging extrudate

3.4 EXTRUDATE CHARACTERIZATION

3.4.1 TEXTURE ANALYSIS

Texture analysis was performed to gather information about the mechanical resilience of the extrudates towards penetration (Figure 6). Additionally, a stretch test was executed with the PEG-PLGA extrudates. For both tests a CT3 Texture Analyzer (Ametek GmbH – BU Brookfield, Dresden, Germany) with the TexturePro CT V1.6 software was utilized.

For the penetration test, the extrudates were placed on microscopic slides and adjusted on the base table (TA-RT-KIT) of the texture analyzer. The TA7 standard probe, which resembles a knife edge, was chosen to penetrate, or respectively cut the extrudates. Extrudates with a diameter of 600 μm had to endure a penetration depth of 0.4 mm, while similarly a depth of 0.2 mm was chosen for extrudates with a 300 μm diameter. The descent speed of the probe was set to 2 mm/s. Upon reaching the sample extrudate, the trigger point of 0.067 N was exceeded, which resulted in a reduction of the probe speed to 0.01 mm/s and the start of data acquisition.

In case of the stretch test, a custom-made measuring body was utilized. This enabled the vertical fixation of extrudates between the base table and the measuring probe. The trigger point was reduced to 0.001 N, to immediately begin with the data acquisition after starting the procedure. With a velocity of 0.01 mm/s the measuring head moved upwards from the base table. The measurement was finished as soon as a sudden drop of stretching force was observed, which was always accompanied by a tearing of the examined extrudate.

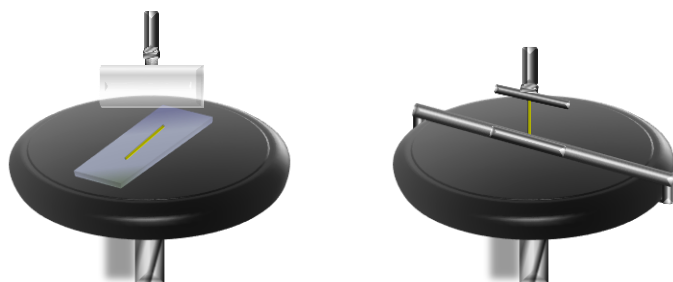


Figure 6: Experimental setup of the penetration test (left) and the stretch test (right)

3.4.2 DIFFERENTIAL SCANNING CALORIMETRY

Differential scanning calorimetry (DSC) examinations were carried out to gain insights into the status within the extrudates. Therefore, all basic compounds and the final extrudates were tested with a DSC 8000 (Perkin Elmer, Rodgau-Jügesheim, Germany). Endothermal Heat Flow curves were acquired in a range from 0 °C to either

100 °C or 200 °C at a 5 K/min heat rate (Table 8). For pure polymers the 2nd heating curve was chosen for evaluation to avoid relaxation peaks within the thermograms.

Table 8: DSC parameters - Temperature ranges and displayed heating curves

Sample	Temperature range	Displayed curve
Minocycline	0 – 200 °C	1 st curve
Magnesium stearate	0 – 200 °C	1 st curve
Physical mixture of minocycline and magnesium stearate	0 – 200 °C	1 st curve
MLC	0 – 200 °C	1 st curve
PEG 1500	0 – 100 °C	2 nd curve
PVM/MA	0 – 100 °C	2 nd curve
PEG-PLGA _{6P}	0 – 100 °C	2 nd curve
PEG-PLGA _{7P}	0 – 100 °C	2 nd curve
All Extrudates	0 – 100 °C	1 st curve

3.4.3 X-RAY POWDER DIFFRACTION

X-ray powder diffraction (XRPD) measurements were executed with a STOE STADI MP - powder diffractometer (Stoe & Cie GmbH, Darmstadt, Germany). To investigate samples via XRPD, especially the extrudates, it was necessary to thoroughly pulverize them beforehand. Therefore, extrudates were cut into pieces with a scalpel and subsequently submitted to a cryomilling procedure. Starting with an automatic precooling phase, the samples were milled with two 4 mm steel spheres at 25 Hz for 60 s. For the pure PEG-PLGA polymers it was necessary to achieve a sufficient crushing. In their case, two milling cycles with two 6 mm grinding media at 25 Hz for 60 s were applied.

Onward, the different powders were applied to the respective X-ray-sample discs, and scanned in an angle range from 5° to 30° in 0.5° steps with an exposure time of 60 seconds per step. Radiation was induced with a molybdenum X-ray tube. For the data evaluation the WinXPOW Software was utilized.

3.4.4 *IN VITRO* RELEASE

3.4.4.1 Prerelease: Drug Extraction

To extract minocycline from the extrudates, an extraction method inspired by Holmkvist et al. 2016 (91) was chosen. The extrudates were weighed and afterwards transferred to 15 ml centrifuge tubes. 2 ml of acetonitrile containing 0.1% trifluoroacetic acid (TFA)

were added to dissolve PLGA. After shaking for 1 min with an IKR-VIBRO-FIX-shaker, 4 ml of methanol were added to solve minocycline and precipitate the polymer. Subsequently, the sample was centrifuged at 1000 rpm for 5 minutes, and filtered through a 0.45 μm Teflon filter to separate the drug from the precipitate, yielding the test solution. With the in 3.4.4.3 described quantification method a recovery rate of 96% was achieved.

3.4.4.2 Sample Preparation and Release Parameters for the *In Vitro* Release

Extrudates with a diameter of 600 μm were cut into pieces of 4 mm length $\pm 100 \mu\text{m}$. For the 300 μm extrudates a length of approximately 16.8 mm was calculated to display a comparable weight to the 4 mm long extrudates with a diameter of 600 μm . Due to the possibility of an insufficient contact between the release medium and a 16.8 mm long extrudate, these extrudates were cut in half. Subsequently, the extrudates were weighed and transferred into 2 ml brown glass vials (600 μm : one 4 mm extrudate; 300 μm : two 8.4 mm extrudates). Per release experiment, five vials per formulation were prepared and incubated in 1 ml of phosphate buffer pH 7.0 at 37 °C in a water bath. From day 0 to 4, sample taking took place daily. From there on, the interval was stretched to every 2 days. During the sample taking the complete buffer was exchanged, and the samples were stored at -20 °C until quantification.

3.4.4.3 Drug Quantification via HPLC coupled to a UV/Vis-Detector

The basic quantification took place on a Waters 600 E HPLC system with an XTerra RP18 5 μm 3.9 x 150 column (Waters). 20 μl sample volume was injected into the system at a flow rate of 1.0 ml/min. The gradient program of the mobile phase can be taken from Table 9. The retention time was 9.5 min and the drug was detected with an UV/Vis detector at 355 nm. Linear calibration curves ($r^2 > 0.999$) were obtained in the range of 2 – 50 $\mu\text{g/ml}$.

Table 9: Mobile phase gradient program of the HPLC – UV/Vis quantification method

Time [min]	Flowrate [$\mu\text{l}/\text{min}$]	25 mM KH_2HPO_4 + 0.06% H_3PO_4 [%]	Acetonitrile [%]
0.00	1000	100.0	0.0
10.00	1000	40.0	60.0
15.00	1000	40.0	60.0
16.0	1000	100.0	0.0

3.4.4.4 Quantification via HPLC coupled to a Tandem Mass Spectrometry Detector (LC-/MS/MS)

In the course of the development, a LC-/MS/MS quantification method with increased sensitivity was established and validated. At the time point of the implementation of this method, the major part of release experiments had already been finished. Nevertheless, it was regarded as valuable, to repeat release experiments with certain promising prototypes (e.g. PEG-PLGA_{6P}-MLC extrudates). Samples were prepared as described above and incubated in phosphate buffer pH 7.0 at 37 °C, and subsequently submitted to the new quantification method.

Therefore, a 1260 Infinity HPLC system (Agilent Technologies) was utilized with a Gemini 3 μ C18 110A, 50 x 2 mm, 3 μ m column (Phenomenex). Tetracycline was used as internal standard. At a flowrate of 400 μ l/min, sample volumes of 5 μ l were injected. The retention times were 1.7 min for minocycline and 2.1 min for tetracycline. Once again, two mobile phases within a gradient program were applied (Table 10).

Subsequently of the separation, the sample was directly injected into the API3200 mass spectrometer (AC Sciex). Within the mass spectrometer, the samples were ionized by electro spray ionization with a positively charged Turbo V source at 650 °C and 5500 V. A quadrupole mass filter served for the mass selection. In case of minocycline, 458.20 Da was the selection mass in quadrupole 1. For tetracycline it was 445.30 Da. In quadrupole 3 the selected mass for the fragmentation ion of minocycline was 441.3 Da with the qualifier at 283.2 Da, while for tetracycline the mass was 410.3 Da with the qualifier at 154.2 Da. Linear calibration curves ($r^2 > 0.99$) were obtained in a range of 10 – 2000 ng/ml.

Table 10: Mobile phase gradient program of the LC-MS/MS quantification method

Time [min]	Flowrate [μ l/min]	Water + 0,1% Formic acid [%]	Methanol + 0.1% Formic acid [%]
0.00	400	95.0	5.0
2.20	400	45.0	55.0
2.50	400	5.0	95.0
3.00	400	5.0	95.0
3.50	400	95.0	5.0
5.00	400	95.0	5.0

3.4.5 MULTISPECTRAL FLUORESCENCE IMAGING

For the first extrudate prototypes, the possibility of monitoring the microenvironment within the extrudates with the fluorescence dye Nile red was explored. Therefore, an initial load of 100 μ l of a 1 mg/ml ethanolic Nile red stock solution was pipetted to an ethanolic minocycline-complex solution, containing 115 mg of minocycline and 297.3 mg magnesium stearate. This was the absolute amount of the educts for a 1g batch for extrusion. Hence, a dye load of 100 μ g/g Nile red was present within the monitored samples. Afterwards, these marked minocycline complex solutions were submitted to the in 3.1, 3.3.1 and 3.3.2 described drying, cryomilling and subsequent extrusion. The adjustment of extrusion parameters due to the addition of Nile red was not necessary. For some extrudates quenching effects were observable. Therefore, these extrudates were also loaded with 10 μ l instead of 100 μ l of the stock solution to avoid these circumstances. For both tested polymers, 3 dyed samples and 1 undyed sample were prepared by cutting them into pieces of 4 mm length. Thereafter, they were incubated in 3 ml PBS pH 6.0 in a water bath at 37 °C.

For data acquisition, the extrudates were transferred from the buffer to a perforated plate and investigated with a LEICA DM 4000 B microscope (Leica Microsystems, Wetzlar, Germany) connected to a CRI Nuance N-MSI-EX imaging system (PerkinElmer LAS, Rodgau, Germany). The program Nuance (version: 3.0.1.2) was used for data analysis. Image cubes were acquired in the range of 590-710 nm in 2 nm steps, using the N2.1 green filter (excitation filter, 515-560 nm; emission filter LP590, 580 nm long pass). The samples were auto exposed to avoid over- or underexposure. Afterwards, minocycline's auto fluorescence in PLGA and the emission of the background were determined. Through manual computation and a fitting procedure with minimal error scale, the auto fluorescence was removed from the extrudates emission spectrum. After unmixing, the purified spectrum from the background and the auto fluorescence, 5 regions of interest (ROI) of the same size were applied across the extrudate. For further analysis, the average scaled counts/s of these 5 measuring areas were used. In addition, the unmixed image cubes were utilized to compare the fluorescence intensity of the single cubes.

3.5 ANTIMICROBIAL *IN VITRO* EVALUATION

The following methods are described according to Prof. Sigrun Eick (92) from the university of Bern, where these experiments were carried out. In addition to the *in vitro* release experiments (3.4.4), extrudates were tested towards their antimicrobial activity,

to evaluate their potential with elevated requirements. These tests were initially carried out with the PLGA_{502/503}-MLC extrudates and later on concluded with a testing of the PEG-PLGA-MLC formulations. The pure minocycline base and the Arestin[®] minocycline microspheres served as positive control. As negative control unloaded extrudates, consisting solely of the polymer and magnesium stearate, were utilized. Care was taken, to protect the formulations from the influence of UV-radiation during storage and the execution of the experiments. By freezing the extrudates and microspheres at -20 °C over night and a subsequent micronization in a porcelain mortar, a homogeneous dispersion of the formulations was reassured.

3.5.1 MICROORGANISMS

A six species biofilm, consisting of *T. forsythia*, *F. nucleatum*, *S. gordonii*, *A. naeslundii* and *P. micra* (2.5, Table 5), was utilized in the following assays. On tryptic soy agar plates (Oxoid, Basingstoke, GB) the bacterial strains were precultured with 5% sheep blood for 24 h at 37 °C with the necessary conditions. In case of *S. gordonii* and *A. naeslundii* 10% CO₂ atmosphere was applied, while the other strains were kept under anaerobic conditions.

For the biofilm assays, all six strains were suspended in phosphate buffered saline according to McFarland 0.5 (approximately 1.5×10^8 microorganisms) and mixed in a ratio of 1:2:4 (*S. gordonii* / *A. naeslundii* / each other strain).

3.5.2 MINIMAL INHIBITORY CONCENTRATION (MIC)

DETERMINATION

MIC determinations were carried out with *P. gingivalis* and *S. gordonii* as test strains. A two-fold dilution series of the formulations was prepared in distilled water, with the highest concentration equivalent to a concentration of 64 µg/ml pure minocycline. Of the negative control an amount, which resembled the loaded extrudates, was utilized. The bacteria were suspended within double concentrated Wilkins-Chalgren-broth with 10% of lysed horse blood and 10 µg/ml β-NAD (approximately 10^6 bacteria/ml). Subsequently, 100 µl of the test dilutions were pipetted onto a 96-well-plate, each followed by 100 µl of bacterial suspension. The concentrations of the tested formulations ranged from 32 µg/ml to 0.125 µg/ml minocycline. After 18 h of incubation, or respectively 42 h at anaerobic conditions, the MIC was evaluated. As MIC, the lowest concentration which could prevent a visible growth, indicated by turbidity, was determined.

3.5.3 ACTIVITY AGAINST BIOFILM FORMATION

Test solutions were prepared by dissolving the test formulations in distilled water to concentrations of 125 µg/ml. 10 µl/well of these solutions were pipetted in the wells of a 96 well-plate. After 1 h, 10 µl/well of PBS with 1.5% bovine serum albumin (PBS/SA) were added. Another 10 minutes later, the mixed bacterial suspension in Wilkins-Chalgren-broth with 5% horse blood and 5 µg/ml β-NAD were added. After 6 h of incubation at 37 °C, or respectively 24 h under anaerobic conditions, the total amount of colony forming units (cfu) was assessed.

Additionally, the quantity and metabolic activity of the formed biofilms were measured. For the quantification crystal violet staining according to Pirrachio et al. 2018 (93), and Kwasny and Opperman 2010 (94) was conducted. Therefore, the biofilms were fixed at 60 °C for 60 minutes and stained with 50 µl of 0.06% (m/V) crystal violet solution per well for 10 minutes. The staining was quantified with a plate reader (ELx808, Biotek Instruments, Winooski, VT, USA) at 600 nm. The metabolic activity of the biofilms was evaluated with resazurin as redox indicator (93,95). Therefore, 5 µl of resazurin reagent were mixed with 100 µl of the nutrient media and pipetted towards the biofilm. After an incubation period of 1 h at 37 °C, the absorbances were measured by spectrophotometric analysis with a plate reader at 570 against 600 nm.

3.5.4 ACTIVITY ON PREFORMED BIOFILMS

Biofilms consisting of a multispecies mixture with six species (3.5.1) have been cultivated for 4 days. After 2.5 days, the nutrient broth was exchanged, and *P. gingivalis* and *T. forsythia* were added anew. After the 4-day incubation period, the nutrient media was removed, the biofilms were shortly washed with PBS. Subsequently, 100 µl of the test solutions were added in concentrations of 1000 µg/ml, 500 µg/ml and 250 µg/ml minocycline. After 10 minutes, 100 µl of nutrient broth were added per well, resulting in final concentrations of 500 µg/ml, 250 µg/ml and 125 µg/ml. Concluded by an incubation over night for 18 h, the cfu, biofilm quantity and metabolic activity were assessed as described in 3.5.3.

The experiments were carried out in quadruplicate, and statistically analyzed with ANOVA with post hoc Bonferroni. The significance level was set to $p = 0.05$ and the Software SPSS 25.0 (IBM SPSS Statistics, Chicago, USA) was utilized.

3.5.5 *IN VITRO* SIMULATION OF GINGIVAL FLOW AND RELEASE KINETICS

Another approach for the *in vitro* evaluation of the extrudates was the simulation of the gingival crevicular flow (CGF). According to Goodson et al. 2003 (55), the resting volume within a periodontal dental pocket is approximately 1.5 μl with a flow of 44 $\mu\text{l}/\text{h}$, which decreases to 15 $\mu\text{l}/\text{h}$ twelve weeks after successful treatment. Therefore, test formulations equivalent to 1 mg of minocycline were weighed into tubes together with 23.5 μl PBS/SA. After incubation for 30 minutes, and centrifugation at 5000 g for 1 minute, 22 μl of the medium were exchanged with fresh 22 μl PBS/SA. The pipetting scheme for the CGF simulation can be taken from Table 11. The obtained eluates were stored at -20 °C until further analyzation. The eluates of T: 1 h, 2 h, 4 h, 6 h, 24 h, 2 d, 4 d, 7 d and from there on weekly were utilized for the determination of the MIC. A two-fold dilution series was prepared and the eluates were submitted to the same procedure as described in 3.5.2. Anew, the lowest concentration, which was able to inhibit the bacterial growth of both tested bacterial strains, was recorded.

Also, the potential of inhibiting the formation of biofilms was tested for the eluates. Eluates of T: 24 h, 2 d, 7 d, 14 d and 28 d were evaluated. 10 $\mu\text{l}/\text{well}$ were pipetted onto a 96 well plate and left untouched for 1 h. From there on, the procedure was similar to 3.5.3, except that the cfu counting took place already after 6 h of incubation.

Table 11: Pipetting scheme for the simulation of the gingival crevicular flow

Time	Removed volume	Added volume	Time	Removed volume	Added volume
0 min		23.5 μl	7 d	3168 μl	3500 μl
30 min	22 μl	22 μl	10.5 d	3500 μl	3500 μl
60 min	22 μl	44 μl	14 d	3500 μl	3304 μl
2 h	44 μl	44 μl	17.5 d	3304 μl	3304 μl
3 h	44 μl	44 μl	21 d	3304 μl	3108 μl
4 h	44 μl	88 μl	24.5 d	3108 μl	3108 μl
6 h	44 μl	792 μl	28 d	3108 μl	2912 μl
24 h	792 μl	1056 μl	31.5 d	2912 μl	2912 μl
2 d	1056 μl	1056 μl	35 d	2912 μl	2716 μl
3 d	1056 μl	1056 μl	39.5 d	2716 μl	2716 μl
4 d	1056 μl	3168 μl	42 d	2716 μl	-

4 RESULTS AND DISCUSSION

Chapters 4.1 to 4.4 are, to a major part, subject of a peer reviewed publication (96). As well, the subsequently presented complexes and their applications are protected by a patent (97).

4.1 CHELATION OF THE TETRACYCLINE DERIVATIVES

Tetracycline derivatives offer a wide spectrum of antimicrobial activity (79) and demonstrated their worth in the local therapy of periodontitis. A problem that all tetracycline derivatives share is their limited stability in aqueous surrounding. Chow et al. 2008 (98) revealed in their work, that additionally to the known susceptibility to light, minocycline is prone to epimerization in water and several organic solvents, especially NMP. After epimerization, only 5% of the initial antibiotic activity remained. They also discovered a delay of such processes, if minocycline has been chelated in advance. A chelate complex is characterized through the formation of bonds between a single central atom and several binding sites of the same ligand (99), which in case of minocycline stabilized the API. Chelate complexes formed with magnesium as central ion proved to be more stable than their calcium counterparts, which probably depended on their higher charge density. Thus, the concept of a chelation arose as first step of development, but with an additional intention: The avoidance of water and the alteration of the APIs physical properties, by choosing fatty acid salts as central ion donor. Therefore, minocycline, doxycycline and oxytetracycline were chosen to be paired in ~70 °C hot ethanol with fatty acid salts, such as magnesium- and calcium stearate to form these lipophilic complexes.

The tested molar ratios of 2:1, 1:1 and 1:2 (tetracycline derivative : fatty acid salt) for minocycline and magnesium stearate yielded in all cases yellow colored solutions (Figure 7). In case of calcium stearate, the 1:2 ratio resulted in a suspension. Thus, this ratio was excluded early from further investigations. Doxycycline demonstrated a compatibility with magnesium stearate similar to minocycline. Clear solutions could be observed with a less intensive yellow coloring. The combination of doxycycline with calcium stearate however, revealed slightly cloudy solutions for the ratios of 1:1 and 1:2. To form a solution between oxytetracycline and magnesium stearate, a prolonged heating of the 1:1 and 1:2 ratios was necessary to eventually solvate initially persistent particles. Noteworthy is that the 2:1 ratio remained turbid even after prolonged heating. This also indicates the formation of a more soluble complex with rising magnesium stearate content. Finally, oxytetracycline and calcium stearate compositions remained turbid, and formed a clearly observable sediment.

Conspicuous was the poor solubility of the calcium stearate compositions compared to their magnesium stearate equivalents. The reason therefore lies within the charge density, mentioned in the first paragraph of this section. Magnesium and calcium are both divalent cations. But due to the smaller atom diameter (Mg: 145 pm; Ca: 194 pm (100)), and its therefore higher charge density, magnesium can easier interact with the chelation site of the ligands. This explains the formation of a suspension between calcium stearate and minocycline in the 1:2 ratio, the turbid solutions with doxycycline and the incompatibility with oxytetracycline.

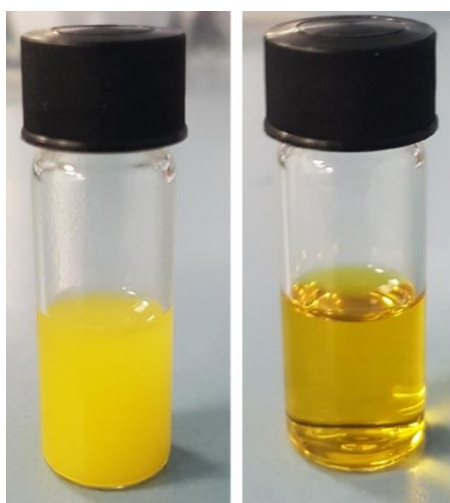


Figure 7: Minocycline paired with magnesium stearate in ethanol (molar ratio 1:2) before (left) and after (right) heating at $\sim 70^{\circ}\text{C}$. Through heating, the prior suspension turned into a solution, which remains stable at room temperature.

4.2 COMPLEX CHARACTERIZATION

4.2.1 UV/VIS-SPECTROSCOPY

A prominent indication for a successful chelation are changes in the absorption spectra (101). Minocycline possesses absorption maxima at 255 and 344 nm in ethanol (Figure 8). After combination with magnesium stearate, the spectrum changed as a function of magnesium stearate concentration. The spectrum shape of the 1:1 and 1:2 ratios were almost identical with a similar position of their absorption maxima. After complexation, the shortwave maximum at 255 nm shifted hypsochromically to 244 nm, while the longwave maximum experienced a bathochromic shift to 385 nm. The ratio of 2:1 did not possess a clear maximum, due to an overlapping spectrum of pure minocycline and the partially developed complex. Thus, the spectra indicated a complexation in the molar ratios of 1:1 and 1:2.

The addition of calcium stearate led to comparable changes within the absorption spectrum. The 1:1 ratio resulted in a hypsochromic shift for the shortwave maximum, and a bathochromic shift for the latter one, while the 1:2 ratio had already been

excluded. Analogous to magnesium stearate, the 2:1 ratio resembled an overlapping spectrum of pure minocycline and a partially formed complex.

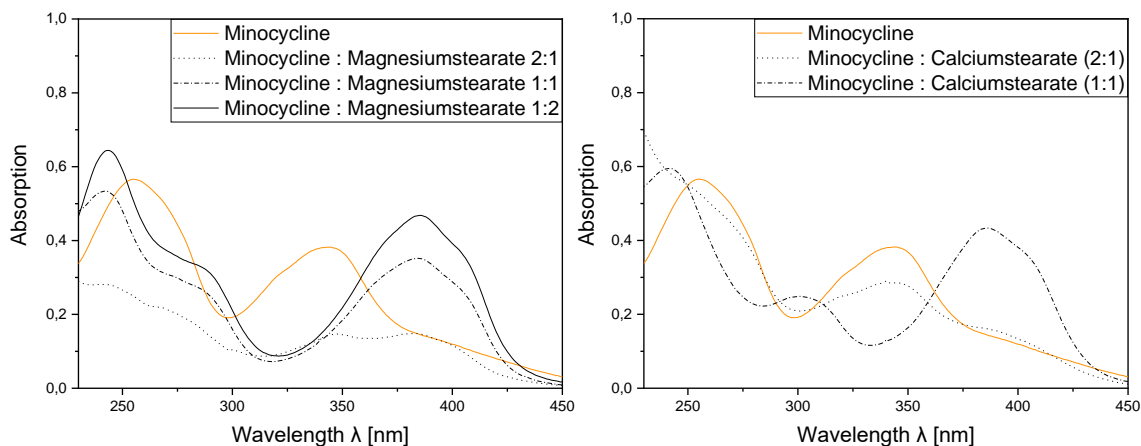


Figure 8: UV/Vis spectra (230-450 nm) of minocycline paired with magnesium- and calcium stearate in different molar ratios

As expected, the results for doxycycline were quite close to minocycline, due to their structural similarity. Deviating from minocycline however, both absorption maxima encountered a bathochromic shift independent from the central ion (Figure 9). For magnesium stearate, minor differences of the absorption maxima were observable depending on the amount of fatty acid salt. Interestingly, the spectra of the 2:1 and the 1:1 ratio were almost congruent. Thus, the complexation appears to be incomplete until the molar ratio of 1:2 yields a clearer shift of the maxima.

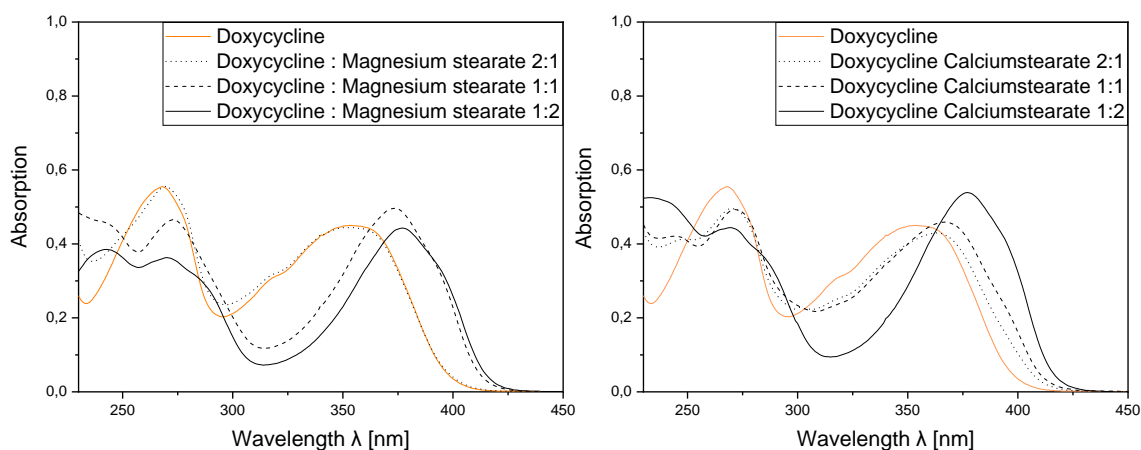


Figure 9: UV/Vis spectra (230-450 nm) of doxycycline paired with magnesium- and calcium stearate in different molar ratios

The prolonged heating period for oxytetracycline to react with the lipophilic fatty acid salts indicate a minor capacity of oxytetracycline to form the desired complexes. Additionally, in case of oxytetracycline the dihydrate salt was utilized for the experiments, which could also contribute to a deviating solubility. In contrast, for minocycline also complexation reactions were executed with the hydrochloride salt,

which equally resulted in the successful formation of solutions. But in comparison, the pure minocycline base appeared to form the complex solutions faster, which is why the pure tetracycline bases should be preferred for this kind of complexation.

Regarding the complexation of oxytetracycline, magnesium stearate was again superior to calcium stearate. In the 1:1 and 1:2 ratios clear solutions emerged, and the maxima at 264 and 365 nm are both shifted bathochromically depending on the concentration of magnesium stearate (Figure 10). The in 4.1 mentioned formation of a turbid “solution” indicated an incomplete complexation. This can also be extracted from the UV/Vis-spectra. The spectra of the 2:1 ratio with magnesium stearate and the pure minocycline were quite similar and only minor maxima shifts were observable. So, the successful complexation of the other ratios resulted in an enhanced solubility in hot ethanol. As expected, the spectra of the supernatants of the oxytetracycline calcium stearate suspensions did not reveal reliable evidence for the formation of stable complexes. The 2:1 and the 1:1 ratio were hardly separable from the original spectrum. Despite the clear demonstration of bathochromic shifts for both maxima for the 1:2 ratio, the unsatisfying solubility contradicted the formation of a complex.

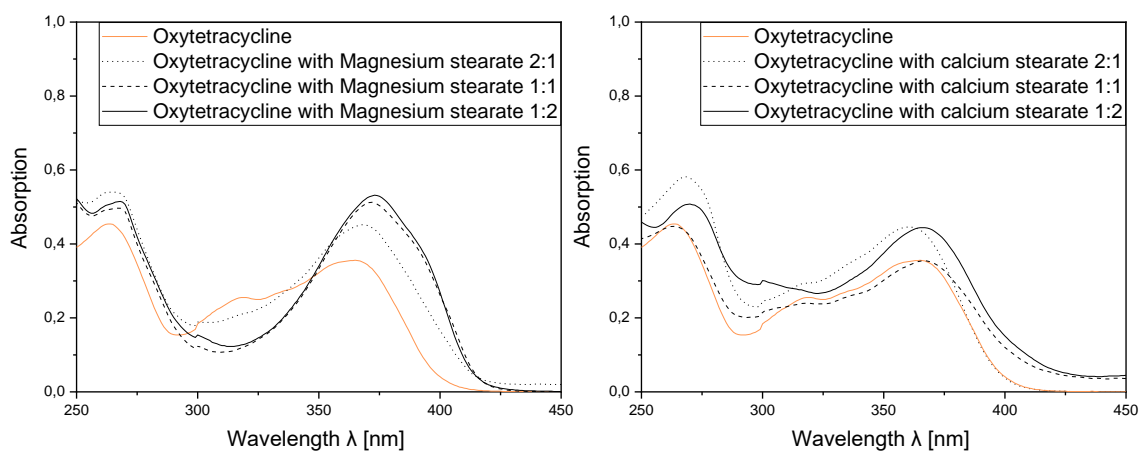


Figure 10: UV/Vis spectra (250-450 nm) of oxytetracycline paired with magnesium- and calcium stearate in different molar ratios

What all complexes, independent from the central ion and the complexing tetracycline derivative, have in common is their sensitivity to pH changes (Figure 11). After addition of small amounts of hydrochloric acid (HCl), the complexes disintegrated and the spectra of the pure tetracycline derivatives aligned with their former complexes. For minocycline the maxima shifted to 264 nm and approximately 355 nm, which will be of use for the subsequent detection during the HPLC analysis. Comparable sensitivity of hydrophilic minocycline chelate complexes to low pH values had also been observed by Zhang et al. 2015 (102).

The UV/Vis-investigation led to the exclusion of all 2:1 ratios. For doxycycline also the 1:1 ratio of the calcium stearate composition was excluded. In case of oxytetracycline even further restrictions were necessary. All pairings between oxytetracycline and calcium stearate were eliminated from further examinations, due to the poor solubility and insufficient complexation capabilities. In summary, the 1:2 ratio complexes between the tetracycline derivatives and magnesium stearate seemed favorable at this point with encouraging hints towards a formation of the lipophilic complexes.

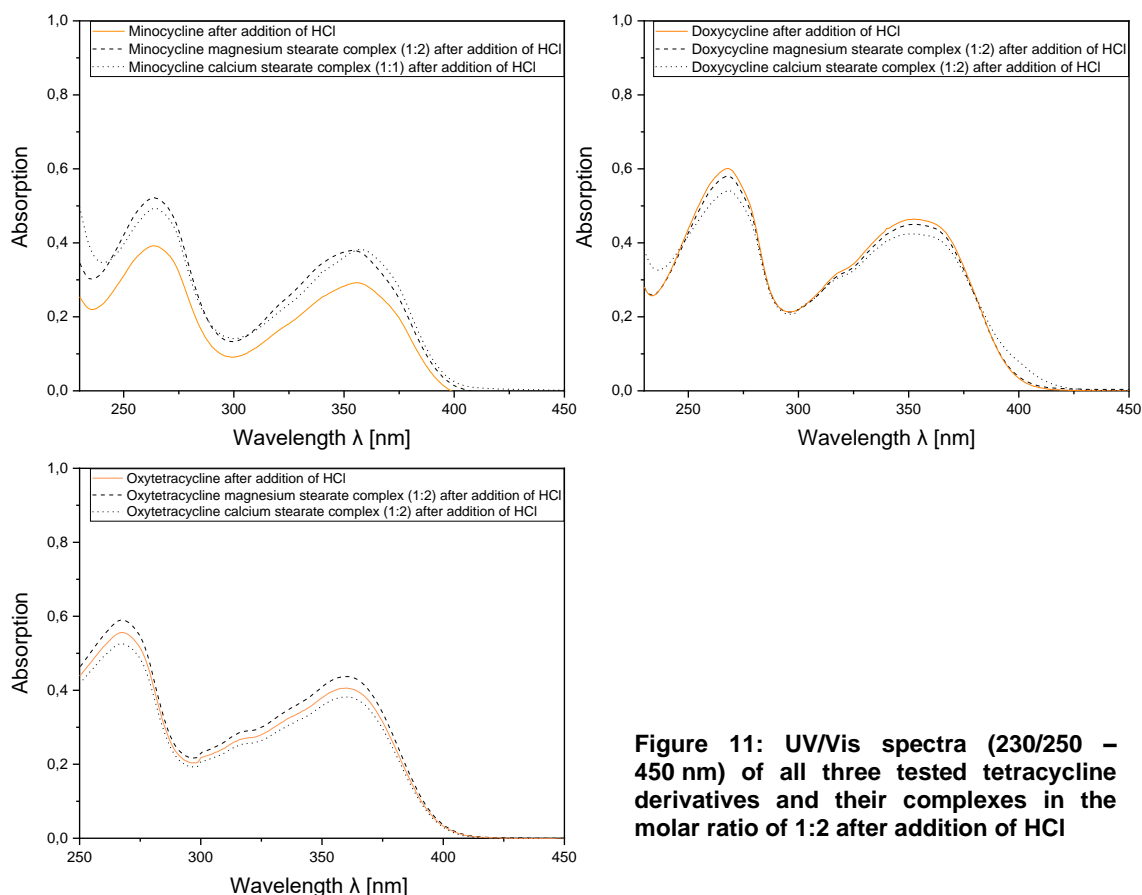


Figure 11: UV/Vis spectra (230/250 – 450 nm) of all three tested tetracycline derivatives and their complexes in the molar ratio of 1:2 after addition of HCl

4.2.2 ATTENUATED TOTAL REFLECTION INFRARED SPECTROSCOPY

With the recording of the IR-spectra further evidence was collected for the formation of the lipophilic complexes. Figure 12 illustrates the spectra of minocycline and its complexes with magnesium- and calcium stearate in the 1:2 ratios. The 1:2 ratios were chosen, due to the results of the prior UV/Vis-investigation. The peak at 3478 cm^{-1} (a) in the pure minocycline spectrum can be assigned to the hydroxide-vibration, which took part in an intramolecular hydrogen-bond. In contrast, the complex displayed a broad peak. This indicated an impediment to the binding sites free vibration, due to the presence of magnesium or calcium acting as central ions. The C-H-vibrations (c) of minocycline were superimposed by the more prominent C-H peaks (g) of magnesium-

or respectively calcium stearate. The carboxylate peak at 1570 cm^{-1} remained plainly recognizable. At 1700 cm^{-1} appeared a new peak, which could not distinctly be assigned to a specific functional group. The fingerprint area also encountered changes, due to the overlapping of vibrations, but offered no further evidence.

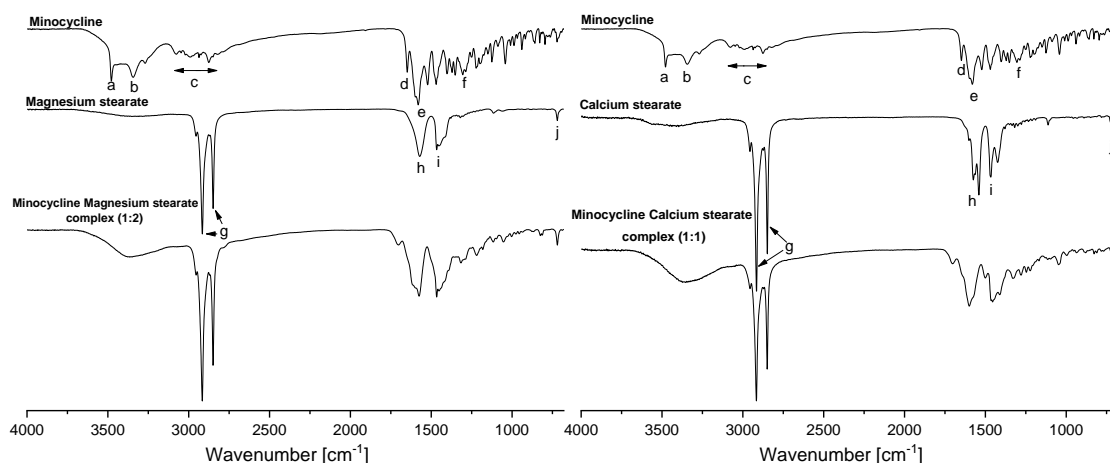


Figure 12: FTIR-ATR-Spectra of minocycline, magnesium- and calcium stearate and their complexes (molar ratio 1:2) ($680\text{-}4000\text{ cm}^{-1}$) Minocycline: a – ν O-H; b – ν N-H; c – ν C-H/=C-H; d – ν CONH₂; e – ν C=C (aromatic); f – ν C-N Magnesium stearate / Calcium stearate: g – ν C-H; h – ν_{as} COO⁻; i – δ C-H; j - CH₂ rocking-vibration

Also, a physical mixture between minocycline and magnesium stearate in the molar ratio of 1:2 was compared to the complex (Figure 13). The spectrum of the physical mixture hardly resembled any of the original spectra. Instead of the clear observable O-H and N-H peaks, a broad peak comparable to the complex, but with a higher intensity was dominating. Additionally, the C-H valence vibration peaks of magnesium stearate are attenuated and slightly shifted. During the compaction for sample preparation a weight of 5 t created by the hydraulic press weighed on the compacts, and this might enforce interactions between them. Thus, a reaction of both components during compression seems possible. But given the high intensity of the peak in the O-H vibration region, these interactions do not impede the vibrations like the formed lipophilic complexes do. The DSC and XRPD data in section 4.7 will support this claim.

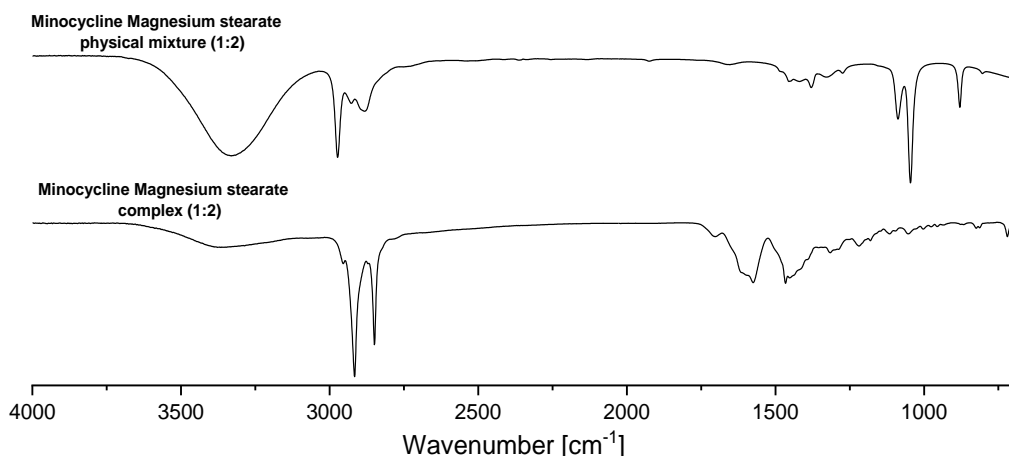


Figure 13: FTIR-ATR-Spectra of minocycline and magnesium stearate in the molar ratio 1:2 as physical mixture and formed complex (680-4000 cm^{-1})

Deviating from minocycline, the IR-spectra for doxycycline revealed a broad peak at approximately 3300 cm^{-1} (a), which could not be distinguished between O-H and N-H vibration (Figure 14). Nevertheless, this peak was also widened and smoothed in presence of divalent cations, which supports the approach of an O-H vibration impediment during and after complexation.

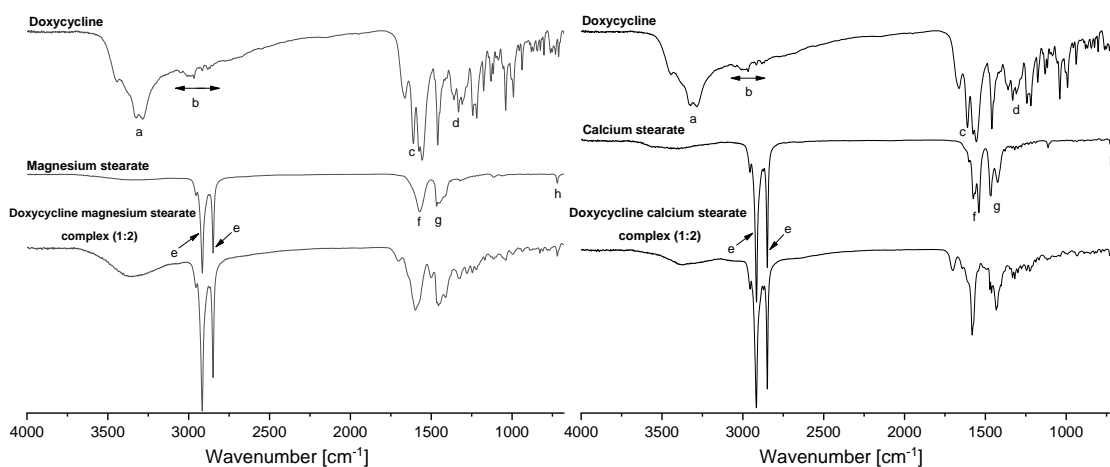


Figure 14: FTIR-ATR-Spectra of doxycycline, magnesium- and calcium stearate and their complexes (molar ratio 1:2) (680–4000 cm^{-1}) Doxycycline: a – ν O-H / ν N-H; b – ν C-H/=C-H; c – ν CONH₂; d – ν C=C(aromatic) Magnesium stearate / Calcium stearate: e – ν C-H; f – ν_{as} COO⁻; g – δ C-H; h – CH₂ rocking-vibration

For oxytetracycline solely the spectrum of the magnesium stearate complex was recorded, due to the previous exclusion of the calcium stearate compositions. Oxytetracycline also displayed the signs of a vibration impediment after contact with magnesium stearate (Figure 15). The O-H and N-H peaks at 3600 and 3370 cm^{-1} merged into a broad peak comparable to precedent spectra. Furthermore, the C-H peaks of the stearate chain dominated in the region of 2900 to 2700 cm^{-1} within the

complex. Concluding, the fingerprint area up to the carboxylate peak at 1600 cm^{-1} of the complex spectrum displayed a superimposition.

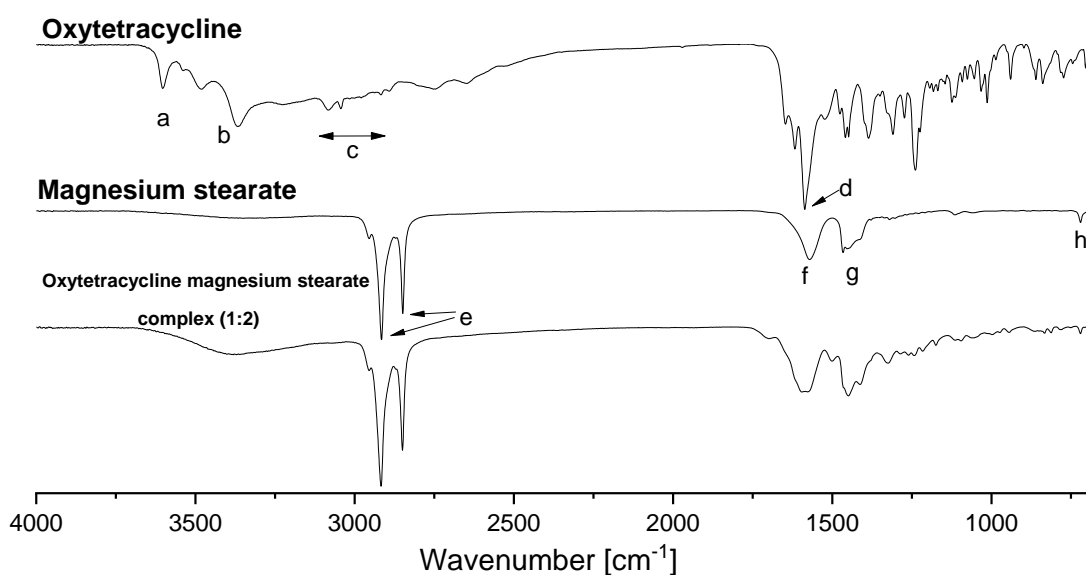


Figure 15: FTIR-ATR-Spectra of oxytetracycline, magnesium stearate and their complex (680–4000 cm^{-1}) Oxytetracycline: a – ν O-H; b – ν N-H; c – ν C-H/=C-H; d – ν CONH₂ Magnesium stearate: e – ν C-H; f – ν_{as} COO⁻; g – δ C-H; h - CH₂ rocking-vibration

4.2.3 MICROSCOPY

For the further evaluation via microscopy of the complexes, they were dried by solvent evaporation, creating glass-like or respectively crystalline structures depending on the molar ratios. Figure 16 illustrates these observations exemplarily for minocycline and doxycycline paired with magnesium stearate. What all three tetracycline derivatives had in common was the glass-like structure on the glass vial's inner surface of the 1:2 ratios, which suggests an amorphous state within the dried film. Contrary, the 1:1 ratios exposed inhomogeneous remnants within in the vials. Unfortunately, the calcium stearate complexes did not yield such homogeneous results for either of both antibiotics (oxytetracycline : calcium – complexes were already excluded).

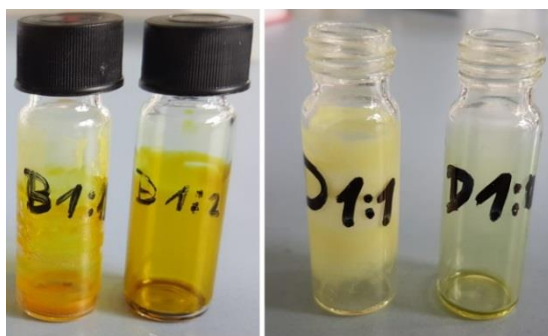


Figure 16: Solidified minocycline/doxycycline : magnesium stearate films within glass vials after evaporation of ethanol;
 Left: Minocycline : Magnesium stearate 1:1 (left) and 1:2 (right)
 Right: Doxycycline : Magnesium stearate 1:1 (left) and 1:2 (right)

These observations were also apparent within the microscopic view (Figure 17). The inhomogeneous nature of the 1:1 molar ratio precipitates was obvious. Crystalline regions with different morphology were apparent in case of the 1:1 minocycline lipid complex (MLC). The 1:1 complex of doxycycline formed powder like nests. Their cloud-like appearance within Figure 16 already suggested such a manifestation. Oxytetracyclines 1:1 precipitated complex displayed semisolid properties, thus the sample had been deformed during application on the microscopic slide. Nevertheless, the crystalline proportions in the center of the presented microscopic section are easy to observe. In contrast, all 1:2 complexes with magnesium stearate formed homogeneous glass-like structures. The compressed regions within the doxycycline and oxytetracycline complexes derived from the sample collection through scraping with a spatula.

These results elucidate the differences between the different molar ratios. The dependence of the complexation degree on the amount of available fatty acid salt has already been demonstrated, but the differences were not clear yet. Even if a complex is formed, the different complexes can vary in their physico-chemical characteristics. For the planned hot-melt extrusion, the complex should ideally be present in form of a homogeneous powder. Though the 1:1 complexes might be suitable for other forms of processing, the 1:2 ratios demonstrated more encouraging properties for the intended use. So, the focus of the following experiments was placed on the molar ratio 1:2 complexes between the three tetracycline derivatives and magnesium stearate.

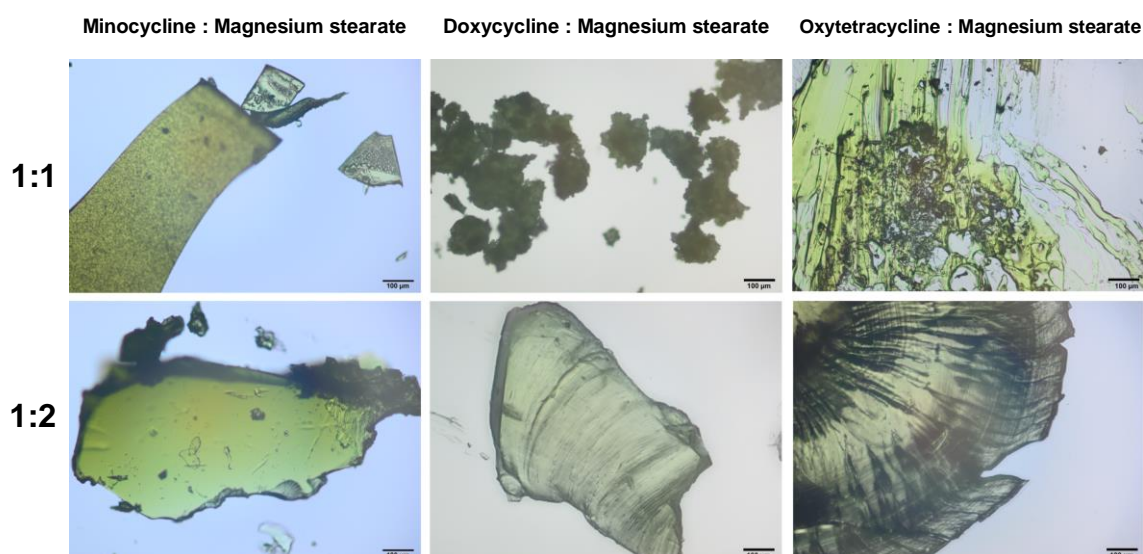


Figure 17: Microscopic view of tetracycline derivative : magnesium stearate complexes in different molar ratios

4.2.4 DISC DIFFUSION TESTS

It is well-known, that the antibiotic capability of tetracycline derivatives can suffer under the influence of polyvalent cations (103). Hence, disc diffusion tests were carried out to clarify any doubts about the antibiotic activity after complexation of the tetracycline derivatives. As just described, the molar ratios of 1:2 were chosen as test solutions. Also, the UV/Vis-spectra (4.2.1) and microscopic data (4.2.3) indicated a stronger interaction between both components, and therefore a higher possible reduction of the antibiotic potential, which had to be clarified. The diameters of the inhibition zones were the decisive value for the evaluation of antibiotic activity (Figure 18).

The control disks loaded solely with ethanol were not able to inhibit the bacterial growth. In contrast, the pure tetracycline derivatives and their complexes were capable of forming inhibition zones. Minocycline accomplished a diameter of 26 mm and the complex achieved 24 mm. In case of doxycycline, the inhibition zones of the pure drug and its complex both measured 25 mm. Likewise, oxytetracycline and its complex formed inhibition zones of 22 mm.

These results indicate a high activity of the lipophilic tetracycline derivative complexes against bacterial pathogens. In most cases the diameters were equally wide. It should be noted, that a statement of superiority between the single tetracycline derivatives should not be extracted from this data, hence inhibition zones do not always correlate with minimal inhibitory concentrations for all bacteria (89,104). A possible explanation for the occurrence of slightly reduced diameters can be decreased diffusion of tetracycline derivative molecules through the agar matrix, due to the interaction with magnesium stearate molecules, creating a larger and more hydrophobic molecule. Nevertheless, these results enabled the next step of progression during our formulation development – the hot melt extrusion.

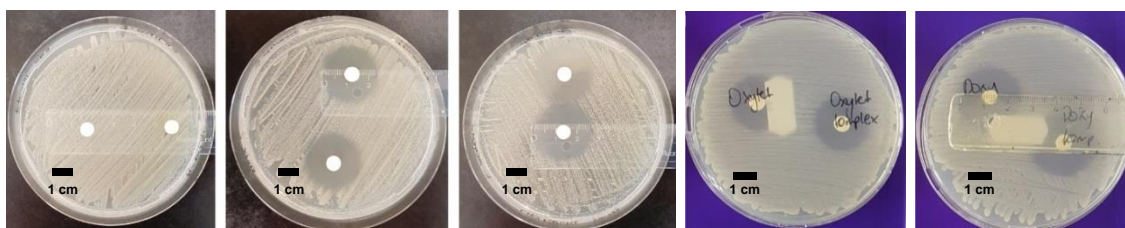


Figure 18: Agar plates incubated with *S. aureus* ATCC 29213..

Left to right: 1st plate: Discs loaded with ethanol; 2nd plate: Discs loaded with ethanolic MLC-solution; 3rd plate: Discs loaded with ethanolic minocycline solution; 4th plate: Oxytetracycline (left) and the complex (right); 5th plate: Doxycycline (left) and the complex (right). The applied scale represents cm.

4.3 FIRST PROTOTYPES

4.3.1 CRYOMILLING AND EXTRUSION OF THE MINOCYCLINE LIPID COMPLEX IN COMBINATION WITH PLGA

For the further development minocycline was chosen as primary API to investigate and process. As described beforehand, due to the comparably lower compliance towards the complex formation, oxytetracycline had to be withdrawn as possible candidate for further processing. Minocycline and doxycycline however, performed equally accessible for the complexation reaction. Also, both antibiotics demonstrate anti-inflammatory properties, (81,105,106), which are beneficial during the treatment of an inflammatory disease like periodontitis. Finally, the reason for giving the preference to minocycline resulted from its broader spectrum of activity and the superior capability of tissue penetration (107). Thus, the following sections cover the minocycline complex – MLC – in the 1:2 ratio incorporated in different PLGA and PEG-PLGA-matrices with varying additional excipients.. For the extrusion, the minocycline lipid complex was dried with a vacuum compartment dryer instead of evaporating the solvent with heat, which led to the manifestation of the complex in form of powder with a more intensive yellow coloring compared to the original minocycline (Figure 19).

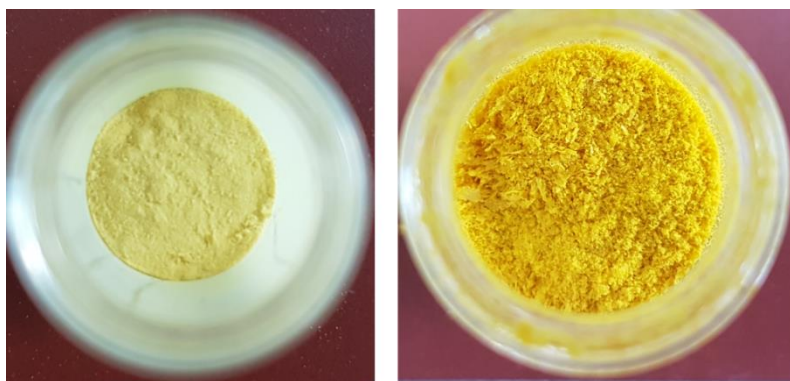


Figure 19: Macroscopic appearance of minocycline (left) and the minocycline lipid complex after drying in a vacuum compartment dryer

In advance of the hot-melt extrusion, this complex powder was submitted to a cryomilling procedure in combination with the desired polymer and additional excipients. The cryomilling ensured the homogeneity and a suitable particle size of the extrusion precursor, while maintaining an environment with minimal thermal stress. In general, cryomilling is regarded as a gentle method for micronization, due to the highly reduced process temperature. But there have also been studies about a chemical activation of APIs and increased upcoming of degradation products, especially during prolonged milling procedures (e.g. >30 minutes) (108,109). These findings may not be applicable to all APIs, but they give reason to choose the cryomilling parameters carefully. We also observed the formation of a crystal disorder for minocycline in

XRPD, but over short milling cycles, unchanged chemical properties for minocycline were described by Dooley 2012 (110). So, extrusion precursor compositions were successfully cryomilled and resulted in a fine powder with a bright yellow coloring.

The hot-melt extrusion itself is a rather fast, simple and well established technology for producing drug delivery systems within the field of pharmaceutical research (111,112). It is an eco-friendly, efficient and continuous process, which is applicable without any (organic) solvent. Additionally, it offers a variety of options for adjusting the product (e.g. diameter, length, addition of property-altering excipients).

On this way, first prototypes were produced with PLGA-polymers, Resomer 502 and 503, from now on referred to as PLGA₅₀₂ and PLGA₅₀₃. The hot-melt extrusion was executed with a 600 µm die, and yielded extrudates in a range from 600 to 900 µm, depending on the chosen polymer (Figure 20). Noteworthy are the viscoelastic properties of PLGA₅₀₃, which resulted in a widening, immediately after the extrusion. The larger diameter led to a deviating amount of available API, in case of application of extrudates with equal length. In terms of reproducibility and a secure dosing, the PLGA₅₀₂-MLC extrudates were favorable, due to the constant diameter of approximately 600 µm. Later on, also blends of both PLGA-polymers were produced and tested. These extrudates did not extend after extrusion. Thus, the viscoelastic properties of PLGA₅₀₃ were reduced within the blend.

Even though these PLGA-MLC extrudates were quite stable after extrusion, they tended to rather break than bend upon exposure to mechanical stress (4.4.1). Within the gingival sulcus such mechanic stress can occur during the application, and through basic daily routines like ingestion. A first approach to bypass this obstacle was the implementation of glycerol monostearate (GMS) as plasticizer (113). The addition of GMS also did not alter the extrudate diameter, but it demonstrated a positive effect on the mechanical resilience by reducing the brittleness.

All these first prototypes were within the desired size range, even the larger specimens. Additionally, extrudates consisting solely of the pure lipophilic minocycline complex were produced to investigate the impact of PLGA on drug release and to explore the possibility to obtain a controlled release without PLGA. It was possible to successfully produce pure MLC extrudates, but they were extensively brittle and exhibited fragile mechanic resilience. Thus, these extrudates were unfortunately not capable to serve any additional purpose than as reference for the *in vitro* release experiments (4.4.2). The absence of potentially toxic solvents lowered the risks during the manufacturing, created a compatible product, and ensured the stability of the API. A limitation of the

laboratory scale production is the manual extruder filling. Thus a discontinuous precursor addition was not completely avoidable.

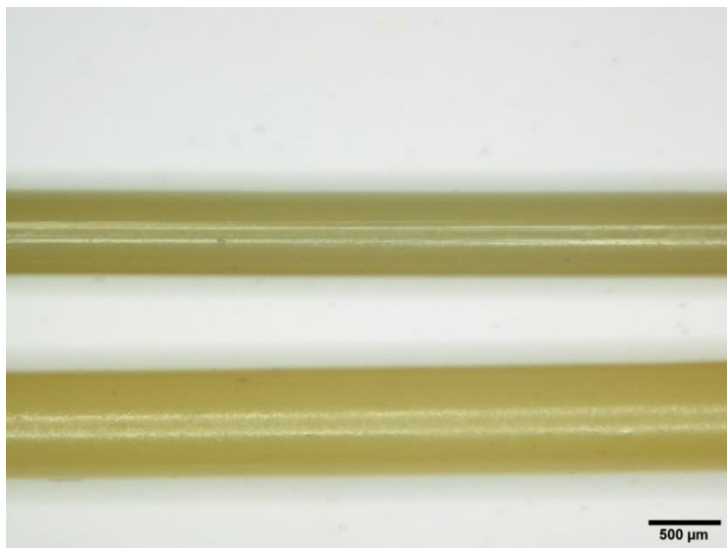


Figure 20: PLGA₅₀₂-MLC (Top) and PLGA₅₀₃-MLC (Bottom) extrudates containing 1.5% minocycline. Both extrudates were extruded with the 600 µm extrusion device. The larger diameter of PLGA₅₀₃-MLC extrudate indicates viscoelastic properties.

Regarding the intended form of application, the first prototypes already united several advantageous properties. Greenstein and Tonetti (114) demonstrated in their work which challenges arose within the gingival sulcus as intended application site. An inflamed dental pocket is at least about 5 mm deep, 3 mm wide and 1 mm thick. The sulcus volume of 15 µl is renewed approximately 40 times per hour. So, the gingival sulcus represents an application site with limited space, a continuous saliva flow, and the likely occurrence of periodic mechanical stress. Consequently, as first step a diameter of < 1 mm should be pursued for a comfortable application. The extrudates meet this requirement and additionally their application does not require any special equipment – a simple tweezer will be sufficient. The achieved drug load of 11.5% is close to the reasonable limit due to the complex composition with magnesium stearate. The overall share of the complex in the extrudate is 41.2%, leaving 58.8% for the release altering polymers. This comparably high drug load and the minor volume within the gingival sulcus enable high local concentrations of the API. Furthermore, diameter and shape of the extrudates are adjustable to the needs of the patient. The use of different diameters – adapted length to the pocket size and the simultaneous application of different diameters (e.g. 600 µm surrounded by 300 µm) - opens up a variety of dosing options and seems highly promising. Also, the release rate can be adjusted by choice of polymer and additional excipients.

4.4 CHARACTERIZATION OF THE FIRST PROTOTYPES

4.4.1 TEXTURE ANALYSIS

The texture analysis confirmed the macroscopically observed limited mechanical resilience of the PLGA-MLC extrudates (Figure 21). Upon penetration, the PLGA₅₀₂-MLC extrudates broke piece by piece, which became apparent by the rise and fall of the required penetration force. Each loss of force could be assigned to a partial breaking, which was occasionally accompanied by splintering of small fragments, especially in case of longer stored samples. Contrary, the PLGA₅₀₃-MLC extrudates broke completely at a penetration depth of 0.14 mm. For both samples a breaking force of 1.5 – 2.0 N was required. The blend of both polymers was also investigated, and displayed a greater mechanical resilience, but did also break like the extrudates of the single polymers. Through the addition of GMS an organoleptic improvement of the mechanical resilience was achieved. These extrudates displayed a higher accessibility to slight bending, but during the texture analysis they broke nevertheless. The reduced breaking force can be attributed to the plasticizing properties of GMS.

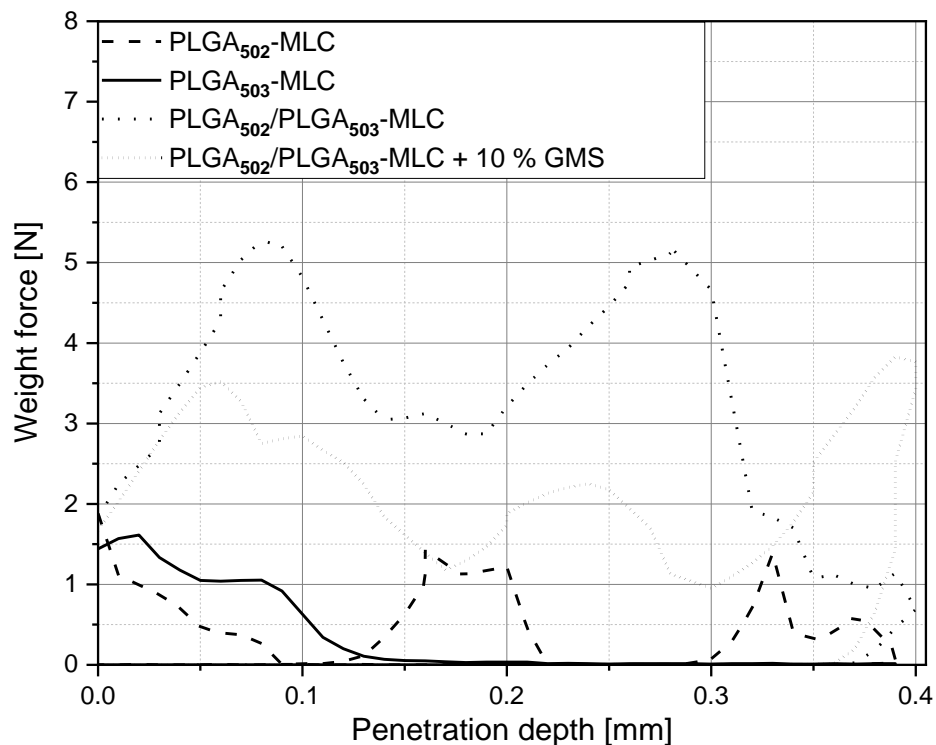


Figure 21: Penetration test: Force-path diagrams of different PLGA-MLC compositions

Concluding, the first prototypes as solid, preformed implants did not fully satisfy the request towards the mechanical properties. But this challenge was handled later on, with the introduction of the second generation prototypes (4.6).

4.4.2 IN VITRO RELEASE

To secure sink conditions during the release experiments, the saturation concentration of the MLC was determined beforehand. Approximately 260 µg/ml minocycline were detected in the supernatant of a saturated MLC suspension in phosphate buffer pH 7.0 after 24 h at room temperature. A differentiation between the MLC and free minocycline was not possible, due to the necessity of an acid in the mobile phase during HPLC and the pH-sensitivity of the MLC (4.2.1). During release from the extrudates, liberation of minocycline, which has a higher saturation concentration (~3 mg/ml) (115), is imaginable. However, even if minocycline would solely be present in form of the complex, 260 µg/ml was sufficient under the given experimental setup to maintain sink conditions.

The *in vitro* release profile of the first prototypes exhibited for all compositions an initially faster release rate, which progressively slowed down during the release period (Figure 22). The pure MLC extrudates displayed the fastest release, but also no burst. After 20 days 60% of the API was released, and from this point no further release was detectable. Nevertheless, the pure MLC was capable of providing a prolonged release up to 20 days. Through the addition of a PLGA polymer the release rate could be modified to a desired level.

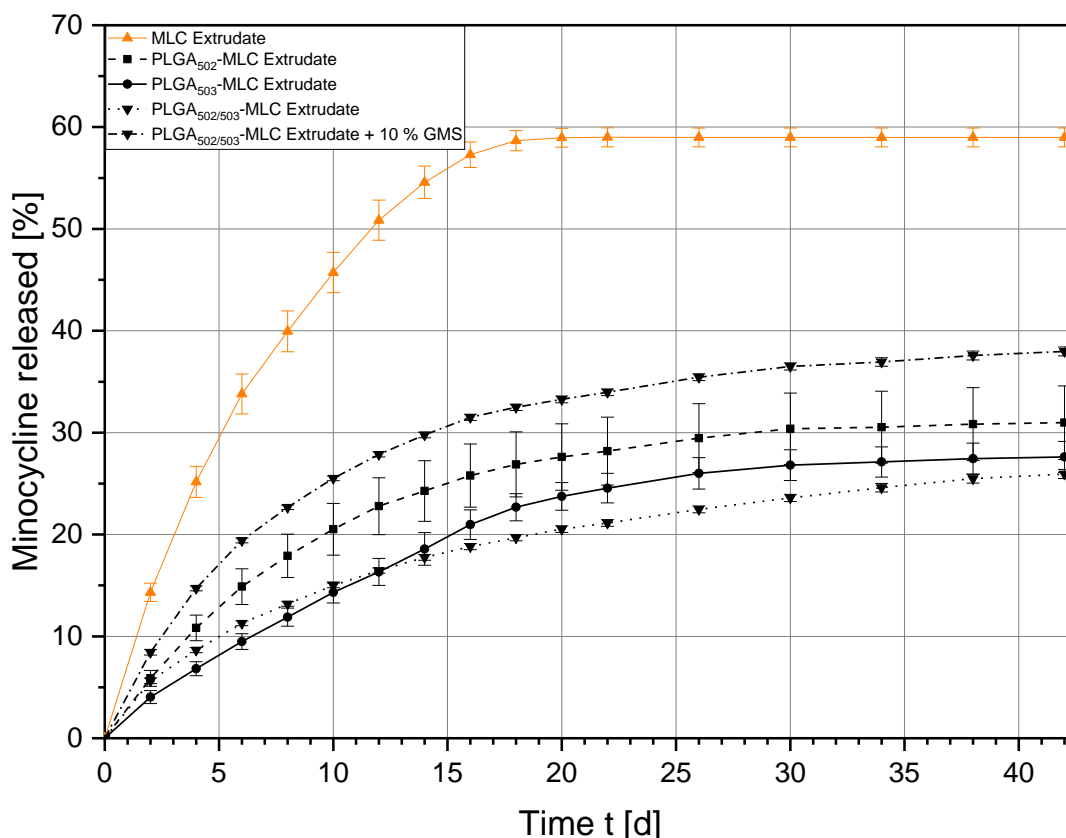


Figure 22: Release profile of several PLGA-MLC extrudates in PBS pH 7.0 at 37 °C

As expected, PLGA₅₀₂ offered a faster release rate compared to PLGA₅₀₃, due to its lower molecular weight (116). This difference was especially dominating within the first two weeks, until their release rates started to align. Remarkable was also the higher standard deviation for PLGA₅₀₂, which can be linked to the lower molecular weight as well. Within the shorter chain PLGA₅₀₂, faster degradation and therefore autocatalysis (87) contribute to more deviating results between the single samples.

For the 1:1 blend of PLGA polymers a release pattern between both curves of the single polymers was expected. Until day 7 these expectations were met, but suddenly the polymer blend fell behind. This sudden drop of the release rate is difficult to explain. Possible explanations can be a batch to batch variation, analytical difficulties or polymer-polymer interactions, which either create a micro-environment that promotes decay of the API, or impedes the release of minocycline. At the end of the release period on day 42, the polymer blend nearly reached the release level of PLGA₅₀₃. Thus, the impact of GMS appeared even greater. The initial purpose of GMS was to act as a softener for extrudates, but the effect was relatively small, even though the stability was enhanced (4.4.1). The greater benefit lay in the significant increase of the release rate. Double the amount was released compared to the batch without GMS within 10 days. From there on, their release rates aligned and no significant difference prevailed.

These in vitro release results demonstrated the controlled release over 42 days, which indicates the high potential of the extrudates as long acting drug delivery system. As described in 1.3, the release period of 6 weeks is desirable, due to the recall-intervals during the periodontal aftercare. So far, this extensive release period was exceptional compared to commercially available systems. At the end of 2019 when these results were published (96), no other local drug delivery system for periodontitis could compete with the extrudates in regards of release duration. A few months later, electrospun membranes loaded with minocycline were introduced by Ma et al. (76), which offer a release over at least 40 days. So, as unique selling points for the extrudates in the direct comparison with these electrospun membranes remain: the significant higher drug load (11.5% : 3%), the increased stability of the API (4.4.3), the absence of toxic solvents (NMP) during the simple and continuous production paired with the easy handling, and their extensive adjustability and effortless application.

However, for all extrudates one observation was striking: with up to 60%, a higher percentage of the API remained undetected during the release experiments. Hence, an investigation of the stability of the MLC in comparison with the pure minocycline was scheduled.

4.4.3 STABILITY STUDIES

The known chemical instability of minocycline in aqueous media led to the assumption, that epimerization, decay and degradation are the cause of the at least 40% undetected API (91,98,117). Thus, the stability of minocycline and the MLC was tested at pH 7.0 and pH 2.3 to clarify the situation of the missing API. The neutral pH reassembles the physiological pH, while the acidic pH imitates conditions, that can occur inside degrading PLGA polymers (118). Even though the elevated temperature of 37 °C promotes degradation processes, this temperature was chosen to simulate the same conditions compared to the *in vitro* release.

Figure 23 illustrates the ongoing decay of minocycline and the MLC depending on the pH value of the medium. Minocycline exhibited extensive degradation at the neutral pH value. Within 3 days the minocycline peak at 4.8 min vanished, while degradation products became noticeable. The vast degradation was also on the macroscopic level unmistakable, due to a color change from yellow to pure black. The MLC however, was capable to protect minocycline up to a certain degree. After three weeks the minocycline peak was still visible, while the peaks of the decomposition products grew progressively. The reduced water solubility of the lipid complex increased drug stability in aqueous surrounding. Additionally, as the incubation period progressed, more parts of the MLC dissolved and became detectable. This can also be noticed in the chromatogram on day 2, where a rise of the minocycline peak was observable. Hence, the onset of a chemical equilibrium between dissolved MLC, which was subject of decay, and not yet dissolved MLC is possible.

In contrast, acidic conditions ensured a longer lifetime of the API. This circumstance was also described by Jain et al. (119) for minocycline. Hence, a less drastic decay was observable for minocycline compared to the neutral pH conditions. The same statement is valid for the MLC, while here an additional dissolution of the MLC over the release period was anew noticeable. From this point on, minocycline and the MLC experienced a similar degree of degradation. As previously demonstrated (4.2.1), minocycline is released from the complex at acidic conditions. Therefore, similar chromatograms and degradation rates were observable.

In summary, the MLC protected the API at neutral pH-values. Nevertheless, minocycline cannot be guarded absolutely from decomposition. Thus, a considerable part of the API decays and cannot be detected during the quantification. A residue analysis performed at the end of the release experiment revealed 10 to 15% of the API

remained within the extrudates. So, it is likely that up to 40% of the API falls victim to decay within the release period.

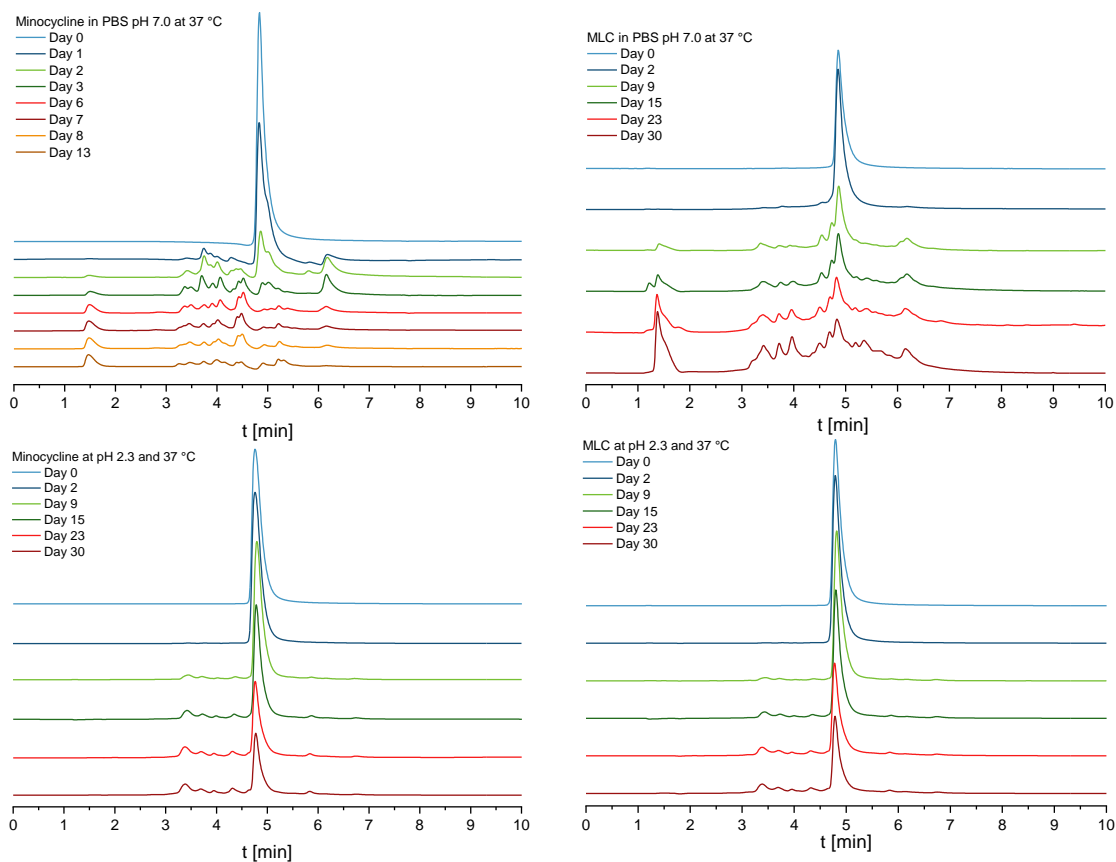


Figure 23: Chromatograms of minocycline and the minocycline lipid complex at pH 7.1 and pH 2.3 at 37 °C

4.4.4 MULTISPECTRAL FLUORESCENCE IMAGING MONITORED WATER PENETRATION

The fluorescence imaging was carried out as an additional experiment, to evaluate the capability of Nile red to monitor these drug delivery systems, and to get an insight on the micropolarity of these systems during incubation. An incubation pH of 6.0, deviating from the *in vitro* release, was chosen for these experiments. The pH within the dental sulcus can vary depending on the dominating bacteria species in combination with the persisting inflammation (120). With this premise, the water penetration experiment was started.

The emission maximum of Nile red depends on the polarity of its environment. In apolar solvents the maxima are around 600 nm but they experience a bathochromic shift in a polar surrounding (121). This shift is similar to the eluotropic series of solvents, while the fluorescence quenches in water. Hence, Nile red can monitor water induced changes in such drug delivery systems (Figure 24).

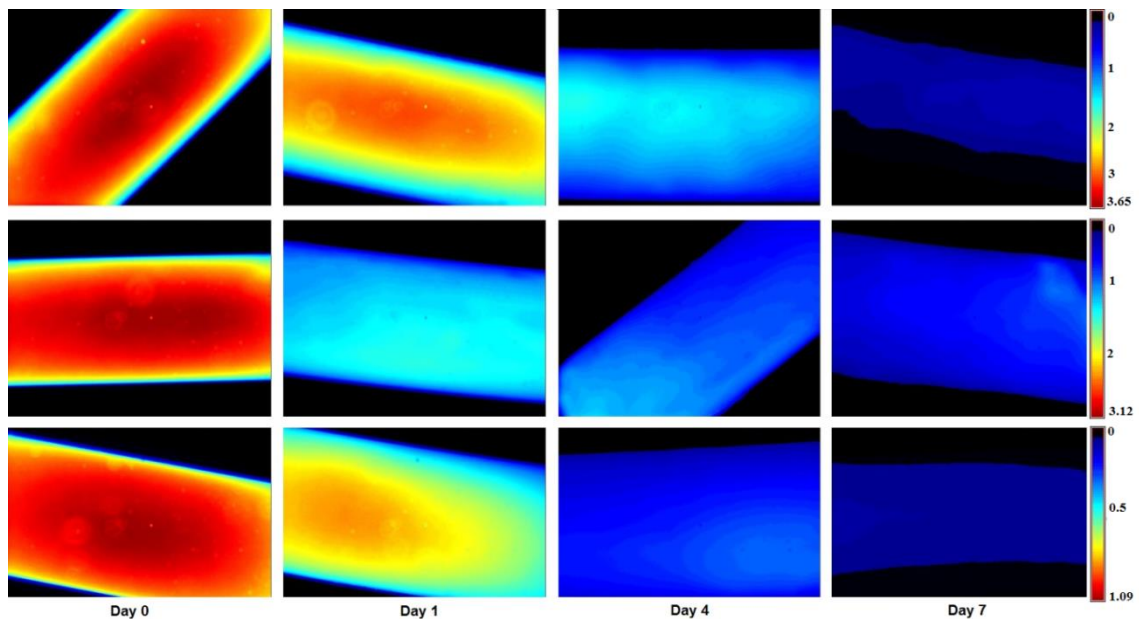


Figure 24: PLGA-MLC extrudates marked with Nile red (NR) in PBS pH 6.0 over time. Top: PLGA₅₀₂-MLC extrudates (100 µg/g NR); Middle: PLGA₅₀₃-MLC extrudates (100 µg/g NR); Bottom: PLGA₅₀₃-MLC extrudates (10µg/g NR); (Display key: Scale Factor : 1, presenting scaled counts/s pixel)

Water diffused from the outer shell, and reduced the fluorescence signal on its way. On day 4, the signal from the inner core started to vanish, while on day 7 the outer domains faded completely. This can also be extracted from Figure 25. The average fluorescence intensity of the PLGA₅₀₂-MLC extrudate decreased constantly with a moderate deviation, hitting a residual level at day 7. Equally loaded PLGA₅₀₃-MLC extrudates exhibited an initially greater deviation, but a comparable drop of signal intensity. For these extrudates, a paradoxical increase of fluorescence intensity above 100% had been observed on day 1 after incubation. Despite the small sample size of $n=3$, it is likely that this circumstance derived from quenching effects. Higher fluorophore concentrations can lead to a self-quenching, for instance through aggregation or energy transfers to non-fluorescent dimers (122,123). Hence, high fluorophore concentrations do not always correlate with high fluorescence intensities. So, it can be assumed that Nile red had a higher solubility within these extrudates, which led to self-quenching. With the following intrusion of water, the Nile red concentration sunk to concentration levels that enabled a higher fluorescence intensity again.

Reviewed from the retrospective, the choice of the same pH as it was chosen during the *in vitro* release experiments, would have been wiser to assess the situation within these extrudates at these conditions more precisely. Nevertheless, it can be concluded, that Nile red is capable of monitoring the microenvironment of these drug delivery systems. Within 6 to 8 days the matrix had been permeated with water. Not detectable diffusion processes contribute to a deviation between the monitored situation and the

actual status within the extrudates at a given time point. However, the existence of a consistent base level of fluorescence beginning around day 7 indicates the change to a more polar environment within this period, and contributes additional information for the *in vitro* release pattern. Around day 7 the release rates of the extrudates started to slowly drop down, which may be linked to then completed water permeation and the onset of an equilibrium state of diffusion.

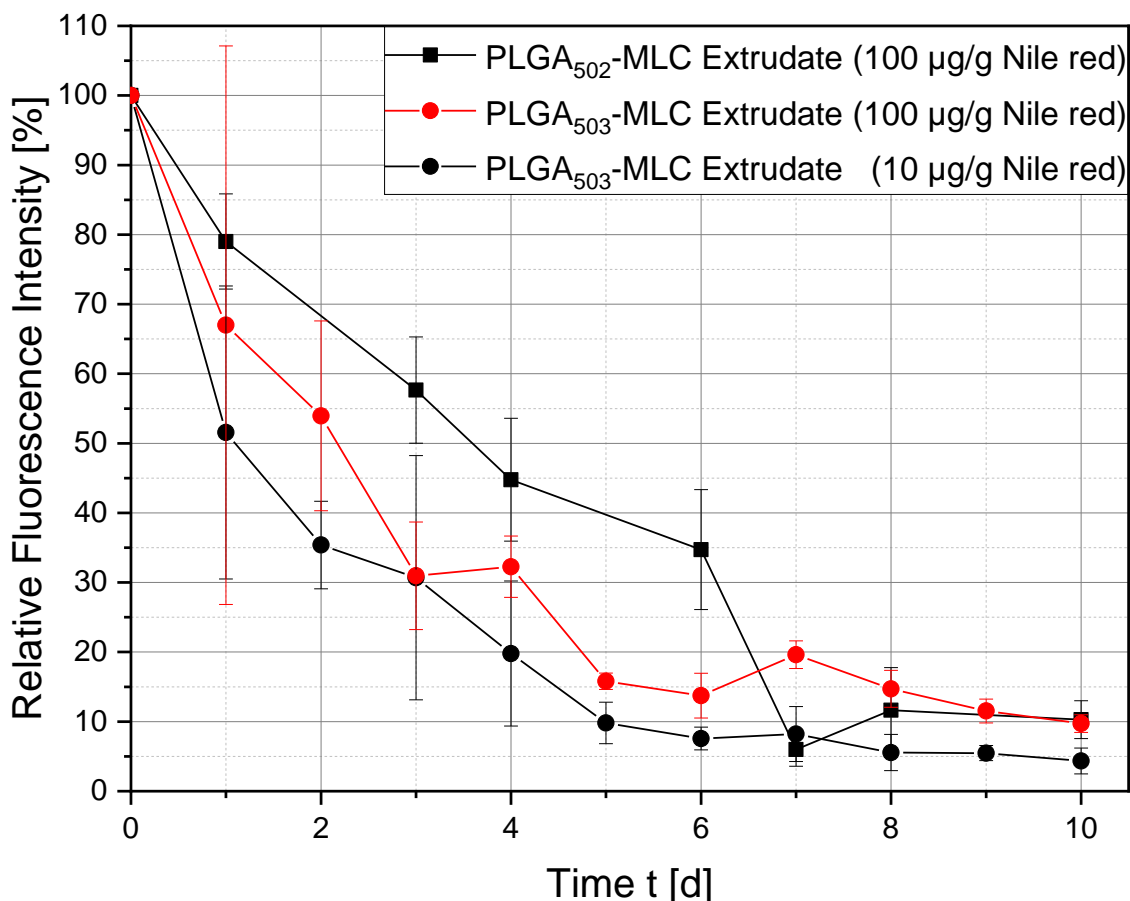


Figure 25: Relative fluorescence intensity change of PLGA-MLC extrudates marked with Nile red

4.5 ANTIMICROBIAL *IN VITRO* PERFORMANCE OF THE FIRST PROTOTYPES

The presented results of this section were gathered within the laboratory of Prof. Dr. Sigrun Eick of the University of Bern during the collaborative work on this project. Also, these results are subject of a peer reviewed publication (92).

4.5.1 ANTIMICROBIAL PERFORMANCE AGAINST PLANKTONIC BACTERIA

The results of the MIC testing are illustrated in Table 12. The performance of the PLGA-MLC extrudates fell slightly behind the competing system. With a MIC of 1-2 µg/ml against *S. gordonii* they were one to two dilution steps behind the pure minocycline, but still within a comparable range. The Arestin® microspheres were as active as the pure drug. As expected, the unloaded placebo-extrudate did not demonstrate any antibiotic activity.

A possible explanation for the moderately lower anti-bacterial activity within this MIC-test can be found within the nature of the MLC. The solubility in water (approximately 260 µg/ml) is relatively poor, and can take additional time, compared to the pure API. Furthermore, the MLC could have adhered to the matrix, despite the careful and thorough dispersion of the formulation.

Table 12: Minimal inhibitory concentrations of tested minocycline formulations in µg/ml

	S. gordonii ATCC 10558	P. gingivalis ATCC 33277
Minocycline	0.5 µg/ml	0.25 µg/ml
Arestin® microspheres	0.5 µg/ml	0.25 µg/ml
PLGA₅₀₂-MLC Extrudate	1 µg/ml	0.25 µg/ml
PLGA₅₀₃-MLC Extrudate	2 µg/ml	0.5 µg/ml
PLGA₅₀₂-Placebo Extrudate	No inhibition	No inhibition

4.5.2 ANTIMICROBIAL ACTIVITY ON THE FORMATION OF BIOFILMS

An inhibition of the formation of biofilms was clearly observable for all experimental formulations and for the positive control (Figure 26). Concerning the count of cfu, the pure minocycline with a reduction of 2.1 Log₁₀ steps after 6 h and 3.6 Log₁₀ steps after 24 h, demonstrated again the highest activity. Within the 6 h period, the extrudates were 1 Log₁₀ step ahead of the microspheres, but within the 24 h time frame the microspheres were capable of keeping the cfu on a lower level. Between both tested PLGA extrudates no significant difference was perceptible in this experimental setup. So, the results from the MIC-testing were confirmed. Interestingly, the PLGA-placebo extrudate could reduce the cfu-count by 0.6 Log₁₀ steps within 24 h compared to the control. Therefore, a minor antibiotic activity of the placebo extrudate consisting of PLGA₅₀₂ and magnesium stearate can be stated.

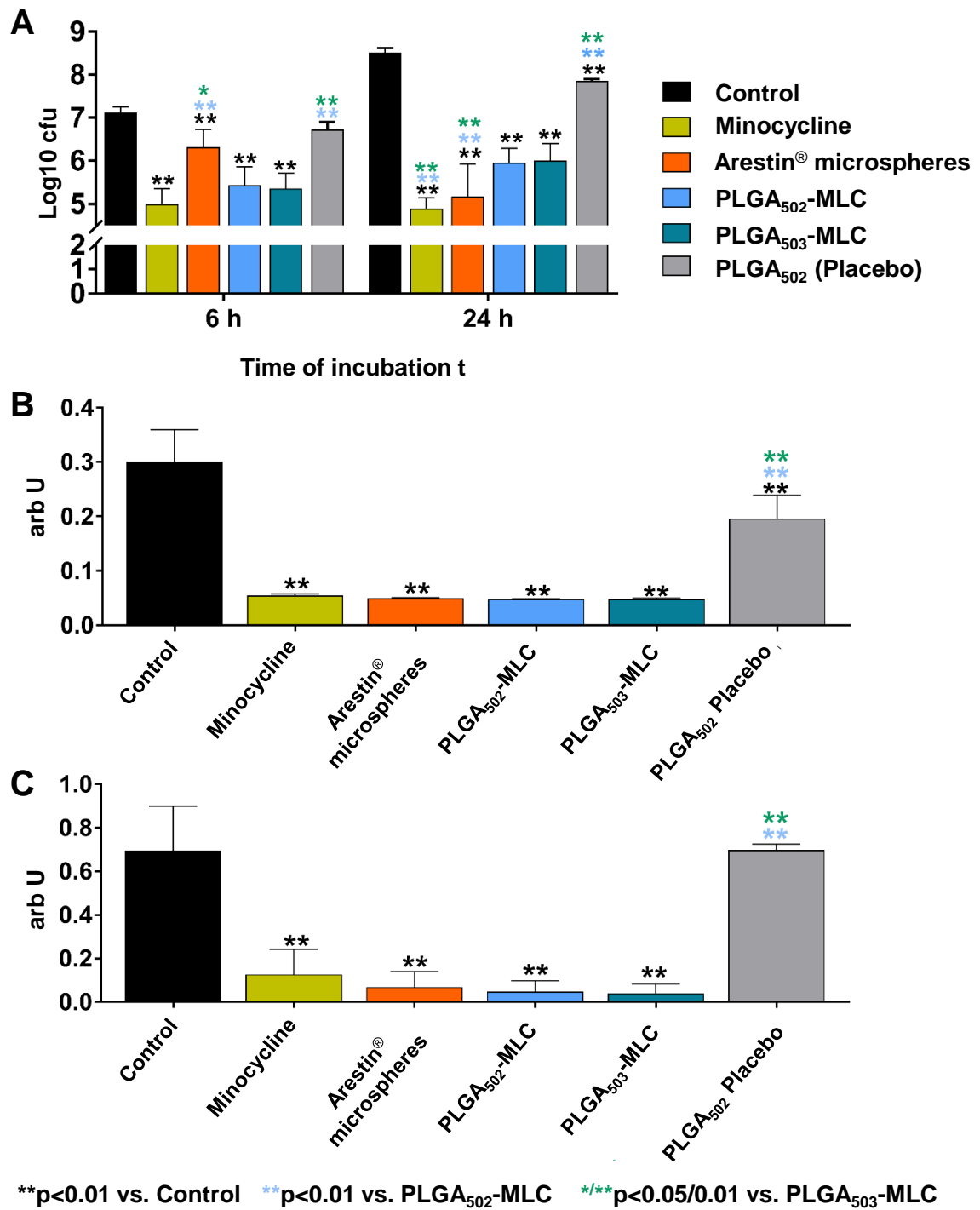


Figure 26: Activity of different minocycline containing formulations on the formation of a six-species biofilm; A - Bacterial counts determined as colony forming units (cfu); B - Biofilm quantity C - Metabolic Activity

Regarding the formation of the six species biofilm, the test formulations all demonstrated a relatively even biofilm quantity reduction of approximately 85% to a total of one sixth of the control. Again, the drug-free extrudate matrix also provided an unexpected, slight antibacterial effect. They diminished the biofilm quantity by one third.

The metabolic activity essentially correlated with its quantity. The PLGA-MLC extrudates and the microspheres effectively cut the activity down by 85 to 90%. A minimal trend in favor of the PLGA-MLC extrudates is noticeable within Figure 26 (C), but the observed effects are not strong enough to declare them as a significant difference. Contrary to both other examined parameters, the placebo extrudates did not have an effect on the metabolic activity.

4.5.3 ANTIMICROBIAL ACTIVITY ON PREFORMED BIOFILMS

Against a preformed biofilm, the tested formulations were capable to diminish the number of cfu as well. Figure 27 illustrates the activity of the different formulations with varying concentrations on a biofilm formed over 3.5 days. As expected, a dependency between the concentration and the reduction of cfu did occur. A reduction of 2.4 to 3.7 Log₁₀ steps was observable, with a stronger inhibition for the higher concentrations. So, the influence on the cfu count was in range of the non-preformed biofilms. Between the extrudates and the microspheres no significant difference was noticeable. In contrast to the prior experiment, the PLGA-placebo extrudate did not have an effect on the cfu count.

Concerning the quantity of the preformed biofilms, there was unfortunately no effect observable for either of the tested formulations. Hence, the PLGA-placebo did also not demonstrate any reduction.

Even though there was no effect on the established biofilm quantity, there was a clear influence on the metabolic activity. All minocycline containing formulations were able to reduce the activity by approximately 75%. Neither the microspheres, nor the extrudates could demonstrate superiority to their competitor. The unloaded extrudates did not decrease the metabolic activity.

Thus, none of the formulations possesses an advantage on the activity against the formation of biofilms. They were all capable to reduce the cfu count, inhibit the formation of new biofilms and they were able to interfere with the metabolic activity of new and established biofilms. But they lacked one crucial property. The activity on preformed biofilms was poor, despite the application of high concentrations way above the MIC. Roy et al. (124) also demonstrated that antibiotics alone do not satisfactorily eradicate bacteria within a biofilm. Thus, these results confirm the established procedure of periodontitis treatment, whereas local antibiotic drug delivery systems are potent as an adjunct, but do not suffice as a single treatment (125).

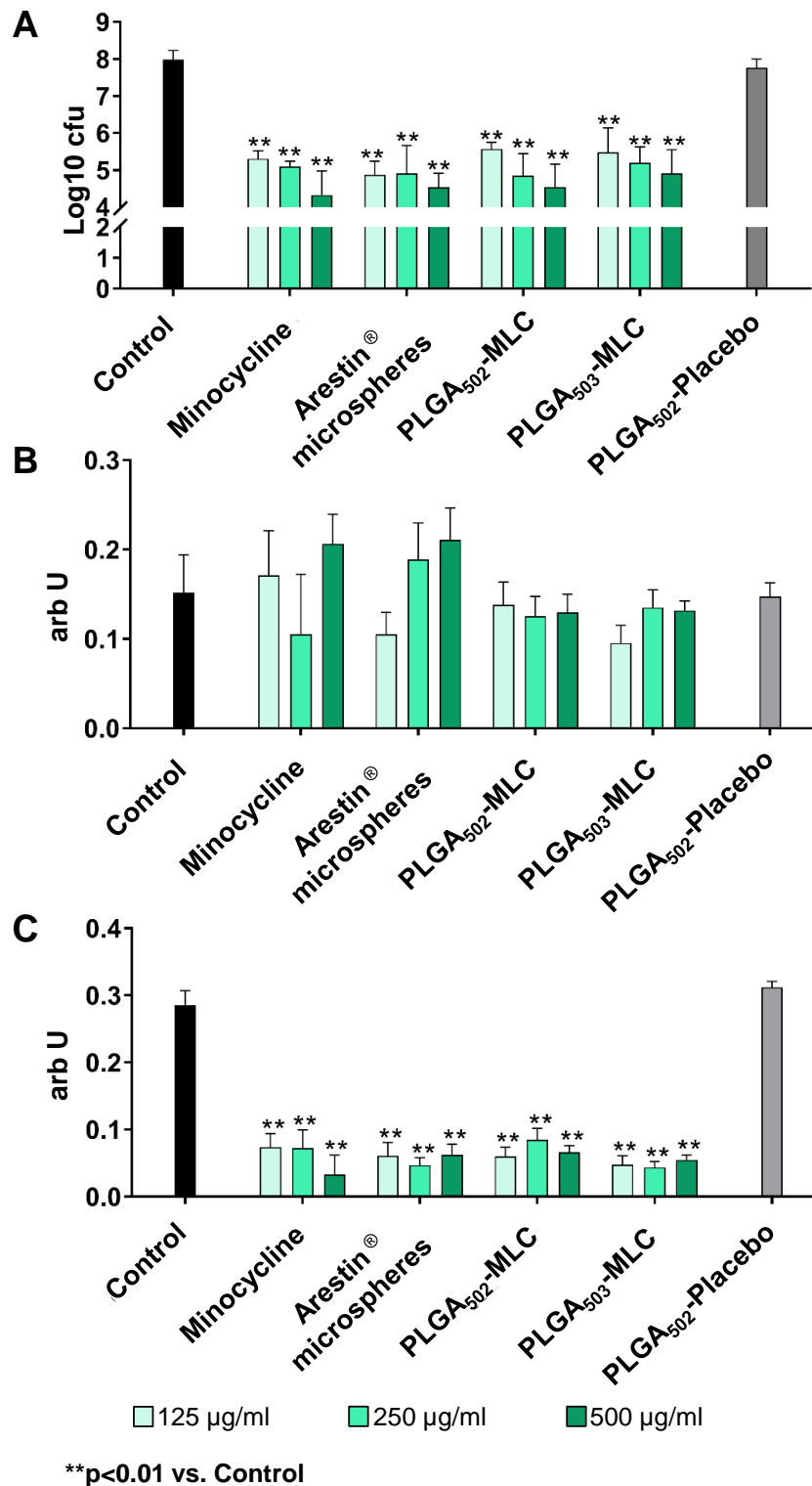


Figure 27: Activity of different minocycline containing formulations on a six-species biofilm formed over 3.5 days; A – Bacterial counts determined as colony forming units (cfu); B – Biofilm quantity; C – Metabolic activity

4.5.4 ANTIMICROBIAL ACTIVITY OF ELUATES OBTAINED FROM THE GINGIVAL FLOW SIMULATION

In vitro drug release experiments are often carried out in constant volumes, which may be exchanged during the observed release period. This is also valid for the simulation

of periodontal applications (126,127) (3.4.4). The aim of this experiment was to create conditions, which are closer to the clinical situation within the gingival pocket, through the simulation of the gingival crevicular flow (CGF). The initial volume of 23.5 μ l was chosen to resemble the volume within a corrupted gingival pocket, and subsequently the exchanged volumes were decreased, due to the reduction of CGF during periodontal therapy (55). In view of the protein composition of the crevicular fluid, a resemblance to diluted serum can be discussed (128). Hence, a buffered saline solution paired with serum albumin was chosen as medium, and the obtained eluates were investigated towards their antimicrobial activity up to 42 days (Figure 28).

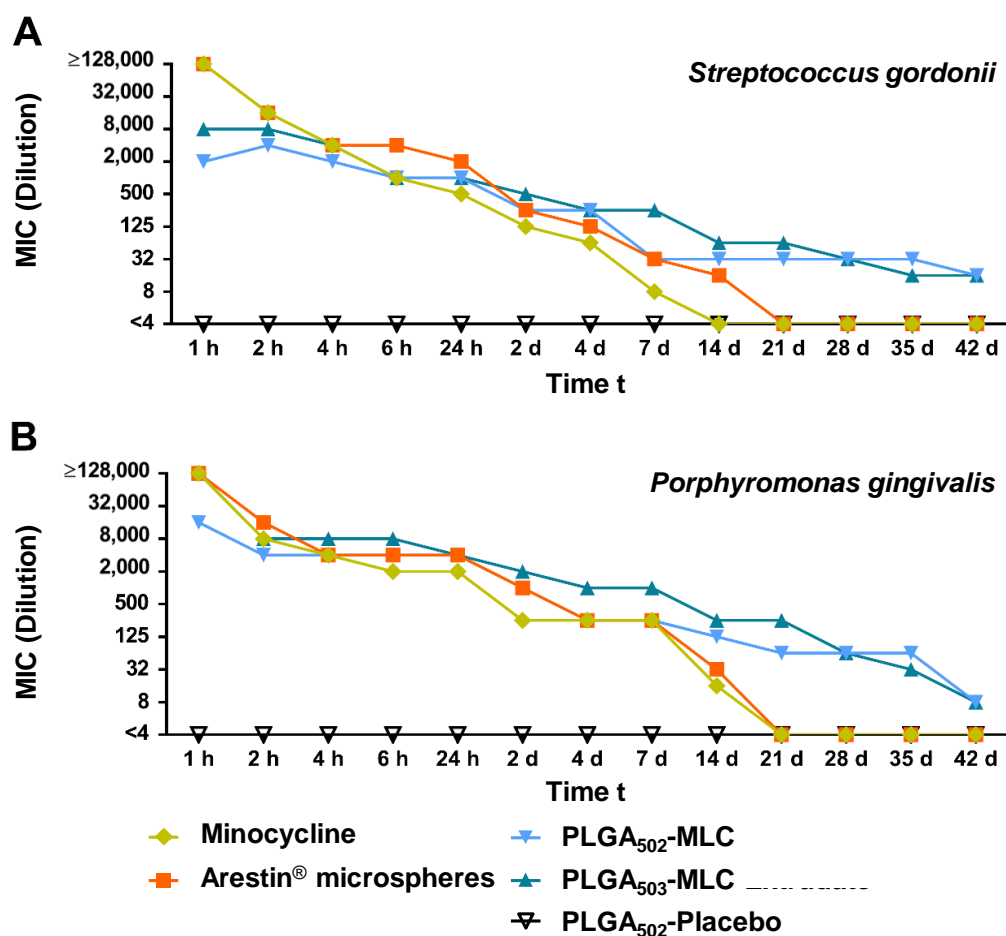


Figure 28: Minimal inhibitory concentrations (maximum dilution) of the eluates of PLGA-MLC formulations obtained over 42 days during simulation of the gingival fluid flow on *S. gordonii* ATCC 10558 (A) and *P. gingivalis* ATCC 33277 (B); PLGA-MLC formulation

As indicated by the prior experiments, all minocycline containing formulations possessed antimicrobial activity against *S. gordonii* ATC 10558 and *P. gingivalis* ATC33277 in the initial phase of the testing. In the beginning, the Arestin® microspheres demonstrated an especially high activity just like the pure substance with active concentrations above 16 mg/ml (Table 13). As expected, the activity decreased during the release period. Especially within the first 24 h a vast reduction was

detectable into the $\mu\text{g/ml}$ concentration range. Within 21 days the activity of the pure API vanquished. During the first three weeks, the microspheres demonstrated a higher activity compared to the pure substance on a near level to the PLGA-MLC extrudates. But they were not able to extend the release beyond this period.

In contrast, the PLGA-MLC extrudates started off with initial lower active concentrations around 2 – 8 mg/ml, except for the placebo extrudates, which were not able to inhibit bacterial growth at any time point. From $t = 24$ h until day 7 their activity decrease was almost equal to the Arestin[®] microspheres, with a slightly higher activity of the PLGA₅₀₃-MLC extrudates. The decisive difference between both systems is that the activity of the extrudates did not end after 21, but after 42 days. Active concentrations of 4 $\mu\text{g/ml}$ were observed at the end of the experiment. Hence, they offered a controlled release with an up to twice the duration compared to the commercial drug delivery system. So, these results align with the findings of the *in vitro* testing from 4.4.2.

Table 13: Calculated concentrations of minocycline ($\mu\text{g/ml}$) containing formulations presented in Figure 28; Calculation based on maximum dilution multiplied with the respective MIC

	Minocycline	Arestin[®]	PLGA₅₀₂-MLC	PLGA₅₀₃-MLC
1 h	>16000	>16000	2000	8000
2 h	4000	4000	1000	2000
4 h	1000	1000	1000	2000
24 h	250	1000	500	1000
2 d	62.5	125	125	250
7 d	31.3	31.3	31.3	125
14 d	<2	8	15.6	31.3
21 d	<1	<1	15.6	31.3
28 d	<1	<1	15.6	15.6
35 d	<1	<1	15.6	8
42 d	<1	<1	4	4

Also, eluates of defined time points were anew tested towards their activity on the formation of biofilms (Figure 29). At day 1 all test formulations were capable of reducing the cfu count by 2 Log₁₀ steps. This situation remained mainly unchanged for the first week. After two weeks however, only the microspheres and the PLGA-MLC compositions could maintain a reduction of more than 1 Log₁₀ step. At day 28, only the eluates of PLGA₅₀₃-MLC were capable of diminishing the cfu count with a reduction of 1.9 log steps. Also noteworthy is the antibacterial effect of the eluates obtained from

the placebo extrudate. On day 14 and 21 they reduced the cfu count by 1.4 Log₁₀ and 1.1 Log₁₀ steps, and therefore mirror the results from 4.5.2.

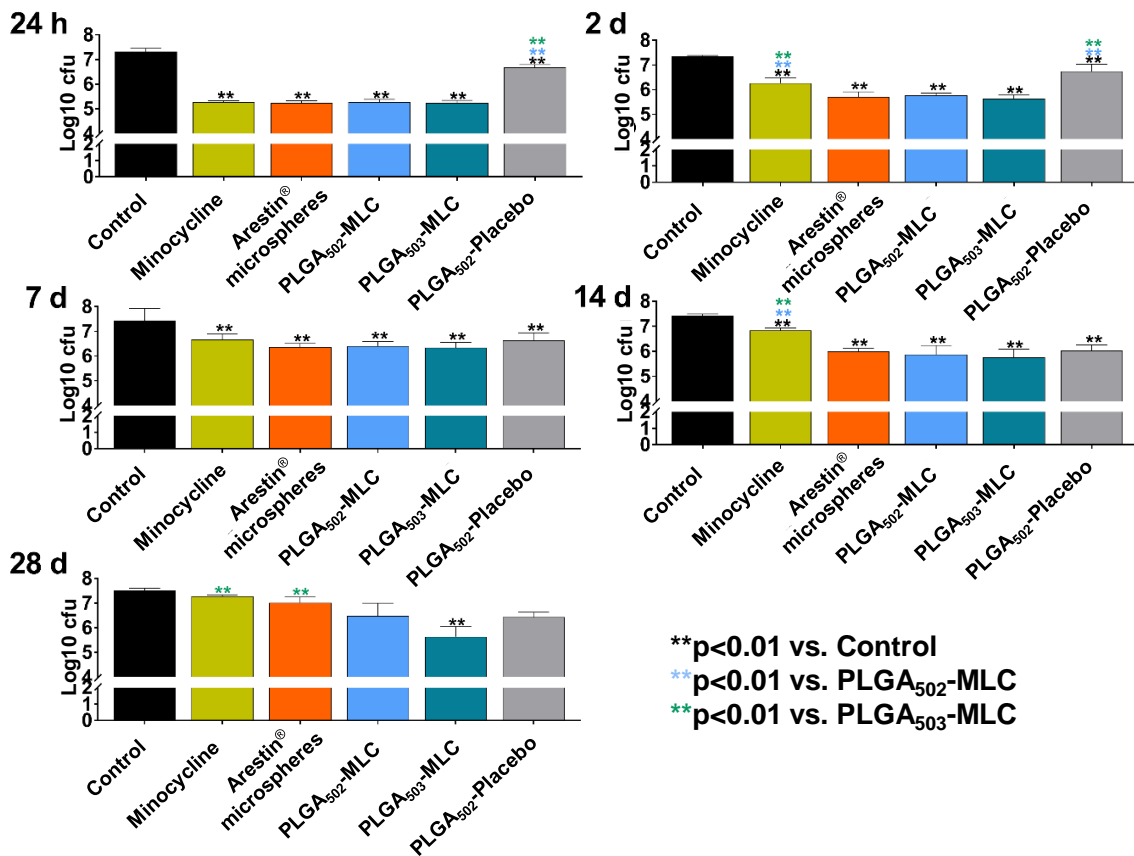


Figure 29: Antimicrobial activity of the eluates obtained during the gingival fluid flow simulation against the formation of biofilms at different time points (cfu count after 6 h)

Local drug delivery systems can achieve high concentrations in the gingival sulcus, and therefore unfold strong effects. Non-biodegradable tetracycline fibers (Actisite®) accomplished concentrations above 1000 µg/ml over a few days (129). Also, doxycycline *in situ* forming depots were capable of realizing local concentrations of 1000 µg/ml within the first two hours of application (130). Depending on the drug load of either 8.5% or 14%, the concentration lowered to 8 µg/ml or respectively to 19 µg/ml after 12 days. Contrary, an oral administration of tetracycline analogues was found to result in gingival crevicular concentrations below 1 µg/ml in approximately 50% of the cases (131). This underlines again the significance of local drug delivery also for periodontitis treatment. Hence, the achieved concentration levels of the tested extrudates are in range of tetracycline derivative containing systems described in the literature. But it has to be considered, that the results described in the literature were observed *in vivo*, and the acquired data about the extrudates represents *in vitro* data, so far.

Despite the positive findings on the performance of the extrudates during this experiment, this *in vitro*-assay has limitations, which need to be labeled. The simulation of the GCF effectively mimics the clinical situation with a limited release medium and varying flow rates. But active transport processes into epithelial cells (132), uptake by fibroblasts (133) and immunologic active cells cannot be depicted. Nevertheless, through the simultaneous examination of approved systems like Arestin[®], data can be extracted for evaluating the suitability for clinical applications. Thus, the observed long lasting and high antimicrobial activity suggest promising potential for the transfer of the extrudates to *in vivo* applications.

Regarding both tested extrudates in comparison to each other, the eluates of PLGA₅₀₃-MLC prototypes possessed a higher inhibitory effect on the bacterial growth as well as on the formation of biofilms. Their higher molecular weight presumes a theoretically slower release rate compared to PLGA₅₀₂, as described in 4.4.2. Thus, a higher antimicrobial activity of PLGA₅₀₃-MLC stands in contrast to the results of the *in vitro* release at first sight. But section 4.4.2 covers extrudates with a defined length, and therefore varying masses depending on the diameter, which was not equal, due to the viscoelastic properties of PLGA₅₀₃. Also, their relative release rate was defined as % [m/m] minocycline, as illustrated in Figure 22 (page 45). During the simulation of the CGF however, all samples were weighed equally to 1 mg minocycline content. Hence, the larger diameter and therefore larger surface of the sample probably had an impact on the initial faster release. For instance, an extrudate with a diameter of 600 µm and a length of 400 µm possesses a surface of 1.319 mm² and a volume of 0.113 mm³. Under the assumption of an equal density, an extrudate with the same volume and a diameter of 800 µm then offers a surface of 1.571 mm². Even though the extrudates are micronized within this assay, the inner surface of these samples could be larger as well. Thus, this circumstance could have contributed to the release of higher API amounts.

Also noteworthy is the observed inhibition of the placebo extrudate on the formation of new biofilms, during the direct contact as well as for the eluates. The composition of the extrudate matrix, consisting of PLGA and magnesium stearate, does not suggest such an interior activity. PLGA served as release controlling matrix for several local antibiotic drug delivery systems for dental applications (69,134). Still, an antimicrobial activity of PLGA had not been described so far (69,135). This is also confirmed by the report of unloaded PLGA-nanoparticles, which were not able to inhibit the formation of biofilms of *Pseudomonas aeruginosa* (135,136). Hence, a connection between magnesium and the disturbed biofilm formations can be discussed. As implant material,

magnesium demonstrated encouraging results with antibacterial activity against planktonic *Staphylococcus epidermidis*, *Staphylococcus aureus*, and *Escherichia coli*, and also suppressed biofilm formation of the mentioned species (137). Also, magnesium oxide nanoparticles had a strong antimicrobial effect on *Escherichia coli*, *Pseudomonas aeruginosa* and *Candida ssp.* (138).

In conclusion, the PLGA-MLC extrudates exhibited suitable antimicrobial properties to serve as a serious alternative to commonly applied systems, especially the PLGA₅₀₃-MLC extrudates. With the stabilized API incorporated in an easily applicable application form, which efficiently acts over a prolonged time period, first successes could be recorded. But for these extrudates adjustments were still necessary. Their reproducible manufacturing and their mechanical properties were not yet adequate enough. Therefore, further development was necessary, and the second generation was introduced, as described below.

4.6 SECOND GENERATION PROTOTYPES

The content of chapter 4.6 and 4.7 are subject of a peer reviewed article (139).

The main purpose for the second generation extrudates was to implement flexibility as well as a higher initial release rate for a comprehensive reduction of the bacterial load at the application side. Therefore, PEG 1500 was explored as a possible plasticizer, PEG-PLGA was considered as an alternative to PLGA. PEG has already been in use for hot melt applications (140) and was part of comparable systems (141). In addition, compatibility between both components seemed likely, due to the intrinsic PEG compound of PEG-PLGA, which could also positively affect the flexibility. A further potential advantage of PEG-PLGA compared to PLGA is the avoidance of low pH-values, polymer autocatalysis and a more linear polymer degradation profile (142). A possible disadvantage is, however, a much faster drug release for small molecules through hydrated PEG nanodomains of the polymer matrix. It was therefore the aim to maintain the long period of controlled release, but to optimize the flexibility. Hence, two PEG-PLGA polymers were investigated: Expansorb DLG 50 – 6P and – 7P. From here on referred to as PEG-PLGA_{6P} and PEG-PLGA_{7P}.

Also, different diameters should be explored. The 600 µm extrudates can be regarded as preformed implants, which can be placed as single or multiple units. In contrast, smaller diameters are expected to yield extrudates with the properties of a filament, which might offer more adjustability with regard to varying dental pocket sizes and geometries. However, smaller diameters are anticipated to be more challenging to

produce and exhibit faster release rates. Hence, we studied the impact of the composition and the reduction of the extrudate diameter to 300 μm on the mechanical properties and drug release rates.

In addition, the characterization was extended with the application of DSC analysis and X-ray powder diffraction. Also, an alternative and more sensitive HPLC- tandem-MS method was developed and applied for the release kinetics.

4.6.1 CRYOMILLING AND HOT-MELT EXTRUSION WITH PEG-PLGA

The process parameters for the extrusion were mostly similar to the extrusion with regular PLGA. Only minor adjustments to the required temperatures were necessary, and empirically applied as listed in 3.3.2.

With PEG-PLGA_{6P} the production was equally successful, like the prior attempts with non-PEGylated PLGA₅₀₂ or PLGA₅₀₃. The inclusion of PEG 1500 however, led to a stronger adhesion of the polymer melt to the extruder matrix during the extrusion. Hence, a slightly minor product yield was the consequence. The extrudates containing 10% PEG seemed the most promising prototypes with regard to their mechanical properties. Therefore, this composition also served as basis for extrudates with a diameter of 300 μm .

As mentioned beforehand, the smaller diameters were expected to be more difficult to produce, and they met this expectation. An indicator therefore was the rise of the temperature within the extrusion chamber during extrusion. The detected temperature rose from the applied 49 °C and 52 °C to 55 °C and 58 °C in the heating zones 2 and 3, during the filling phase, and remained on this level during extrusion.

Unfortunately, the extrusion with PEG-PLGA_{7P} resulted in brittle extrudates with an inhomogeneous appearance (Figure 30). A possible explanation therefore may be found in the different molar weights of the used polymers. PLGA₅₀₂ and PLGA₅₀₃ displayed an adequate compatibility and their molar weight ranged from 7 to 38 kDa (116), as well as PEG-PLGA_{6P} with 30 to 60 kDa (143). PEG-PLGA_{7P} exceeds these weight ranges with 60 to 85 kDa. So, the insufficient compatibility of the MLC and PEG-PLGA_{7P} possibly originated therefrom. Due to this circumstance, the PEG-PLGA_{7P}-MLC extrudates were excluded from the texture analysis.

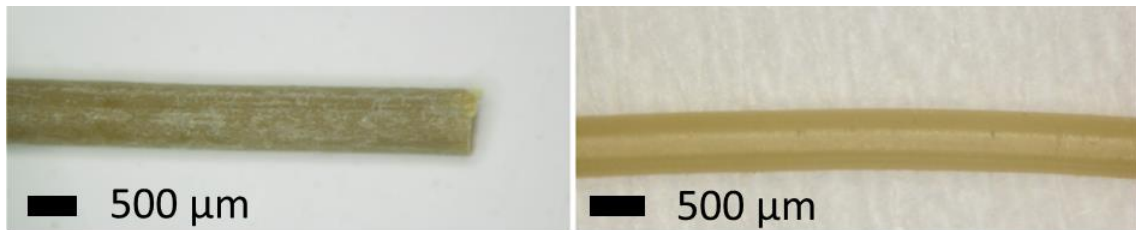


Figure 30: Microscopic view of PEG-PLGA_{7P}-MLC extrudate (left) and PEG-PLGA_{6P}-MLC extrudate containing 10% PEG 1500 (right) extruded with a 600 µm die

4.7 CHARACTERIZATION OF THE SECOND GENERATION PROTOTYPES

4.7.1 TEXTURE ANALYSIS

Similar to the previously presented data in 4.4.1, weight force – penetration depth diagrams were recorded. In comparison to the PLGA polymers, the PEG-PLGA polymers behaved quite differently (Figure 31).

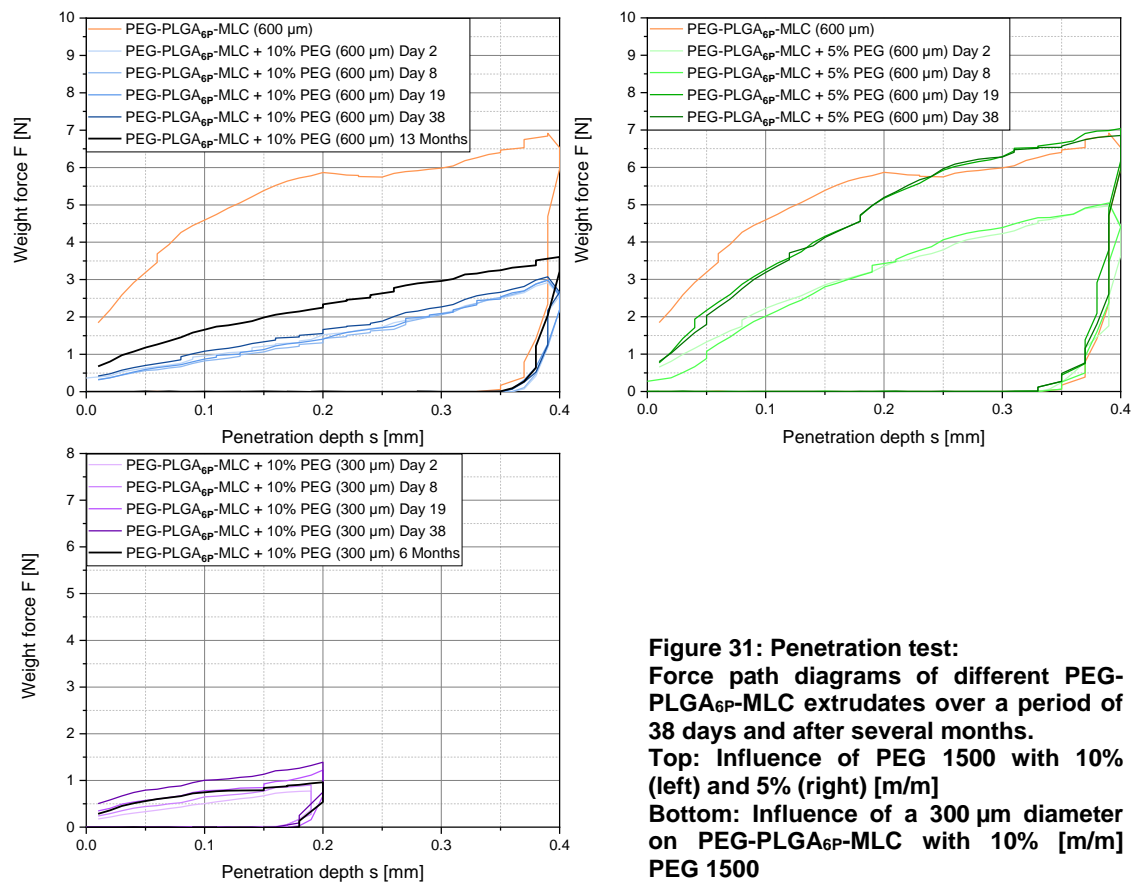


Figure 31: Penetration test: Force path diagrams of different PEG-PLGA_{6P}-MLC extrudates over a period of 38 days and after several months. Top: Influence of PEG 1500 with 10% (left) and 5% (right) [m/m] Bottom: Influence of a 300 µm diameter on PEG-PLGA_{6P}-MLC with 10% PEG 1500

For all samples, a continuous acceleration of penetration force depending on the penetration depth was observable. The absence of a force drop and the force values of 0 N during the withdrawal movement of the probe demonstrated a plastic

deformation without fracturing. For the pure PEG-PLGA_{6P}-MLC extrudates a final force of 6 to 7 N was measured. This force could be reduced through the addition of PEG 1500 as plasticizer. A content of 5% PEG ended up with 5 N as maximal force, but within three weeks these extrudates hardened and behaved quite similar to the pure PEG-PLGA_{6P}-MLC extrudate. The 10% PEG containing extrudates kept their flexible properties even after a longer storage period while reducing the peak force to 3 N. Within a year these extrudates became harder, but nevertheless they remained flexible. Only a slight force increase was observable within 13 months, while stored at 2 to 8 °C in an opaque falcon tube. The reduction of the diameter had a minor effect on the mechanical properties. Initially, a slightly lower force was required to penetrate the 300 µm extrudates compared to their 600 µm counterparts. During the investigated storage period these penetration forces remained similar, even after 6 months.

The ductility test also gave interesting insights towards the mechanical properties and corresponded with the penetration experiment (Figure 32). The pure PEG-PLGA_{6P}-MLC extrudates confirmed their high mechanical resilience with 7 N peak force, which were necessary, to pull the extrudate apart. Unfortunately, the low flexibility permitted a stretching of only 0.4 mm. A content of 5% PEG led to a flexibility enhancement, but could not extend the stretch distance. The tear force was also reduced to 4.5 N. 10% PEG content however, resulted in a clearly different behavior. At 0.3 mm the force remained constant at 1.5 N until these extrudates finally teared at around 9 mm. The 300 µm extrudates with a PEG content of 10% behaved similar. They also reached a stretching distance of almost 9 mm, while the necessary force was reduced to 0.25 N.

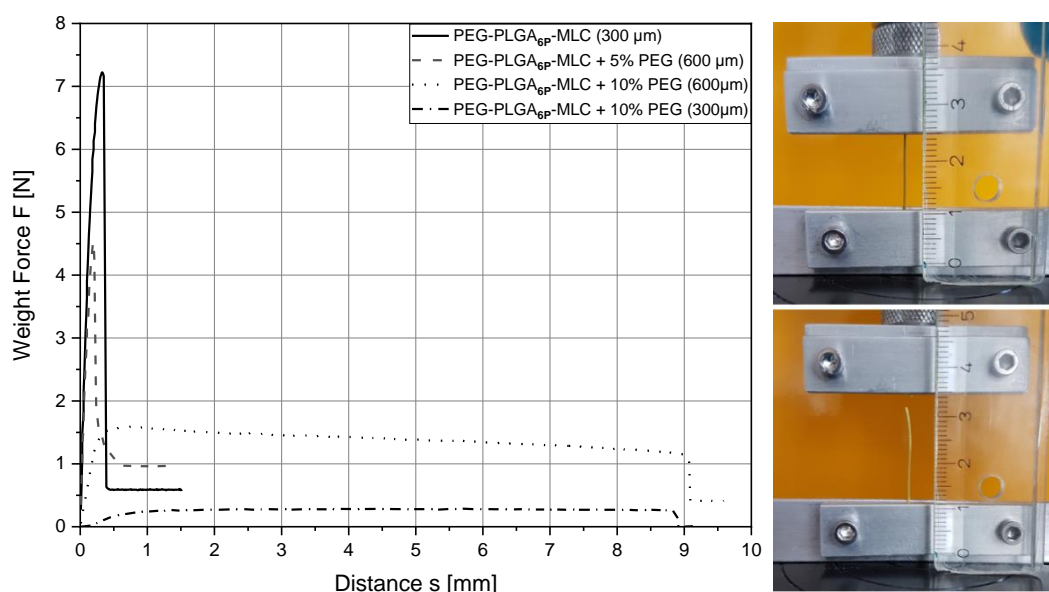


Figure 32: Left: Ductility test: Force path diagram of PEG-PLGA_{6P}-MLC extrudates with and without addition of PEG 1500; Right: Experimental setup (top) and outcome (bottom) for a 600 µm PEG-PLGA_{6P} + 10% PEG extrudate with visible elongation

The favorable flexible traits were also obvious on the macroscopic level (Figure 33).

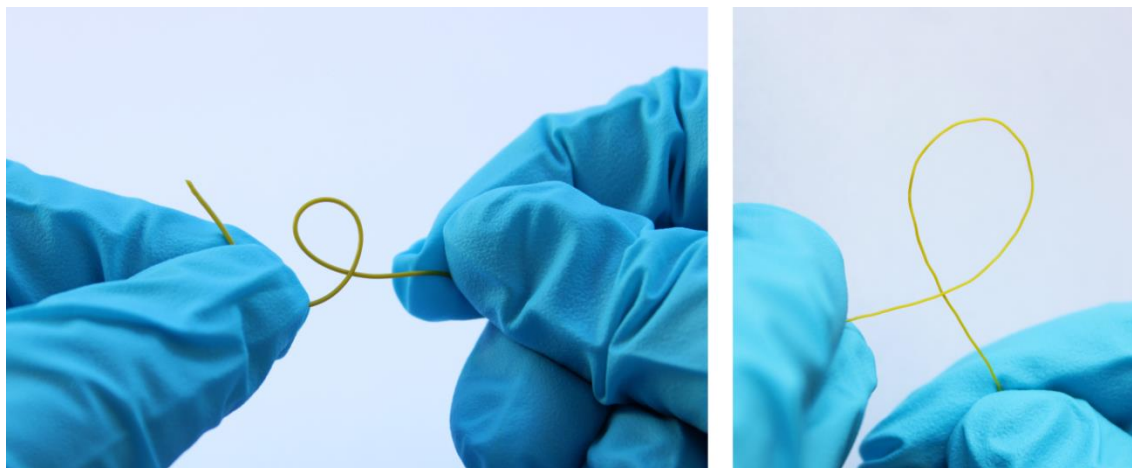


Figure 33: Application proof of flexibility of PEG-PLGA_{6P}-MLC extrudates containing 10% PEG; Left with a diameter of 600 µm; Right with a diameter of 300 µm

The penetration test and the ductility test both demonstrated a change of force parameters depending on the PEG concentration. Unfortunately, the flexibility did not last with a PEG content of 5%. 10% of PEG 1500 however, led to a prevailing, excellent flexibility with only minor hardening after months of storage. It has to be noted, that the measurable solidification after 13 months did not impair the handling. These extrudates were still effortlessly bendable without macroscopic signs of material fatigue. Also, the extrudates with a reduced diameter remained flexible.

The results of the ductility test basically mirrored the results of the penetration test. With an extension of up to 150% of their original length, the 10% PEG containing extrudates anew demonstrated their desirable mechanical traits. In contrast, 5% PEG 1500 were again not enough to achieve such a performance.

Hence, the PEG-PLGA_{6P}-MLC extrudates paired with 10% PEG established their claim as favorable prototypes early. With this combination of polymer and plasticizer the aimed degree of flexibility was now realizable.

4.7.2 X-RAY POWDER DIFFRACTION

The investigation with X-ray powder diffraction in combination with the DSC analysis yielded novel information on the nature of the extrudates and on the MLC. The X-ray spectra of the basic compounds are illustrated in Figure 34. Minocycline's spectrum possesses sharp bands with a high intensity, especially in the range from 5° to 15°. Commercial magnesium stearate exists in several polymorphic manifestations (144). The magnesium stearate utilized here was partially amorphous, which can be recognized by the two broad peaks in the XRPD-spectrum. A physical mixture of both

reactants in a molar ratio of 1:2 (minocycline : magnesium stearate), resulted in a superposition of both spectra. The sharp crystalline peaks of minocycline remained clearly observable besides the broad bands of magnesium stearate. In contrast, these sharp peaks disappeared as soon as the chelation took place. Only one broad peak remained, indicating an at least partial amorphous state of the MLC. The absence of these peaks underlines the formation of the claimed complex.

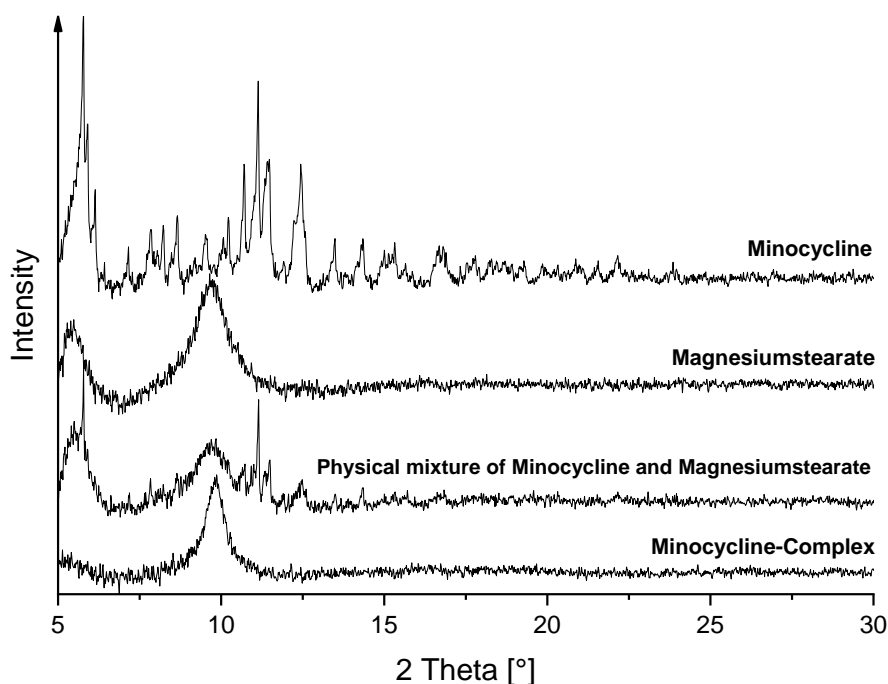


Figure 34: XRPD-diffractograms of minocycline, magnesium stearate, their physical mixture and the MLC

The upper diagram of Figure 35 illustrates the spectra of the PEG-PLGA polymers and the influence of PEG 1500 on the extrudates. PEG 1500 was primarily crystalline, which can be observed from the high intensity peaks at 8.75° and 10°. These values match with literature statements, if the utilized X-ray tube (copper (0.153 nm) and molybdenum (0.072 nm)) are considered during conversion with the Bragg's law (145). Both PEG-PLGA polymers demonstrated an amorphous manifestation, due to the broad low intensity peaks. The spectrum of the PEG-PLGA_{6P}-MLC extrudate contained an evident peak of the MLC. The addition of 5% PEG 1500 results in an intensification of the MLC peak at 10°, which implies the formation of crystalline regions. This effect was even further increased by addition of 10% PEG 1500, and also led to a new peak at 11.5°, which could be assigned to pure crystalline PEG 1500. The PEG-PLGA_{7P}-MLC extrudate spectrum displayed no alteration through the addition of the MLC compared to the pure polymer. Hence, the X-ray data by itself could suggest a compatible, amorphous status of this extrudate in strong contrast to the macroscopic appearance.

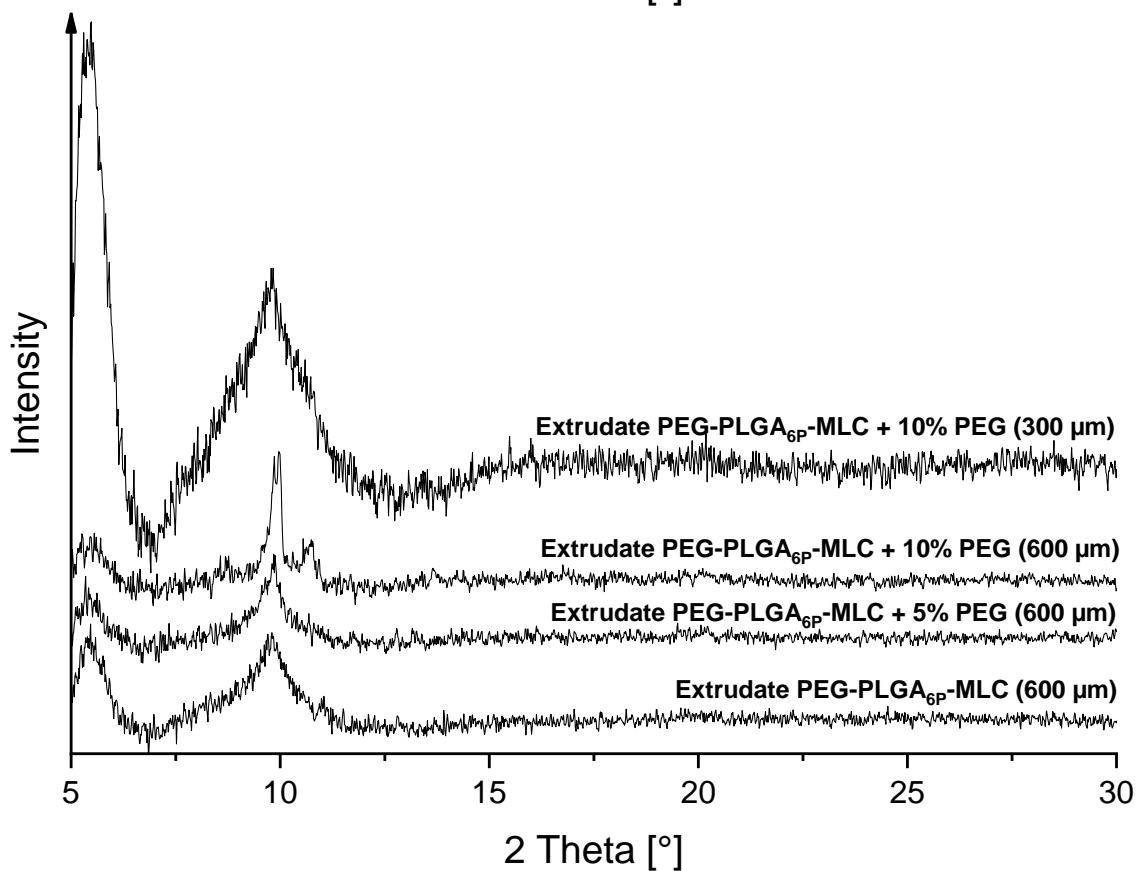
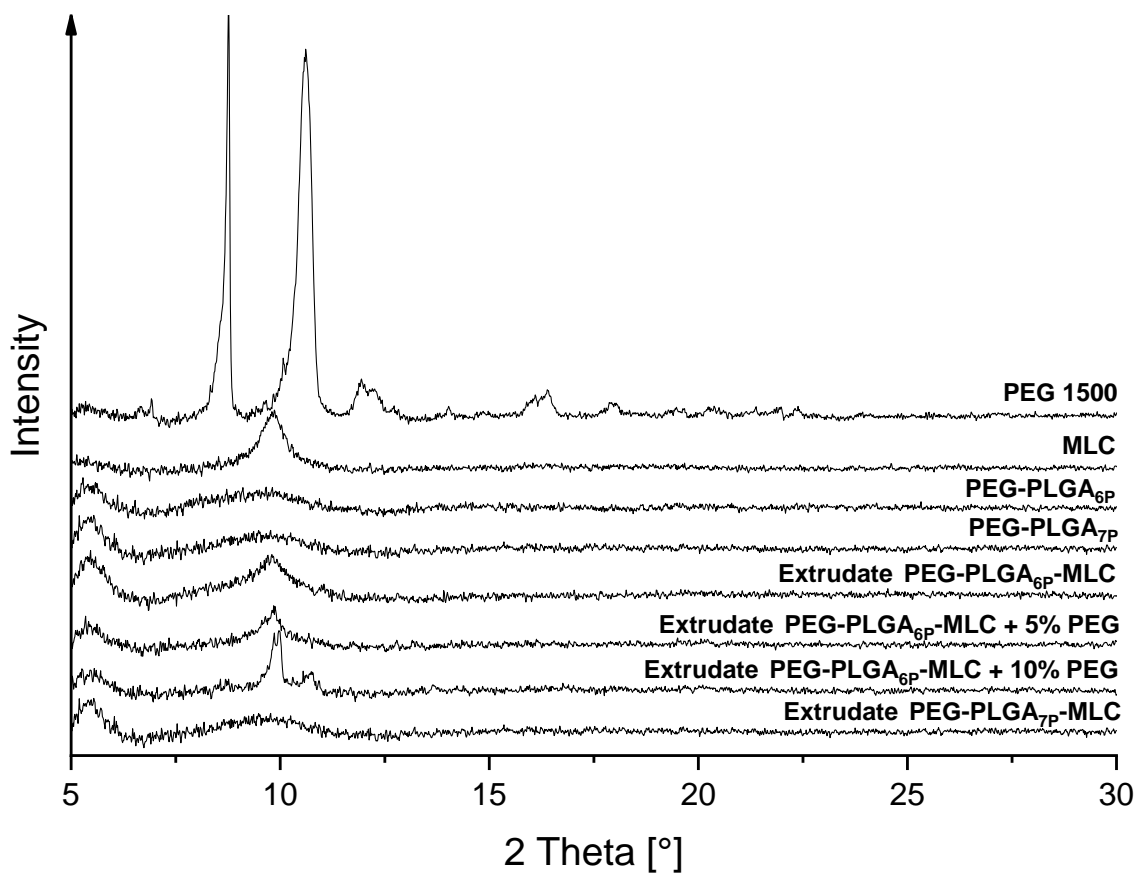


Figure 35: Top: XRPD-diffractograms of the components and several extrudates (600 μm) consisting of PEG-PLGA polymers, the MLC and PEG 1500 as plasticizer; Bottom: XRPD-diagrams of PEG-PLGA_{6P}-MLC extrudates with 10% PEG and varying diameters

The impact of the smaller diameter, and therefore more demanding conditions during extrusion are observable in the lower diagram of Figure 35. Dominating were a high intensity peak at 6° and a broadened peak with likewise high intensity at 10° in range of the complex. A differentiation between PEG and MLC was not possible anymore. The increased peak intensity could be attributed to the formation of crystalline regions. The higher shear rate, elevated temperature and pressure, which are caused by the extrusion with a 300 µm nozzle, could be responsible for amplifying crystallization (146).

For comprehensive conclusions the XRPD-data alone would not suffice. But in combination with the subsequent DSC analysis, more precise statements could be generated.

4.7.3 DIFFERENTIAL SCANNING CALORIMETRY

The DSC analysis gave additional insights on the nature of the components and the extrudates. DSC is a common technique for the characterization of extrudates (147), but thermograms of extrudates can be challenging to interpret. The formation of the complex, the cryomilling and the extrusion contribute to the thermal history of the final product. Also, the extrusion leads to a molecular orientation within the extrudate, which might influence the glass transition (T_G) (148). During the DSC analysis of an extrudate, the contact area and therefore the measured signal can change, which results in varying thermograms of equal samples. Hence, the following thermograms have to be interpreted with caution. Reproducible results can be obtained with pre-heated samples, but this would include an erasure of the thermal history of the investigated sample. Considering these aspects, we decided to explore the thermograms of the 1st heating procedure.

Figure 36 illustrates thermograms of minocycline, magnesium stearate, their physical mixture and the MLC. Minocycline does not possess a melting point and disintegrates at temperatures above 175 °C (149). The thermal event in the range of 60 to 140 °C could be attributed to water, which was not removable by drying in a vacuum compartment dryer. Magnesium stearates thermograms also display peaks, which could be attributed to the evaporation of water, due to its hygroscopic character (150), or to the presence of free stearic acid. The physical mixture of both components led to a superimposition of both thermograms, in which the disintegration peak of minocycline is smoothed. The analysis of the MLC did not reveal any familiar peaks of its basic components. Instead a broad peak at 65 °C was observable, which is either a sign of a chemical reaction or a broad melting point. These differences between the physical

mixture and the MLC support the formation of the complex, especially in combination with the XRPD data. The broad peak in the MLC thermograms suggests an intermediate state of an amorphous complex with crystalline parts.

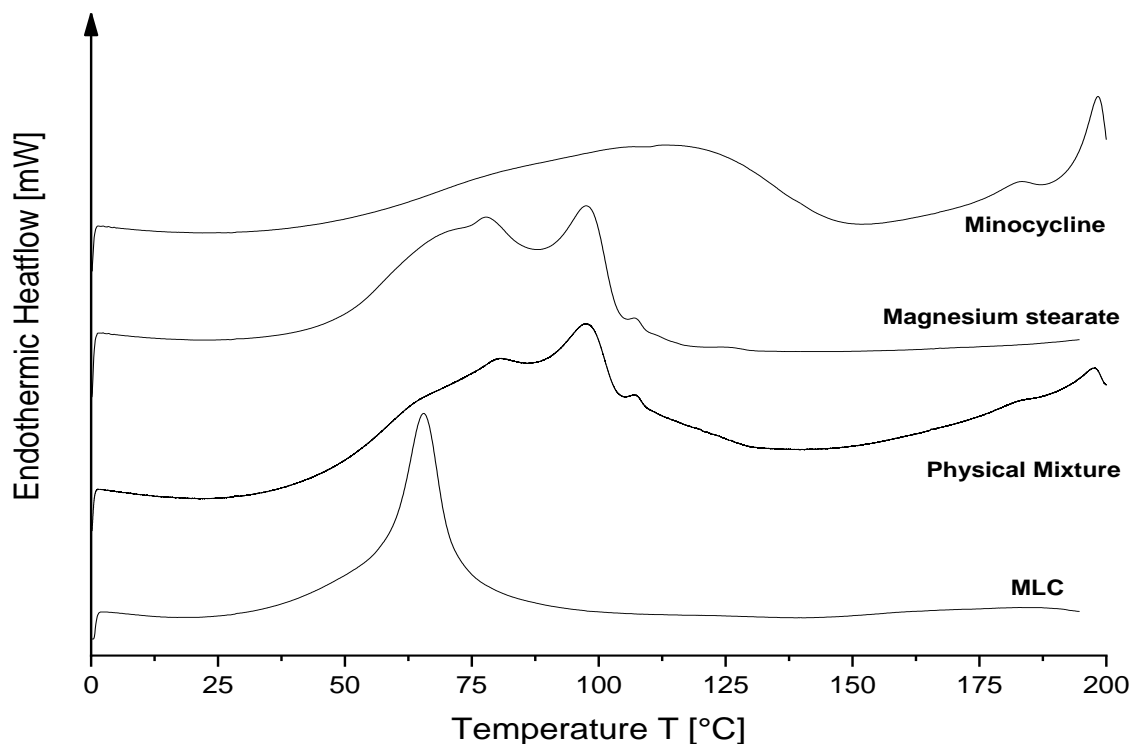


Figure 36: DSC-thermograms of the MLC compounds, their physical mixture and the MLC in a temperature range of 0 - 200 °C; Heat rate: 5 K min⁻¹

The thermograms of the PEG-PLGA polymers, the MLC and their extrudates are presented in Figure 37. Due to its higher molecular weight, the T_G of PEG-PLGA_{7P} at 37.0 °C lay above the T_G of PEG-PLGA_{6P} at 25.6 °C. The T_G of the PEG-PLGA_{6P}-MLC extrudate was elevated to approximately 37.3 °C through the addition of the MLC. Also, a reduction and broadening of the glass transition step height was observed for PEG-PLGA_{6P}. A second glass transition at 69 °C indicated a not completely homogeneous composition, even though the absence of the broad minocycline melting point hints towards a compatibility of both components. The subsequent thermal event up to 80 °C could have originated from undissolved magnesium stearate within the polymer matrix. In the case of the PEG-PLGA_{7P}-MLC extrudate, a novel melting point at 40 °C was observable, which is accompanied by the glass transition of the PEG-PLGA_{7P}. Additionally, three broad melting points occurred in the range of 45 to 80 °C, leaving the impression of an incompatible mixture, in contrast to the XRPD-data.

Combining the results of both analytical procedures, the complex is likely to be mainly present in form of a solid solution inside the PEG-PLGA_{6P}-MLC extrudates. As

mentioned beforehand, the XRPD-data could suggest a similar situation for PEG-PLGA_{7P}, but the DSC-data confirms the macroscopic noticeable deficits.

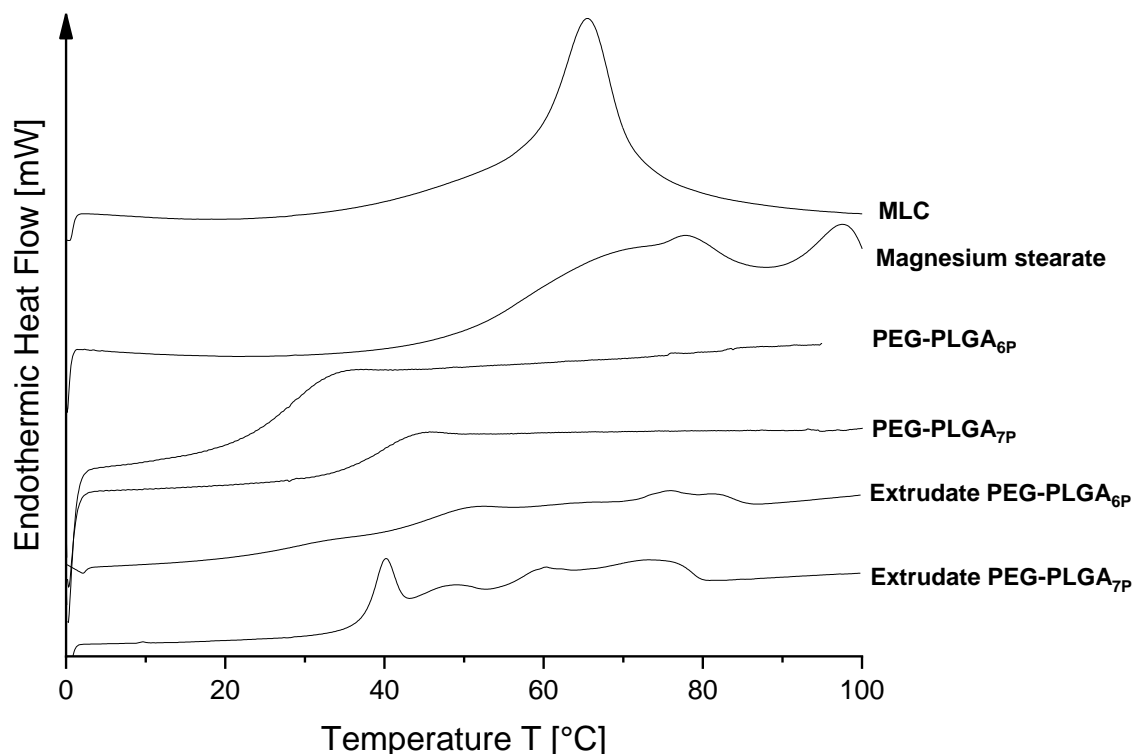


Figure 37: DSC-thermograms of different PEG-PLGA-MLC extrudates and their basic compounds in a temperature range from 0 to 100 °C; Heat rate: 5 K min⁻¹

Figure 38 illustrates the influence of PEG 1500 and the impact of the reduced diameter. It has to be noted that the thermogram of PEG 1500 has been scaled down. The reason therefore is the high intensity melting peak of PEG 1500 at 50 °C. A depiction with a shared scaling would result in indeterminable peaks, due to their comparably low intensity.

The thermograms revealed a not completely homogeneous state inside the PEG-PLGA_{6P}-MLC extrudates, when paired with PEG. The addition of PEG created novel peaks in the range of 55 °C to 60 °C and around 80 °C. Notably, a content of 5% PEG led to peaks with greater intensity compared to the PEG-PLGA_{6P}-MLC extrudates with 10% PEG. The intensification could imply the presence of more crystalline regions compared to the extrudates with 10% PEG content. Contrary, the findings of the XRPD-data exhibited reversed results (4.7.2). There, hints for a higher crystalline partition within the 10% PEG containing extrudates were recorded. The higher PEG content may have resulted in a more efficient filling of the interstitial space between the PEG-PLGA-polymer chains. This could explain the less prominent thermal events in the thermogram of the 10% PEG extrudates and would also give account of their enduring flexibility in contrast to their 5% PEG counterparts. It is also possible, that the

lipophilic complex hinders the implementation of lower concentrations of a hydrophilic plasticizer. Regarding the formation of a higher crystalline share inside the PEG containing extrudates, these systems should be addressed as solid dispersions.

The increased mechanic and thermal stress during the extrusion of the 300 μm extrudates, was also noticeable during the DSC analysis. The recorded peaks at 60 °C and 80 °C were more distinct compared to their 600 μm relatives. So, their thermogram resembles an intermediate of the just discussed 600 μm extrudates with 5% and 10% PEG. In consideration with the broad high intensity peaks of the XRPD-analysis, these 300 μm extrudates equally qualify as solid dispersions.

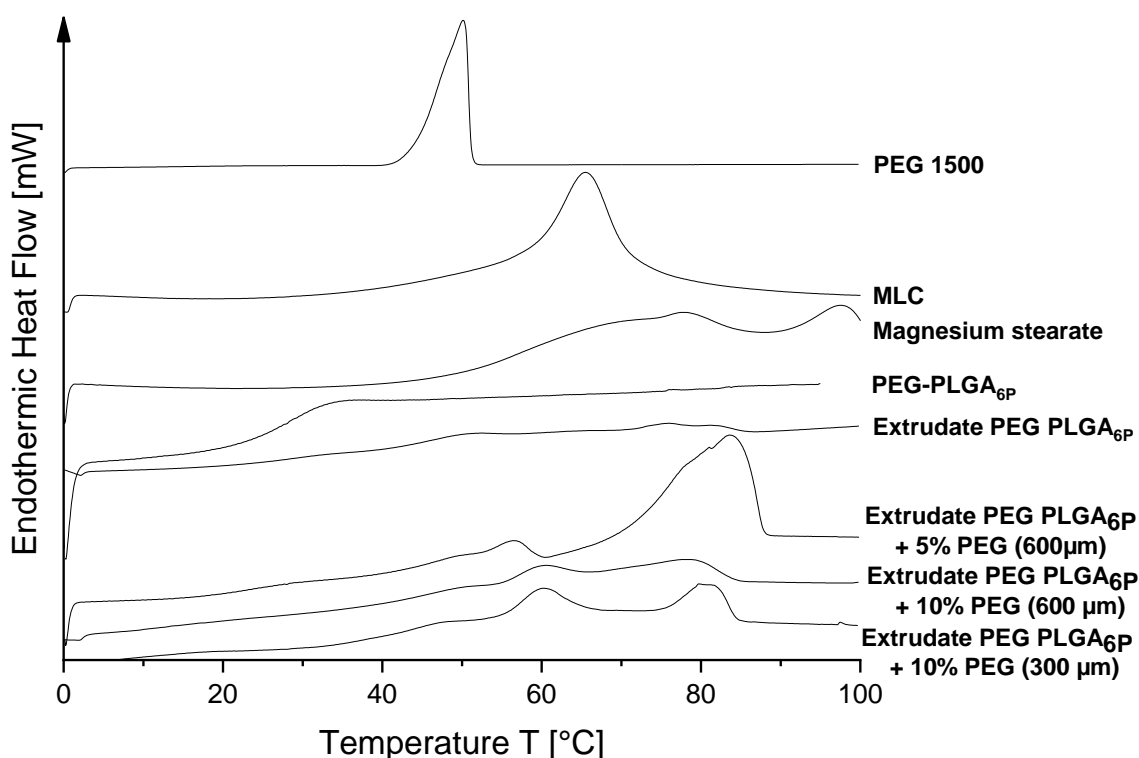


Figure 38: DSC-thermograms of PEG-PLGA_{6P}-MLC extrudates combined with PEG 1500 and varying diameters (300 and 600 μm)

Thus, if XRPD and DSC analysis are unitedly applied, they can offer an in-depth representation of the situation within solid systems. For the extrudates, different solid states were observable depending on their composition and on the applied extrusion parameters. Hence, these values could serve as quality markers for the further development. Also, valuable data concerning the MLC was gathered, which complements the characterization of the complex in chapter 4.2.

4.7.4 IN VITRO RELEASE

Initially, a release experiment in accordance to the release study of the PLGA-polymers in 4.4.2 with similar conditions was carried out (Figure 39). The polymer free MLC

extrudates were used as control. For comparative reasons the release profile of PLGA₅₀₂-MLC- and PLGA₅₀₃-MLC extrudates are illustrated within this figure as well. As already described in 4.4.2, the polymer free drug MLC extrudates were able to release the API over 21 days. The addition of PEG-PLGA could extend this period to 42 days, as could PLGA.

However, the differences between the single PEG-PLGA polymers were conspicuous. The PEG-PLGA_{7P}-MLC extrudates demonstrated a release profile, which is close to the pure MLC. Despite their higher molecular weight, these extrudates possessed a higher release rate compared to all PEG-PLGA_{6P} compositions. But from day 12 on, this release rate subsided rapidly. In contrast, the PEG-PLGA_{6P}-MLC extrudates expressed a more constant release over the period of 42 days. The reason for these differences is the incompatibility of the MLC and PEG-PLGA_{7P}. Hence, the release behavior matches with the previously described brittle properties, their inhomogeneous surface and the results of the DSC analysis.

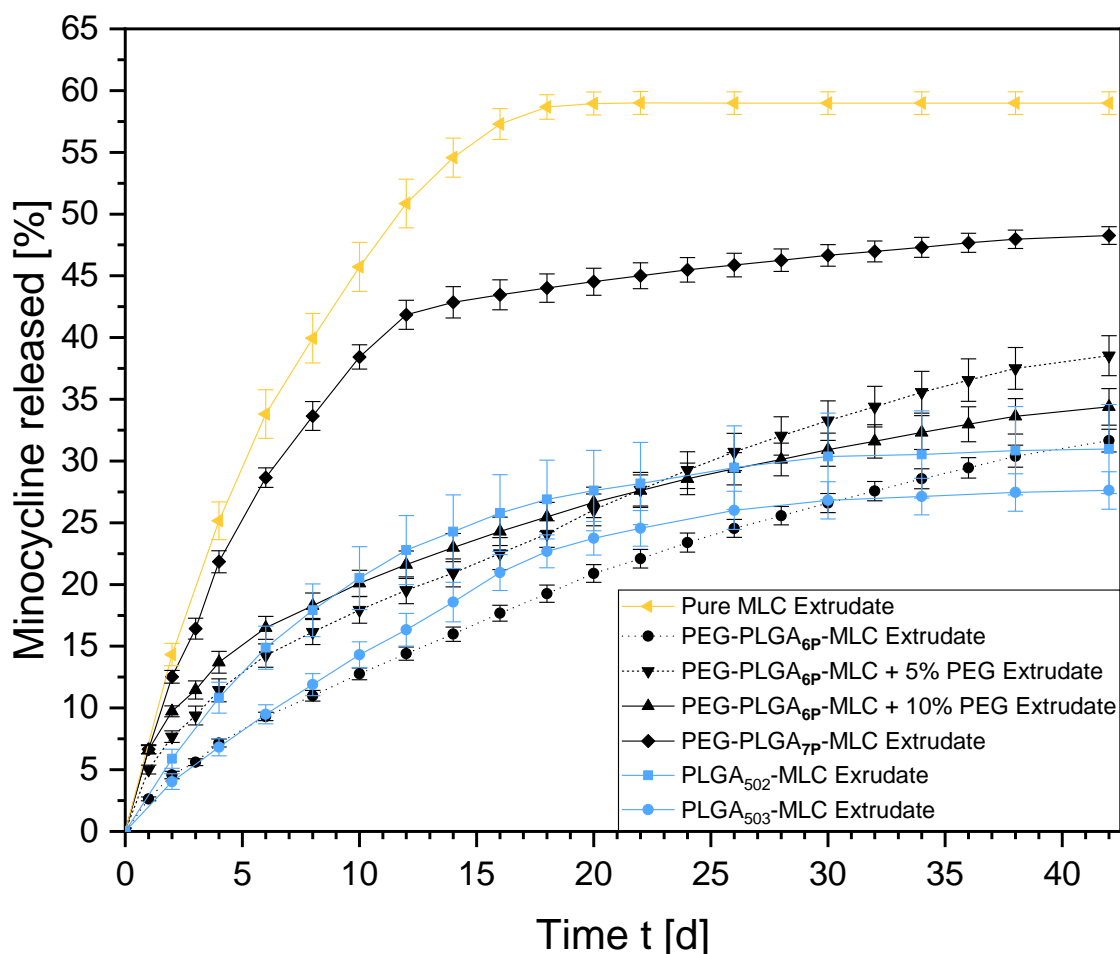


Figure 39: In Vitro release profiles of PEG-PGLA-MLC extrudates (600 μm) in phosphate buffer at 37 $^{\circ}\text{C}$; Release profile of PLGA-polymers included as reference (Quantification by UV/Vis-detector)

The impact of PEG 1500 on the PEG-PLGA_{6P}-MLC extrudates can also be observed within this figure. PEG provoked moderate changes of the release profile. The addition of 5% and 10% PEG 1500 successfully increased the initial release rate, doubling the amount of released API within the first days. This increased release rate was desired to reduce the microbial load during the beginning of the therapy. In comparison with the PLGA-MLC release patterns, the PEG-PLGA-MLC composition with supporting PEG offers a more favorable course. The initially faster release is valuable, combined with the overall higher release amount and the stable release rate. Interestingly, the extrudates containing 5% PEG 1500 overtook the 10% PEG extrudates after three weeks. A possible explanation therefore can be the emergence of a more hydrophilic climate inside the extrudates caused by the higher PEG content, which promotes interaction with the buffer and therefore degradation.

In comparison with the PLGA-MLC extrudates, the PEG-PGLA-MLC extrudates with addition of PEG demonstrated the fastest release rate during the first 5 days until they were passed by PLGA₅₀₂-MLC. This situation lasted until day 24, from where on the PEG-PLGA-MLC compositions consolidated their leadership through their constant release rate. Surprisingly, PEG-PLGA-MLC_{6P} without supplement of PEG 1500 required the whole release period to finally catch up with the previously conducted PLGA-MLC release profiles. A reason for this unexpected observation could again lie in the molecular masses. Even the “high” molecular weight PLGA has a lower molecular weight than PEG-PLGA_{6P}. The additional functionalization with PEG was not able to overcome this circumstance.

The newly developed quantification method with LC-MS/MS was applied to the 300 μm and 600 μm versions of the PEG-PLGA_{6P}-MLC formulations (Figure 40). The lower limit of quantification enabled a higher recovery-rate of the released drug. Therefore, the overall cumulative release of the 600 μm extrudate is with 47.5 % at day 42 higher compared to the original method. Apart from that, they demonstrated a comparable course.

Initially, the 300 μm specimens exhibit a higher release. Before the release rate started to slow down at day 10, they released > 55% of their load - ~25% more than the 600 μm extrudates - and in total they were able to release an absolute amount of 60% within 42 days. It has to be noted, that from day 10 on the released amount was comparably low and might not suffice to inhibit bacterial growth. The observed higher release rate for these extrudates was expected, due to the higher volume specific surface compared to the original prototypes with a 600 μm diameter. At a constant volume, the surface is increased, while the diffusion paths within the extrudate are

reduced, which results in a higher diffusion rate. Regarding their significant lower release rate after 10 days, a combination of both extrudates might be a notable dosing option for the clinical use. Concerning the remaining 40 to 65% of API, a similar fate, like it was recorded for the PLGA-MLC extrudates is probable (4.4.2, 4.4.3). Around 10 to 15% of the API remained detectable within the extrudates. Thus, up to 50% of the API is likely to fall victim to decomposition and decay.

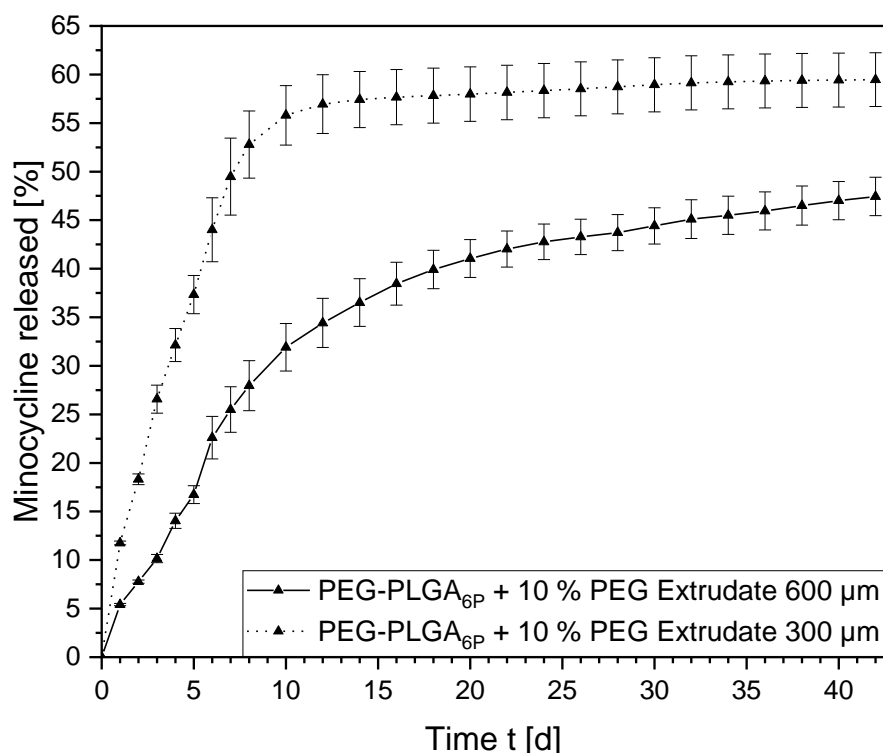


Figure 40: Impact of extrudate diameter (300 µm / 600 µm) on the release kinetics of PEG-PLGA_{6P}-MLC extrudates in phosphate buffer pH 7.0 at 37 °C (Quantification by LC-MS/MS)

Overall, the 10% PEG extrudates emerged as the most favorable composition during the second development cycle. Their optimized mechanical properties offer an even easier application and a more comfortable fitting in the gingival sulcus, while the favorable traits of the lipophilic drug complex remain unchanged, with a slightly increased initial release. Hence, the antimicrobial potential of these enhanced prototypes required further evaluation to establish their claim as most advanced prototype.

4.8 ANTIMICROBIAL *IN VITRO* PERFORMANCE OF THE SECOND GENERATION PROTOTYPES

The results of the present section were obtained at the laboratory of Prof. Dr. Sigrun Eick from the University of Bern.

4.8.1 ANTIMICROBIAL ACTIVITY ON THE FORMATION OF BIOFILMS

Similar to the experiments described in 4.5, the antimicrobial performance of the PEG-PLGA_{6P}-MLC composition with supporting PEG content was evaluated. Their activity on the formation of new biofilms in comparison to PLGA₅₀₂-MLC is illustrated in Figure 41.

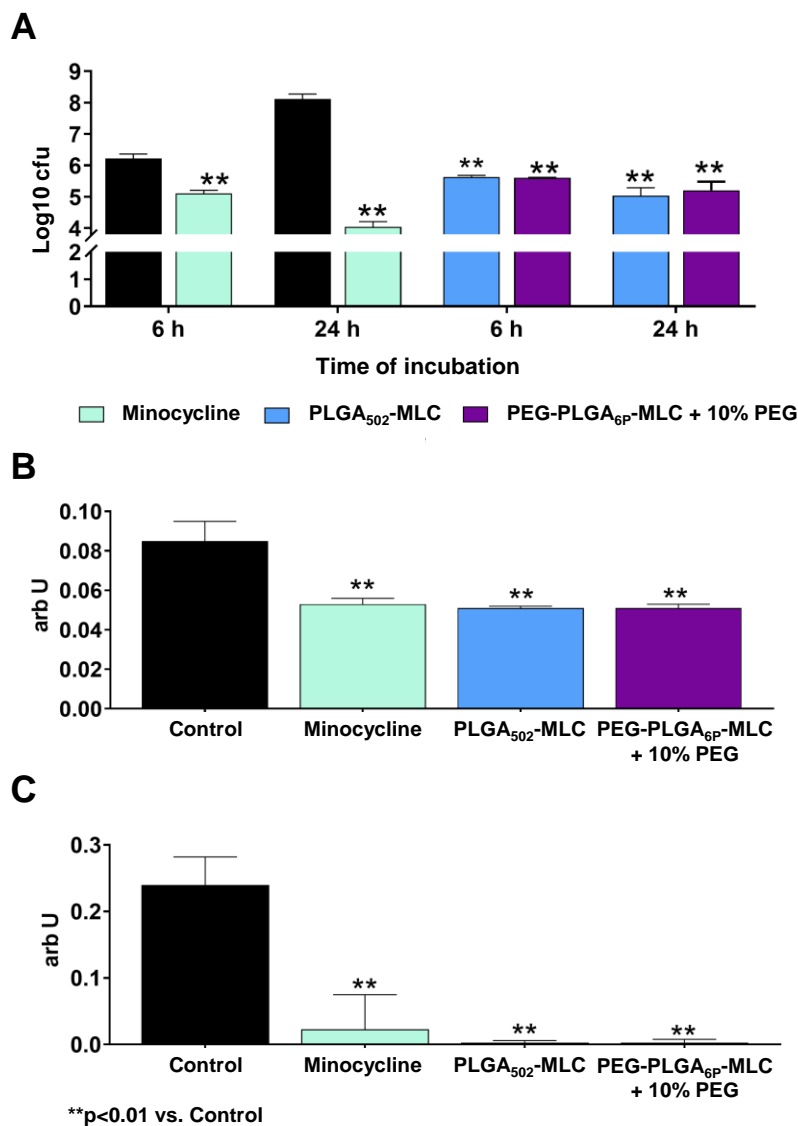


Figure 41: Activity on the formation of a six-species biofilm of PEG-PLGA_{6P}-MLC with 10% PEG in comparison to PLGA₅₀₂-MLC: A - Bacterial counts determined as colony forming units (cfu); B - Biofilm quantity; C - Metabolic Activity

Minocycline reduced the number of cfu in comparison to the control, as well as both test formulations. Confirming the results from the biofilm formation testing in 4.5.2, the pure drug demonstrated the highest effect on the cfu count with a reduction of

1.1 Log₁₀ steps after 6 h, and 4 Log₁₀ steps after 24 h. The PLGA- and PEG-PLGA-MLC formulations both achieved a reduction of 0.6 Log₁₀ steps after 6 h, and 2.9 to 3.08 Log₁₀ steps within 24 h. Hence, no difference between PLGA-MLC and PEG-PLGA-MLC was detectable in this case.

The level of biofilm quantity was for the control and for the test formulations on an equal level. They achieved a reduction by approximately 40%. These results also matched with the findings from the previous test of the first prototypes.

As expected, the reduction of the biofilm is also mirrored in its metabolic activity. Mean reductions of 95% for minocycline, and up to 98% for the MLC containing systems demonstrated high activity.

4.8.2 ANTIMICROBIAL ACTIVITY ON PREFORMED BIOFILMS

At the time point of this assays execution, there were unfortunately no samples of PLGA₅₀₂-MLC left in Prof. Eick's laboratory. Hence, minocycline alone had to serve as positive control. However, the activity of PEG-PLGA-MLC on preformed biofilms was, as anticipated, close to their PLGA-MLC relatives (Figure 42). Test formulation and control were both able to diminish the cfu count to a similar extent. A reduction in a range from 1.38 Log₁₀ steps to 1.94 Log₁₀ steps was observable. Hence, during this procedure the general effect on the cfu count was for the positive control and the test formulation at the lower end of their activity spectrum, compared to the achievements against newly developing biofilms. Given the minor activity of the positive control compared to the prior execution of this experiment (4.5.3), paired with the corresponding performance of the test formulation, a deviation, as it can occur within microbiological assays, seems possible (151,152). It should also be noted, that for the PEG-PLGA-MLC formulation, a concentration dependency of the effect on the cfu count was not directly extractable.

An effect on the quantity of the established biofilm was not detectable. This outcome also aligns with the findings of the PLGA-MLC compositions (4.5.2).

Nevertheless, a reduction of the metabolic activity was measurable. Mean reductions of 38% for the positive control, and approximately 55% for the test formulation were observed. Thus, the effects were less intensive in comparison with the previous run, but in reference to the positive control, the PEG-PLGA-MLC + 10% PEG formulations demonstrated a similar behavior and capability.

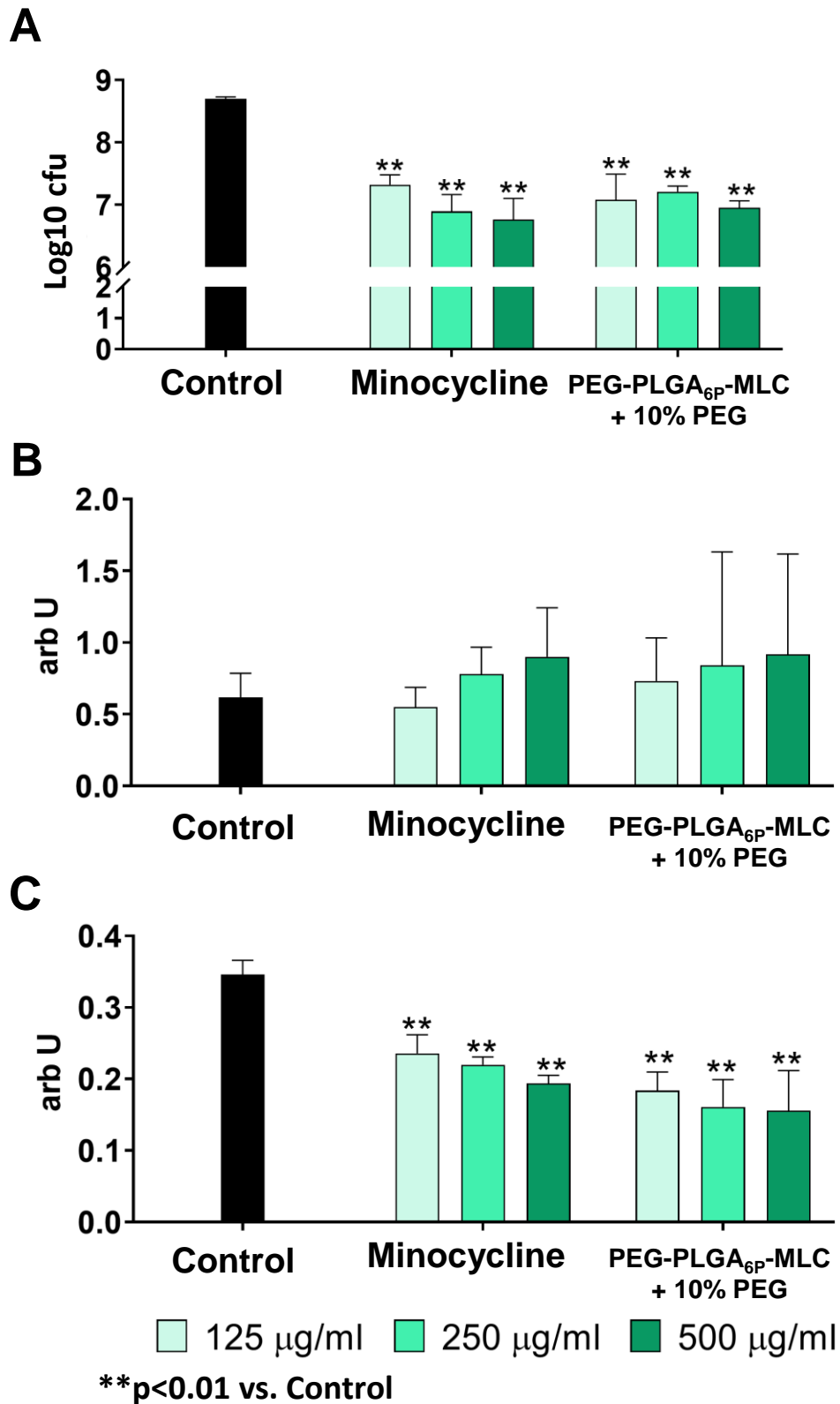


Figure 42: Activity of PEG-PLGA_{6P}-MLC + 10% PEG on a six-species biofilm formed over 3.5 days with minocycline serving as control; A – Bacterial counts determined as colony forming units (cfu); B – Biofilm quantity; C – Metabolic activity

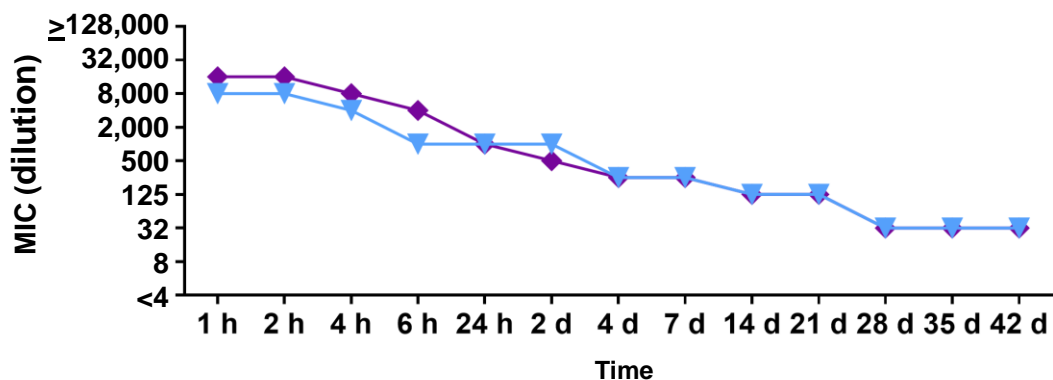
The absolute effects were moderately lower during the second run of this microbiological assay. Nevertheless, it can be stated that the second generation

prototypes possess an equal antimicrobial potential on the interaction with new and established biofilms like their predecessors. In relation to the pure minocycline, both formulations performed uniformly. Given the deviating results for the positive control, the differences could be attributed to the sensitivity of the microbiological assay, as stated above.

4.8.3 ANTIMICROBIAL ACTIVITY OF THE ELUATES OBTAINED FROM THE GINGIVAL FLOW SIMULATION

The activity of the eluates of PLGA₅₀₂-MLC and PEG-PLGA_{6P}-MLC with 10% PEG as their maximum dilution is displayed in Figure 43. Against *S. gordonii*, the PEG-PLGA-MLC extrudate exhibited a higher initial activity, but aligned with the PLGA-MLC extrudate at day 4. In case of *P. gingivalis*, both formulations demonstrated an almost identical activity, besides an advantage of one dilution step in favor of PLGA-MLC at day 42.

S. gordonii



P. gingivalis

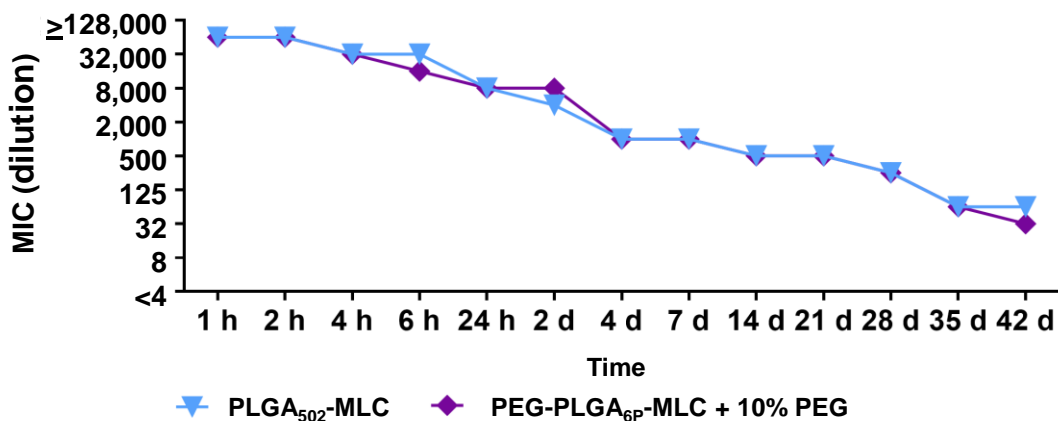
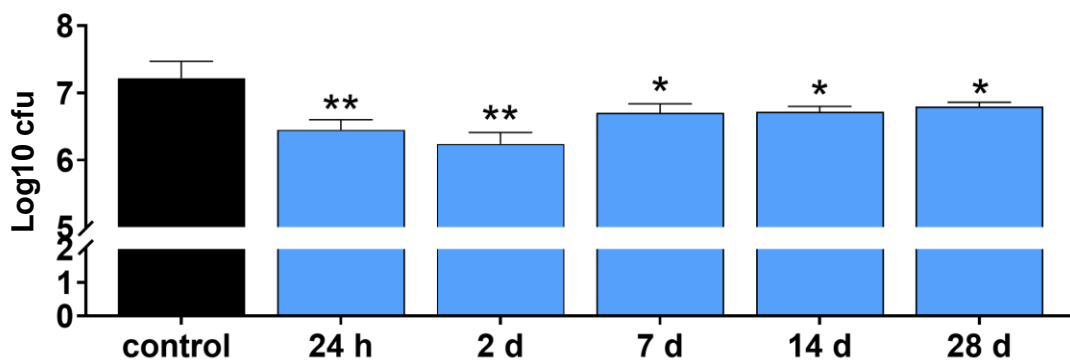


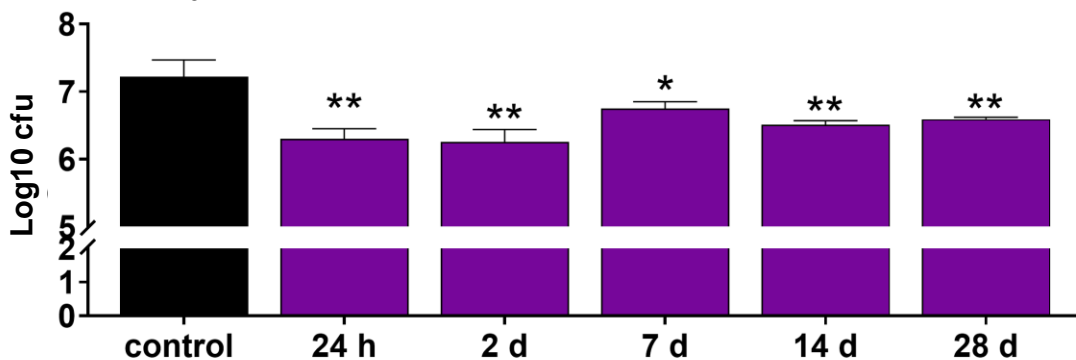
Figure 43: Minimal inhibitory concentrations (maximum dilution) of eluates of PEG-PLGA_{6P}-MLC + 10% PEG formulations compared to PLGA₅₀₂-MLC obtained over 42 days during simulation of the gingival fluid flow on *S. gordonii* ATCC 10558 (A) and *P. gingivalis* ATCC 33277 (B); PLGA-MLC formulation

Of course, the activity of these eluates was also of interest, as it was for the first prototypes. The growth inhibition capability of the eluates at different time points is illustrated in Figure 44 in comparison to PLGA₅₀₂-MLC. Within the first two days, both MLC-containing formulations were able to lower the cfu count by 0.97 Log₁₀ steps. Subsequently, a slight increase of the cfu count was observable for both of the tested systems on day 7. Even though PLGA₅₀₂-MLC demonstrated an effect against the control on day 14 and 28, a stronger impact for PEG-PLGA_{6P}-MLC + 10% PEG was ascertainable.

PLGA₅₀₂-MLC



PEG-PLGA_{6P}-MLC + 10% PEG



*p<0.05, **p<0.01 vs. Control

Figure 44: Antimicrobial activity of the eluates obtained during the gingival fluid flow simulation against the formation of biofilms at different time points (cfu count after 6 h)

However, it should be pointed out again, that the positive control, which was in this case PLGA₅₀₂-MLC, was anew slightly behind its previously measured results. But this does not affect the extractable conclusion retrieved from this antibacterial *in vitro* performance evaluation. The comparative confrontation between the first generation prototype PLGA₅₀₂-MLC and the flexible PEG-PLGA_{6P}-MLC + 10% PEG extrudates revealed a similar antibacterial potential for both applicants in all matters. None of them was clearly superior in any of the assessed parameters. Hence, the second generation

prototypes enforced their claim as favorable composition, due to their excellent mechanical behavior and simplified handling.

4.9 AN APPROACH TO FURTHER IMPROVEMENT THROUGH THE IMPLEMENTATION OF PVM/MA

Even though the second generation prototypes already unified several advantageous traits, ideas of features remained, which could further improve this novel drug delivery system. Exemplarily, an enhanced mucoadhesion would add another beneficial attribute to the extrudates. As possible candidate the poly(vinyl methyl ether/maleic anhydride) copolymer (PVM/MA) was chosen (Figure 45). PVM/MA itself is water-insoluble. In presence of water however, the anhydride is hydrolyzed, yielding free carboxylic acid groups, which generate the polymers mucoadhesive properties (153,154). PVM/MA is often an ingredient in healthcare products, such as dentifrice, denture adhesives or as ingredient within transdermal patches. It has also been of interest for other pharmaceutical applications. For instance, bioadhesive PVM/MA-nanoparticles for oral administration and microspheres with PVM/MA-content were successfully manufactured (155,156).

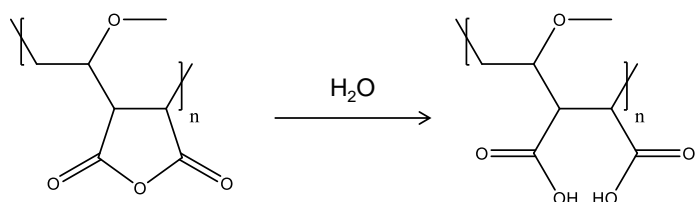


Figure 45: Structure of PVM/MA (left) and its hydrated form (right)

Especially due to the common application within dental hygiene products, and the classification as a safe ingredient (157), the choice fell on PVM/MA as mucoadhesive adjuvant. Contrarily to these points in favor, anhydrides are considered to be reactive. Hence, an interaction with the MLC, the plasticizer or PEG-PLGA cannot be excluded. Yoncheva et al. (2005) (158) fabricated pegylated PVM/MA-nanoparticles by dissolving both components in acetone with a subsequent precipitation. PEG 2000 yielded a higher pegylation efficiency in comparison to PEG 1000. Hence, a certain degree of chemical interaction during the manufacturing process with PEG 1500 or the remaining ingredients seemed possible.

Nevertheless, PVM/MA was added with 5% [m/m] to the second generation prototypes, thereby reducing the share of PEG-PLGA_{6P} within the composition. Cryomilling with the additional excipient did not cause any anomalies, and the extrusion precursor was of similar quality. Concerning the hot melt extrusion however, minor adjustments to the

extrusion parameters were applied (3.3.2 - Table 7). The extrusion of 300 μm extrudates led to a temperature increase within the extruder, similar to the prior extrusion described in 4.6.1. The temperature in the heating zones 2 and 3 were elevated from 51 $^{\circ}\text{C}$ and 53 $^{\circ}\text{C}$ to 52 $^{\circ}\text{C}$ and 56 $^{\circ}\text{C}$. Macroscopically observed, the addition of PVM/MA to the flexible second generation extrudates did not cause any noticeable defects (Figure 46). Extrudates with larger diameters tend to appear darker under the microscope in comparison with the thinner specimens. Also batch to batch variations can cause darker shades, but there were no deviations in the subsequent characterization of such extrudates observable, so far. A reason for such deviations during the manufacturing process can be found in the manual filling of the extruder, as described in 4.3.1. The manual filling does not enable a standardized transfer of mass per time unit to the extrusion chamber. Hence, if the production of the extrudates should become of interest of upscaling, attention should be paid on the standardization of this process parameter.

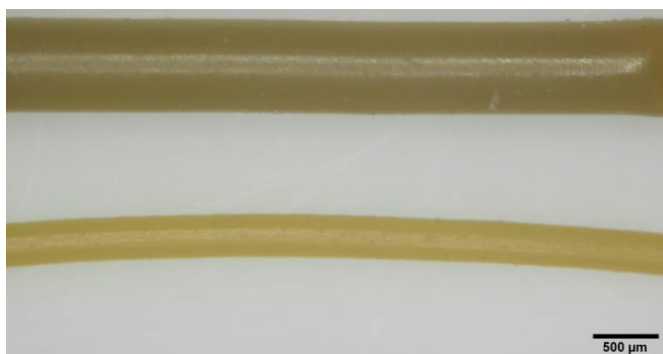


Figure 46: Extrudates with supplement of 5% PVM/MA; extruded with 600 μm (top) and 300 μm (bottom) die

However, after the successful implementation of the additional mucoadhesive excipient, the influence on the total composition demanded examination. Thus, the impact on the flexibility was the first parameter to be tested (Figure 47). In case of the 600 μm extrudates, a rise of the required penetration force was observed by up to 1.3 N. Initially, the increase of the required force correlated with the duration of the storage period, but paradoxically the force decreased again at day 38 during several measurements. Nevertheless, the force was still above the narrow range exhibited by the second generation prototypes without supplement of PVM/MA. In contrast, the 300 μm extrudates did not experience a noticeable alteration through the additional polymer. Even though the required force also slightly rose during the storage period, their force path diagrams remained close to the ones of the extrudates without PVM/MA. With peak forces at 0.2 mm, they were even slightly below the level of the PVM/MA-free extrudates. During the manual handling and bending however, no striking differences to the original extrudates were noticeable, independent of the diameter.

During the stretch test however, the influence of PVM/MA became more present. Independent of the diameter, the peak force to commence the elongation of the extrudates was decreased. At first sight, this could imply a further softening of the extrudates, but paired with the early rupture at 4 mm or respectively 4.5 mm in comparison to the 9 mm, this scenario becomes unlikely. The early breach and the lowered peak force could hint towards the emergence of micro-ruptures, due to a lowered flexibility. The areas affected by these proposed micro-ruptures within the extrudate would not be able to support the tensile strength of the drug delivery system. With this premise, the peak force and the early tearing seem more plausible. So, how did PVM/MA possibly lower the plasticity? The answer therefore might be found in the earlier described reactive nature of the anhydride. Hence, the formation of ester bonds between terminal alcohol groups of a PEG-chain and a carboxylic acid group of a hydrolyzed anhydride can be suggested. Even a cross-linking cannot be excluded. Thus, the formation of such covalent bonds would restrain the capability of PEG to act in the interstitial space as plasticizer, and therefore elucidate the slight hardening and premature tearing of the extrudates.

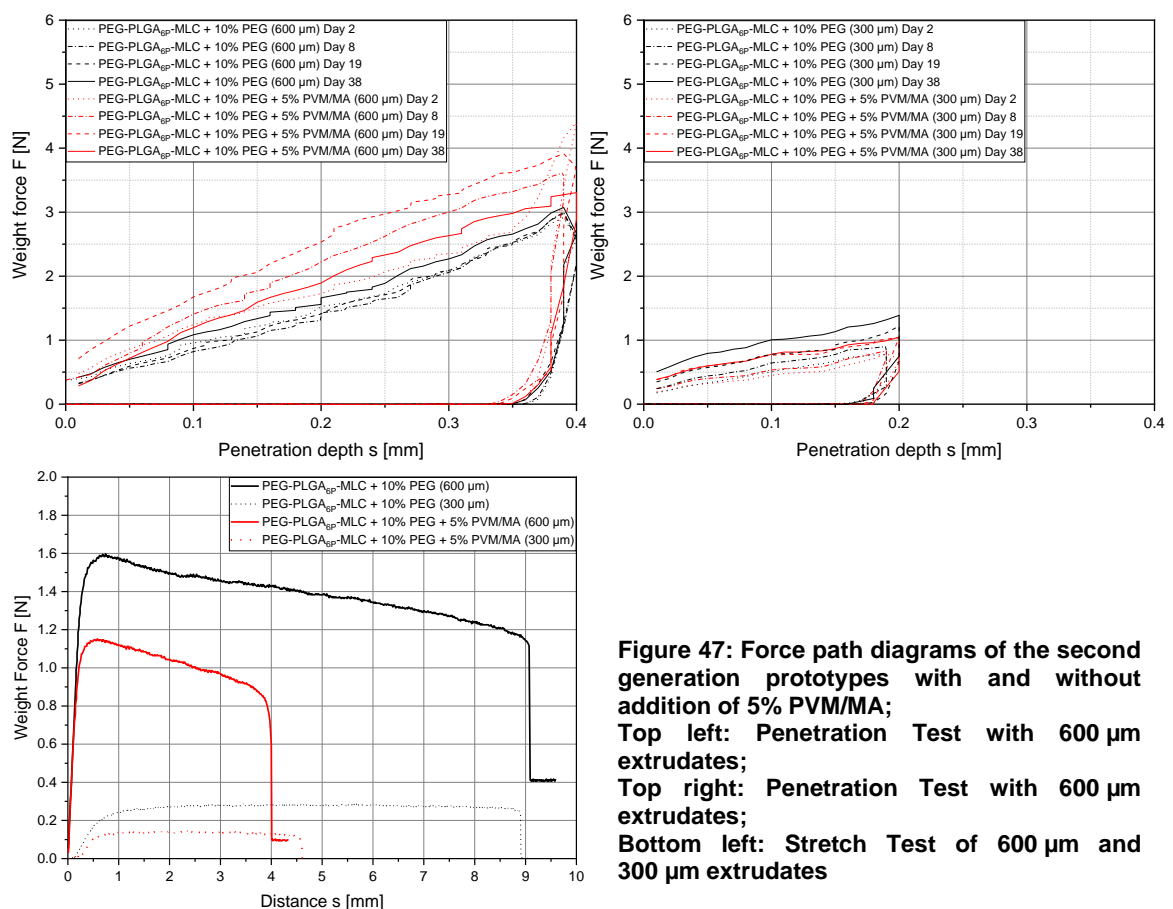


Figure 47: Force path diagrams of the second generation prototypes with and without addition of 5% PVM/MA;
Top left: Penetration Test with 600 μ m extrudates;
Top right: Penetration Test with 300 μ m extrudates;
Bottom left: Stretch Test of 600 μ m and 300 μ m extrudates

In summary, the addition of PVM/MA negatively influenced the extrudates plasticity. Interactions between the reactive anhydride and the plasticizer seem likely, as initially

implied. Nonetheless, these drawbacks may be part of an acceptable bargain, if favorable traits like mucoadhesion could be gained in return. Thus, these extrudates were further characterized to obtain a more conclusive picture about possible benefits and disadvantages.

Therefore, the DSC-analysis was the subsequent step to clarify, if the mechanic observations are also reflected by changes within the phase composition (Figure 48). PVM/MA itself does not demonstrate any thermal events in the exhibited temperature range, but the T_G is expected at 157 °C (159). Within the 600 μm extrudates, PVM/MA led to an intensification of the transitions and thermal events of the pure second generation prototype. The burdensome conditions during the extrusion with the 300 μm die enforced this situation further. The thermogram of the 300 μm extrudate containing PVM/MA had a strong resemblance with PEG-PLGA_{6P}-MLC. These observations suggest the increased occurrence of crystalline regions within the extrudates, especially within the 300 μm specimens.

This can explain the hardening of the PVM/MA-containing extrudates during storage. Hence, an even stronger effect for the 300 μm could have been expected during the texture analysis of these extrudates, but a penetration depth of 0.2 mm was probably not sufficient to emphasize such differences more clearly.

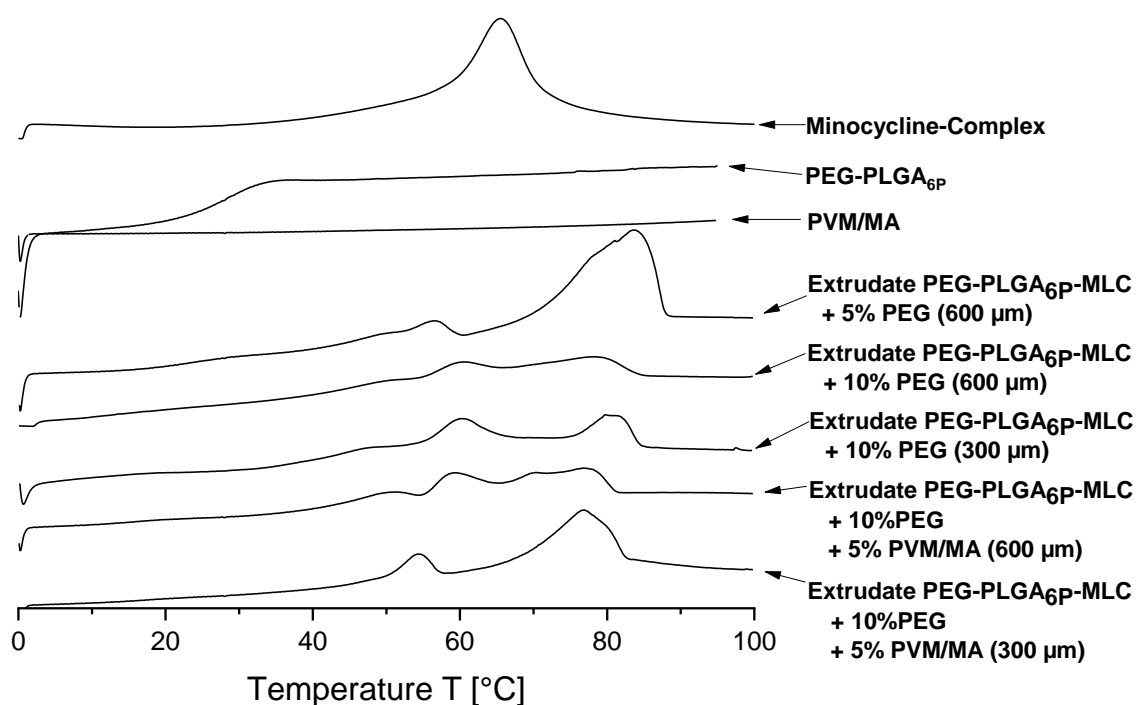


Figure 48: DSC-thermograms of the second generation prototypes with and without supplement of 5% PVM/MA

The impact of PVM/MA on the X-ray patterns of the extrudates is illustrated in Figure 49. Two broad peaks in the range of 5 to 6.5° and 7 to 14° confirmed the amorphous nature of PVM/MA. However, PVM/MA was not able to promote such conditions within the extrudates. In fact, crystallinity was increased distinctively. Under the presence of PVM/MA, the peaks of the second generation prototypes were decisively intensified. The 300 μm extrudates with additional PVM/MA content emulated their larger counterparts, but surprisingly the intensity of the main peak at 9.86° was lowered. Contrary to the 300 μm extrudates without PVM/MA supplement, these extrudates demonstrated several separable peaks, instead of two broad high intensity peaks. Also both the PEG-peaks gained further sharpness. Hence, it can be extracted, that the 300 μm PVM/MA extrudates also possess more crystalline regions compared to the PVM/MA-free extrudates.

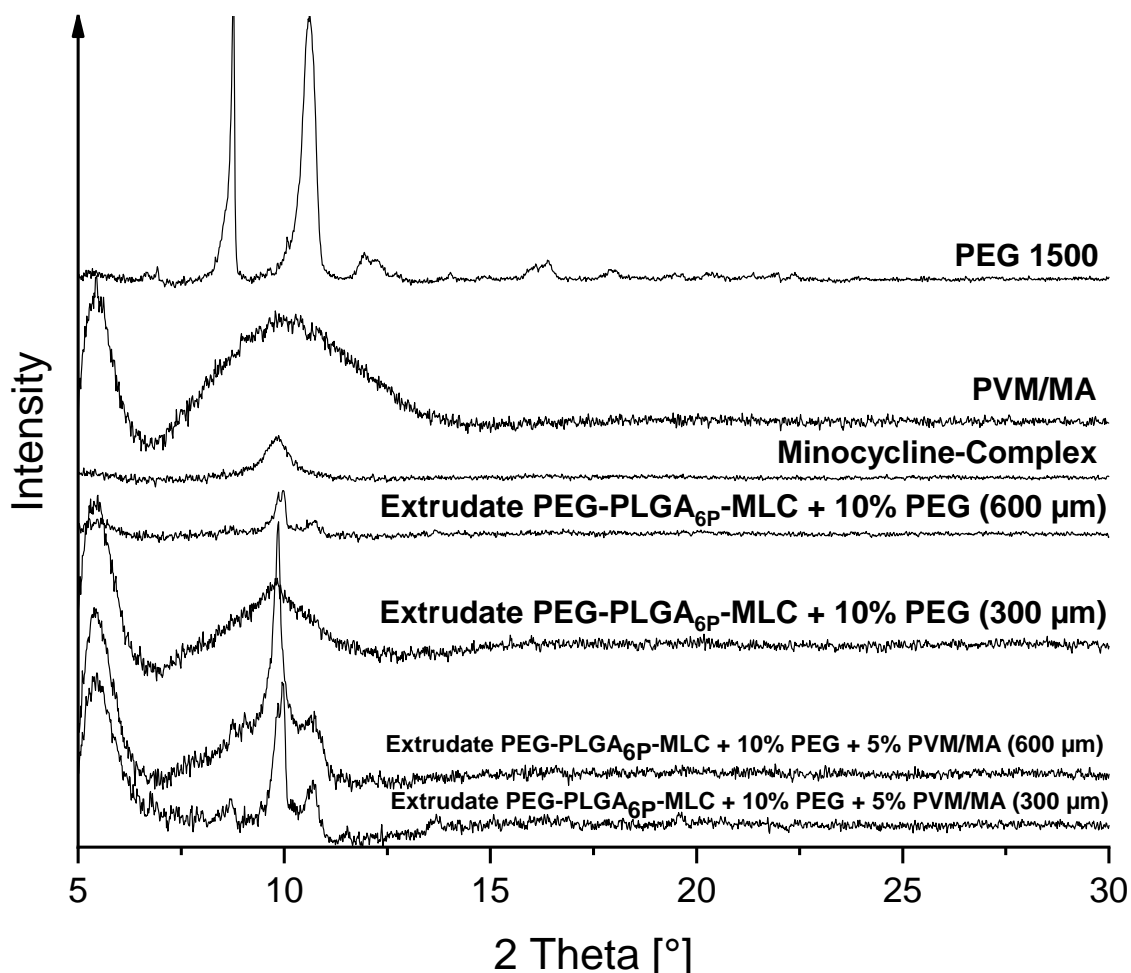


Figure 49: XRPD-diffractograms of the PEG-PLGA_{6P}-MLC + 10% PEG extrudate (600 μm) and the influence of 5% PVM/MA on the diffraction pattern of these extrudates (300 and 600 μm)

XRPD and DSC-analysis both hint towards the expression of crystalline regions through the implementation of PVM/MA. As initially explained, the possible reaction between PVM/MA and the remaining components is likely to play a critical role in this

observation. These crystalline regions contribute to an inhomogenization of the phase composition, which in first line negatively affects the flexibility. Thus, an effect of these internal changes of state seemed likely, and they demanded clarification.

Therefore, another *in vitro* release experiment was executed under deployment of the improved HPLC-method (Figure 50). In general, PVM/MA led to an accelerated release of minocycline. With PVM/MA supplement, the 600 μm extrudates release pattern was almost identical with the untreated 300 μm second generation prototype, within the first 10 days of release. From there on, their cumulative release values were separated by barely a minimum. Hence, the 600 μm extrudates with additional PVM/MA also released only minor amounts of API from day 12 on. Within the 300 μm extrudates, the release rate was even further increased through addition of PVM/MA. After 6 days, already 60% of the API were set free, but in the following weeks solely 1.4% of minocycline were additionally releasable.

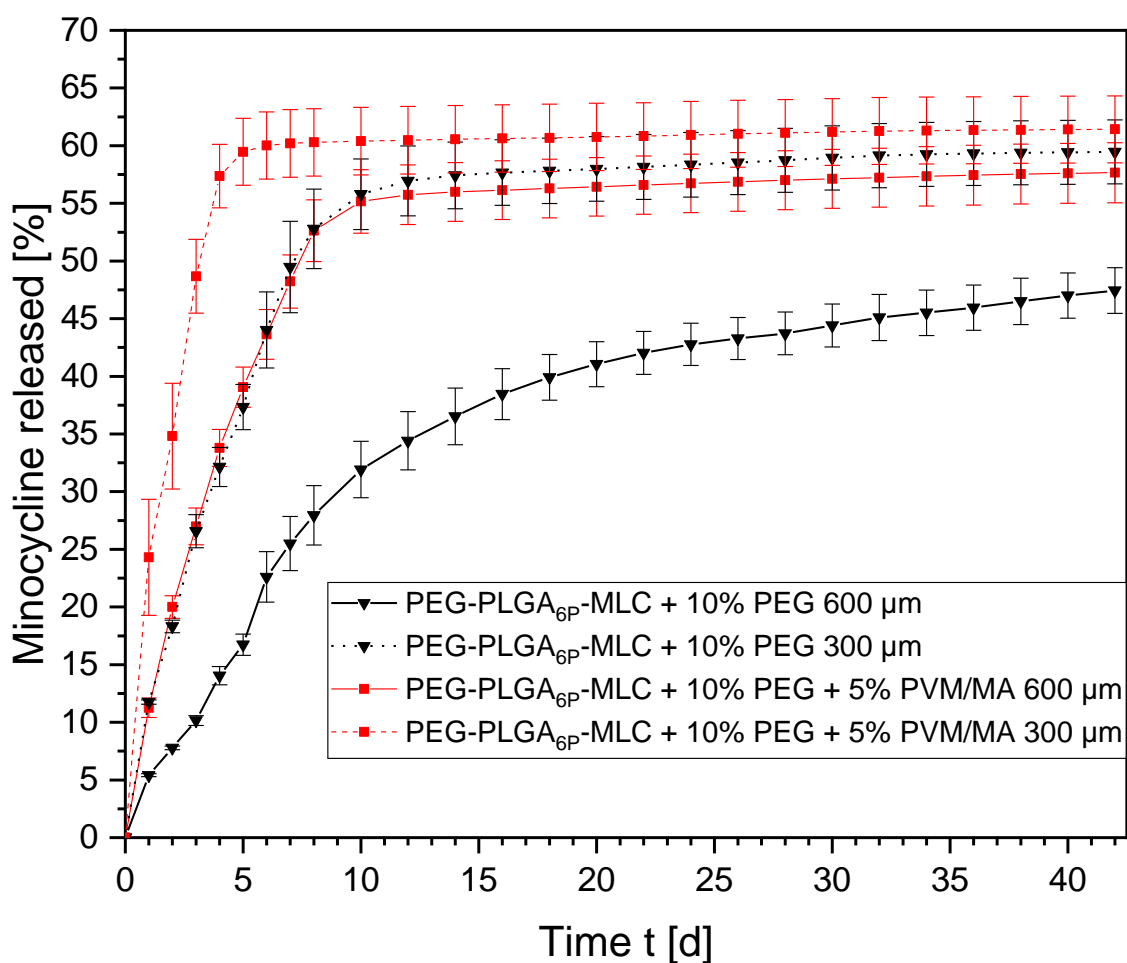


Figure 50: Influence of 5% PVM/MA content on the drug release of PEG-PLGA_{6P}-MLC + 10% PEG extrudates with 300 and 600 μm diameter

Apparently, the changes within the extrudates promoted a faster release of minocycline from either the polymer matrix or the complex. For an accelerated release from the

MLC, the pH-sensitivity mentioned in 4.2.1 may be responsible. The free carboxylic acid groups, which are likely to be present during the incubation in the phosphate buffer, could cause an acidic microenvironment within the extrudates. Hence, these conditions could stimulate the release of minocycline from the MLC. This acidic microenvironment could also catalyze the degradation of PEG-PLGA_{6P}, and therefore partially contribute to the faster release. Usually, PEG-PLGA polymers show lower rates of autocatalysis, due to an early water penetration caused by the PEG content, and a therefore swift diffusion of acidic degradation products (88). A premature release of the API from PEG-PLGA_{6P} due to the higher crystalline proportions however, seems improbable. According to the DSC and XRPD analysis, PVM/MA did cause an increase of the crystalline shares. But the crystalline proportions of implemented components alone did not affect the release rate in such a drastic manner, at least in case of the examined PLGA- and PEG-PLGA-MLC extrudates. Principally, the phase situation within the release defining matrix is of greater importance for the release pattern of such systems (160), and the here used polymers did not demonstrate alterations during the processing. However, according to the results of the DSC (4.7.1), the general compatibility of the components is also a key factor in terms of drug release. The only extrudates with an equally fast release were the incompatible PEG-PLGA_{7P} extrudates with their macroscopically noticeable flaws, and their on inhomogeneity hinting DSC thermogram. In case the exploration of these interactions should be of greater interest in the future, the changes in the microenvironment of the PVM/MA containing extrudates should be monitored. For instance, pH sensitive fluorescence dye or electro spin-resonance probes could serve as capable tools.

Even though PVM/MA did so far not offer any improvements after its implementation, the prospect of its mucoadhesion was still of interest. Thus, an *ex vivo* mucoadhesion test was carried out. The intension of this experiment was to measure the required force to detach extrudates with and without PVM/MA-supplement from oral rat mucosa after a contact time of 1 minute. In this case, the extrusion precursor was prepared in form of 13 mm diameter discs, through pressing with a hydraulic press (IR-compact-press (3.2.2); 100 mg extrusion precursor, 5 t pressure, 40 s pressing time). Oral mucosa was obtained from rats, which were sacrificed during an unrelated animal test. Each sacrificed rat yielded two pieces of oral rat mucosa. Hence, each rat mucosa was treated with a PVM/MA-loaded and a PVM/MA-free disc. These mucosae were stored in ice cooled, closed petri dishes with droplets of neutral phosphate buffered saline, to prevent the tissue from drying out during transport. The measuring was executed with the texture analyzer (Figure 51). A polystyrene plate was placed and fixated on the base table. On the polystyrene plate the mucosa was fixated with needle pins and

wetted with one droplet of neutral phosphate buffered saline. The discs were attached to the bottom of a cylindrical measuring probe with fixative tape. The measuring probe was manually decelerated until it reached the mucosa. After 1 minute incubation time the measurement was started.

Unfortunately, this experiment did not lead to any evaluable results. Macroscopically, for some samples an attachment over short distances was noticeable, but there was no trend in favor of any formulation recognizable. The measured forces were widely spread between 0.2 N to 8.3 N. The measured force path diagrams did not reveal any signs of detachment (e.g. force drops after visible detachment of the mucosa). The deplorable outcome of this experiment had multifactorial causes. First of all, it was unexpectedly difficult to obtain mucosa of approximately the same size. The mucosal area covers just a few square centimeters, and a certain degree of force was required to extract the mucosa. In most cases, the retrieved mucosa did not cover the 13 mm diameter of the discs. Hence, a standardized contact area was not adjustable. Additionally, the histology of the rat oral mucosa could interfere with the mucoadhesion, due to the keratinized epithelium (161), which deviates from human mucosa. Another factor was the sensitivity of the texture analyzer. The necessary detachment forces were expected to be low, which could have interfered with the sensitivity minimum of the device. Also, the experimental setup did not lie within the device's specification. The higher observed detachment forces can in two cases be assigned to the contact between fur remnants and the upper fixative tape, which should have been avoided. Thus, for an improved experimental setup, larger tissue samples of unkeratinized tissue from non-rodents should be utilized in combination with a more suitable device.

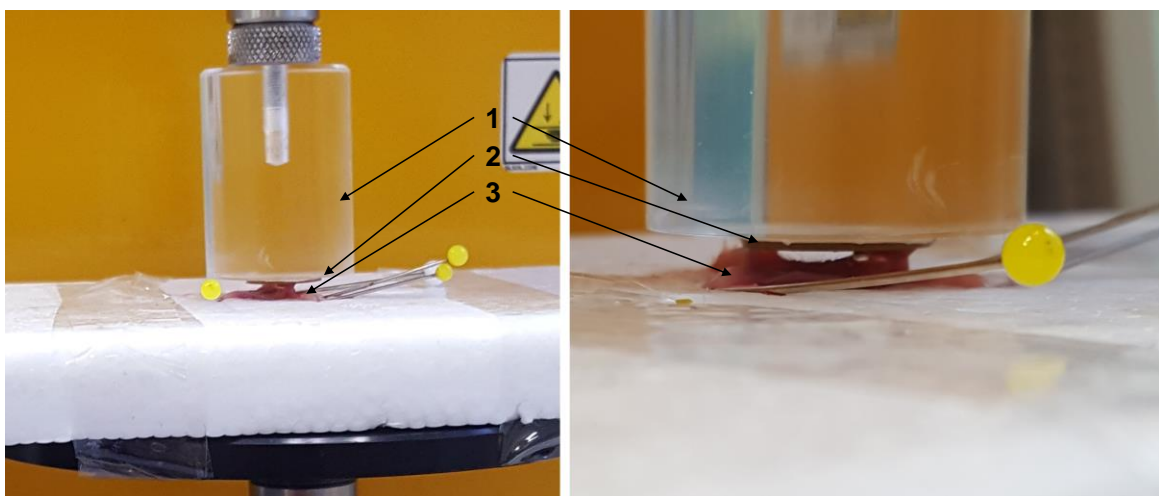


Figure 51: Setup of the mucoadhesion test; 1 - Cylindrical measuring probe; 2 - Test formulation disc (in this case loaded with PVM/MA) attached to the cylindrical measuring head; 3 - rat oral mucosa

At first sight, the hot melt extrusion with supplement of PVM/MA led to serviceable extrudates. But on closer inspection, the 5% PVM/MA content interfered extensively on physical and probably molecular level with the functional extrudate and resulted in an unfavorable product. Crystallization was promoted, the extrudates hardened and an acidic microenvironment can be assumed, which altered the release profile negatively. The microbiological potential was not further explored, due to the adverse impact on the drug release. The exploration of lower mass ratios of PVM/MA (e.g. 2.5%, 1%) could be enticing, but with the unfortunate results from this series of experiments, another mucoadhesive supplement may be more promising

In summary, the PEG-PLGA_{6P}-MLC + 10% PEG extrudates remain the superior prototypes.

5 SUMMARY AND PERSPECTIVES

In the present work, novel tetracycline derivative complexes with sustained activity were explored, and subsequently incorporated into highly flexible extrudates as local drug delivery system for the treatment of periodontitis. During the development of these complexes, oxytetracycline, minocycline and doxycycline were examined towards their capability to form lipophilic complexes with the fatty acid salts magnesium- and calcium stearate.

The purpose of this endeavor was to stabilize the active pharmaceutical ingredients, since they are less susceptible to degradation and epimerization in the form of chelate complexes. The formation of these lipophilic complexes was characterized with UV/Vis-, IR-spectroscopy and microscopy. Thereby, varying capabilities of the tetracyclines to form these complexes were revealed. Minocycline and doxycycline demonstrated equal potential in terms of complex formation. In contrast, oxytetracycline was less capable to form complexes, especially with rising fatty acid salt content. This circumstance possibly derived from the more hydrophilic nature of this tetracycline derivative. Generally, complexes with magnesium stearate were more reliable to form, due to the smaller atom diameter in comparison to calcium. The smaller atom diameter eases the interaction of the divalent cation with the chelating functional groups. Furthermore, the complex formation was dependent on the molar ratio of the two components. Molar ratios of 2:1, 1:1 and 1:2 (tetracycline derivative : fatty acid salt) were examined. The 1:2 ratios emerged as favorable, as they demonstrated homogeneous amorphous structures after drying. The interaction of tetracyclines with polyvalent cations is also recognized as a factor, which can reduce their antimicrobial activity. Hence, a disc diffusion test was carried out, which proved the integrity of their antimicrobial activity after interaction with the fatty acid salts.

From this starting point, the main objective of this work could be pursued. This main objective involved the production of a locally applicable, biodegradable drug delivery system, offering controlled release over several weeks. Ideally, this application form should also be simple to handle, mechanically resilient and uncomplicated to produce. Thus, the fabrication of hot-melt extrudates seemed as promising pathway to fulfill these ambitious aims.

For the hot-melt extrusion minocycline and doxycycline 1:2 complexes were both potent candidates. But the choice fell on the minocycline complexes, due to their broader activity spectrum and superior tissue penetration. The first prototypes, with a diameter of 600 μm , were produced with PLGA as release controlling polymer. They

became the basis for the implementation of additional features. Initially, however, these first extrudates were examined towards their mechanical stability and release properties. They were easy to handle with a tweezer, but did not withstand mechanical stress. Premature material fracture was the main drawback of these extrudates. Their release properties, however, already matched the desired time frame. The minocycline lipid complex (MLC) – PLGA extrudates offered a controlled release of at least 42 days, which was exceptional so far. Also, the MLC was investigated towards its stability in aqueous surrounding in comparison to the pure drug. This experiment demonstrated enhanced stability towards degradation of the MLC and therefore prolonged life time. Additionally, the extrudates were loaded with the fluorescence dye Nile red to monitor water penetration into the prototypes. The results indicated a complete permeation of water into the matrix within a week. To conclude this first development cycle, the extrudates were tested in microbiological assays in comparison to Arestin[®] microspheres, to evaluate their antimicrobial *in vitro* activity. The extrudates were equally effective against newly forming biofilms, but additionally their activity lasted over a longer time period.

Most of the summarized results so far are subject of the first two peer reviewed articles, published in the “International Journal of Pharmaceutics” and in “Pharmaceutics”. Furthermore, the concept of the described lipophilic tetracycline complexes with sustained activity is protected by a patent.

From there on, PEG-PLGA was explored as matrix polymer, to alter the release profile in direction of a higher initial release rate. As well, two plasticizers (GMS and PEG) were incorporated to enhance the mechanical properties. The second development cycle culminated in highly flexible extrudates with excellent mechanical features and the desired release rate. Their phase composition was explored in detail with XRPD and DSC analysis. MLC-PEG-PLGA extrudates, consisting of Expansorb DLG 50 – 6P with supplement of 10% PEG 1500, emerged as the prototype with the most favorable traits. Additionally, 300 µm extrudates with thread-like behavior were successfully produced and characterized. These results are also published in the “International Journal of Pharmaceutics”. After publication, the antimicrobial potential of these prototypes was examined in similar manner to the first generation of extrudates. They performed equally pleasing, but were not superior to the MLC-PLGA extrudates in this regard.

At this point, the extrudates already fulfilled the aspired requirements of the proposed, ideal, local application form for the treatment of periodontitis:

- The API is successfully stabilized by complexation with magnesium stearate
- The extrudates offer a controlled release over a period of at least 42 days
- They consist of a biodegradable matrix
- The production by hot-melt extrusion is eco-friendly, continuous, offers potential for upscaling and free of toxic solvents
- The extrudates are highly flexible, bendable and mechanical resilient
- The mechanical traits enable an easy handling for the dentist and simplify the application process

As just listed, the extrudates unify several advantageous traits and circumvent the drawbacks of several (former) commercial systems. To bring some of them back to mind: lack of biodegradability, short antimicrobial acting periods and complicated application processes were reasons, which led to market withdrawal in the past.

Nevertheless, the further improvement of the extrudates was pursued through the implementation of an additional polymer. PVM/MA was chosen as mucoadhesive supplement to secure the desired position within the gingival sulcus after application. Unfortunately, PVM/MA negatively affected the release profile and also had an undesired impact on the mechanical behavior. Thus, PVM/MA was disclosed as potential mucoadhesive polymer, and the MLC-PEG-PLGA extrudates with 10% PEG supplement remained the final prototypes.

In the future, other mucoadhesive excipients should be tested, if this feature should be implemented into the extrudates. Thereby, focus should be laid on keeping the release profile and the flexible traits unaffected. To substantiate the proposed explanation of PEG-PLGA – PVM/MA interactions, gel permeation chromatography experiments could be useful. Changes in molecular weight, especially after extrusion and subsequent incubation in release medium, could give insight on the ongoing chemical reactions. Also, PEG 1500 concentration and extrusion parameters could be varied for further fine tuning. As well, the compatibility of the lipophilic tetracycline derivative complexes with other polymers offers potential research themes. Regarding the complexes in connection with (PEG-)PLGA, a wide range of application fields besides the therapy of periodontitis is imaginable. For instance, minocycline is discussed as a drug for neurologic applications, due to its pleiotropic effects. Therefore, the complexes could be incorporated into suitable drug delivery systems, like nanoparticles or electrospun fleeces. Preliminary tests in the early phase of this work demonstrated, that the

fabrication of the MLC in other application forms is conceivable. Exemplarily, these unrepresented results revealed a possible fabrication of MLC-PLGA microspheres with the solvent-evaporation method.

However, this work derived from a cooperative project between the Martin-Luther-University Halle-Wittenberg, the Fraunhofer Institute for Cell Therapy and Immunology IZI, the Fraunhofer Institute for Microstructures and Materials IMWS and the University of Bern. During this project, a potent drug delivery system for the local treatment of periodontitis was conceptualized and realized. Currently, this cooperation is making efforts to set the environment for a transfer of these promising drug delivery systems into clinical applications. Thus, these extrudates might already be available to dentists and patients in the near future.

REFERENCES

1. Pihlstrom BL, Michalowicz BS, Johnson NW. Periodontal diseases. *Lancet* [Internet]. 2005;366(9499):1809–20. Available from: <http://www.ncbi.nlm.nih.gov/pubmed/16298220>
2. Könönen E, Kumar PS. Bacteriology of Periodontal Diseases. In: *Molecular Medical Microbiology* [Internet]. Elsevier; 2015. p. 957–68. Available from: <https://linkinghub.elsevier.com/retrieve/pii/B9780123971692000536>
3. Nazir MA. Prevalence of periodontal disease, its association with systemic diseases and prevention. *Int J Health Sci (Qassim)* [Internet]. 2017;1(2):72–80. Available from: <http://ieeexplore.ieee.org/document/4554114/>
4. Paster BJ, Olsen I, Aas JA, Dewhirst FE. The breadth of bacterial diversity in the human periodontal pocket and other oral sites. *Periodontol* 2000. 2006;42(1):80–7.
5. Hojo K, Nagaoka S, Ohshima T, Maeda N. Bacterial Interactions in Dental Biofilm Development. *J Dent Res* [Internet]. 2009 Nov 14;88(11):982–90. Available from: <http://journals.sagepub.com/doi/10.1177/0022034509346811>
6. Jakubovics N, Kolenbrander P. The road to ruin: the formation of disease-associated oral biofilms. *Oral Dis* [Internet]. 2010 Nov;16(8):729–39. Available from: <http://doi.wiley.com/10.1111/j.1601-0825.2010.01701.x>
7. Nobbs AH, Lamont RJ, Jenkinson HF. Streptococcus Adherence and Colonization. *Microbiol Mol Biol Rev* [Internet]. 2009 Sep;73(3):407–50. Available from: <https://mmbbr.asm.org/content/73/3/407>
8. Kolenbrander PE, London J. Adhere today, here tomorrow: oral bacterial adherence. *J Bacteriol* [Internet]. 1993;175(11):3247–52. Available from: <https://jb.asm.org/content/175/11/3247>
9. Marsh PD. Dental plaque: biological significance of a biofilm and community lifestyle. *J Clin Periodontol* [Internet]. 2005 Oct;32(s6):7–15. Available from: <http://doi.wiley.com/10.1111/j.1600-051X.2005.00790.x>
10. Chalmers NI, Palmer RJ, Cisar JO, Kolenbrander PE. Characterization of a *Streptococcus* sp.-*Veillonella* sp. Community Micromanipulated from Dental Plaque. *J Bacteriol* [Internet]. 2008 Dec 15;190(24):8145–54. Available from: <https://jb.asm.org/content/190/24/8145>
11. Holmberg K, Hallander HO. Production of bactericidal concentrations of hydrogen peroxide by *Streptococcus sanguis*. *Arch Oral Biol*. 1973;18(3):423–34.
12. Stingu C-S, Eschrich K, Rodloff AC, Schaumann R, Jentsch H. Periodontitis is associated with a loss of colonization by *Streptococcus sanguinis*. *J Med Microbiol* [Internet]. 2008 Apr 1;57(4):495–9. Available from: <https://www.microbiologyresearch.org/content/journal/jmm/10.1099/jmm.0.47649-0>
13. Darveau RP. Periodontitis: a polymicrobial disruption of host homeostasis. *Nat Rev Microbiol* [Internet]. 2010 Jul 1;8(7):481–90. Available from: <http://www.nature.com/articles/nrmicro2337>

14. Mahanonda R, Pichyangkul S. Toll-like receptors and their role in periodontal health and disease. *Periodontol 2000* [Internet]. 2007 Feb;43(1):41–55. Available from: <http://doi.wiley.com/10.1111/j.1600-0757.2006.00179.x>
15. Ren L, Jin L, Leung WK. Local expression of lipopolysaccharide-binding protein in human gingival tissues. *J Periodontol* [Internet]. 2004 Aug;39(4):242–8. Available from: <http://doi.wiley.com/10.1111/j.1600-0765.2004.00732.x>
16. Lourenço TGB, Heller D, Silva-Boghossian CM, Cotton SL, Paster BJ, Colombo APV. Microbial signature profiles of periodontally healthy and diseased patients. *J Clin Periodontol* [Internet]. 2014 Nov;41(11):1027–36. Available from: <http://doi.wiley.com/10.1111/jcpe.12302>
17. Socransky SS, Haffajee AD, Cugini MA, Smith C, Kent RL. Microbial complexes in subgingival plaque. *J Clin Periodontol* [Internet]. 1998 Feb;25(2):134–44. Available from: <http://doi.wiley.com/10.1111/j.1600-051X.1998.tb02419.x>
18. Hajishengallis G, Lamont RJ. Breaking bad: Manipulation of the host response by *Porphyromonas gingivalis*. *Eur J Immunol* [Internet]. 2014 Feb 8;44(2):328–38. Available from: <https://onlinelibrary.wiley.com/doi/abs/10.1002/eji.201344202>
19. Wang M, Krauss JL, Domon H, Hosur KB, Liang S, Magotti P, et al. Microbial Hijacking of Complement-Toll-Like Receptor Crosstalk. *Sci Signal* [Internet]. 2010 Feb 16;3(109):ra11–ra11. Available from: <https://stke.sciencemag.org/lookup/doi/10.1126/scisignal.2000697>
20. Potempa M, Potempa J, Okroj M, Popadiak K, Eick S, Nguyen K-A, et al. Binding of Complement Inhibitor C4b-Binding Protein Contributes to Serum Resistance of *Porphyromonas gingivalis*. *J Immunol* [Internet]. 2008 Oct 15;181(8):5537–44. Available from: <http://www.jimmunol.org/lookup/doi/10.4049/jimmunol.181.8.5537>
21. Di Benedetto A, Gigante I, Colucci S, Grano M. Periodontal Disease: Linking the Primary Inflammation to Bone Loss. *Clin Dev Immunol* [Internet]. 2013;2013:1–7. Available from: <http://www.hindawi.com/journals/jjir/2013/503754/>
22. Page RC, Korman KS. The pathogenesis of human periodontitis: an introduction. *Periodontol 2000* [Internet]. 1997 Jun;14(1):9–11. Available from: <http://doi.wiley.com/10.1111/j.1600-0757.1997.tb00189.x>
23. Cope G, Cope A. Gingivitis: symptoms, causes and treatment. *Dent Nurs* [Internet]. 2011 Aug;7(8):436–9. Available from: <http://www.magonlineibrary.com/doi/10.12968/denn.2011.7.8.436>
24. Savage A, Eaton KA, Moles DR, Needleman I. A systematic review of definitions of periodontitis and methods that have been used to identify this disease. *J Clin Periodontol* [Internet]. 2009 Jun;36(6):458–67. Available from: <http://doi.wiley.com/10.1111/j.1600-051X.2009.01408.x>
25. Pihlstrom BL. Measurement of Attachment Level in Clinical Trials: Probing Methods. *J Periodontol* [Internet]. 1992 Dec;63(12s):1072–7. Available from: <http://doi.wiley.com/10.1902/jop.1992.63.12s.1072>
26. Genco RJ, Borgnakke WS. Risk factors for periodontal disease. Enersen M, editor. *Periodontol 2000* [Internet]. 2013 Jun 24;62(1):59–94. Available from: <http://www.eurekaselect.com/node/52541>
27. Axelsson P, Lindhe J, Nystrom B. On the prevention of caries and periodontal

- disease. Results of a 15-year longitudinal study in adults. *J Clin Periodontol* [Internet]. 1991 Mar;18(3):182–9. Available from: <http://www.embase.com/search/results?subaction=viewrecord&from=export&id=L21842173%5Cnhttp://elvis.ubvu.vu.nl:9003/vulink?sid=EMBASE&issn=03036979&id=doi:&atitle=On+the+prevention+of+caries+and+periodontal+disease.+Results+of+a+15-year+longitudinal+study+>
28. Tomar SL, Asma S. Smoking-Attributable Periodontitis in the United States: Findings From NHANES III. *J Periodontol* [Internet]. 2000 May;71(5):743–51. Available from: <http://doi.wiley.com/10.1902/jop.2000.71.5.743>
29. Bergström J, Preber H. Tobacco Use as a Risk Factor. *J Periodontol* [Internet]. 1994 May;65(5):545–50. Available from: <http://doi.wiley.com/10.1902/jop.1994.65.5.545>
30. Pitiphat W, Merchant AT, Rimm EB, Joshipura KJ. Alcohol Consumption Increases Periodontitis Risk. *J Dent Res* [Internet]. 2003 Jul 13;82(7):509–13. Available from: <http://journals.sagepub.com/doi/10.1177/154405910308200704>
31. Preshaw PM, Alba AL, Herrera D, Jepsen S, Konstantinidis A, Makrilakis K, et al. Periodontitis and diabetes: a two-way relationship. *Diabetologia* [Internet]. 2012 Jan 6;55(1):21–31. Available from: <http://link.springer.com/10.1007/s00125-011-2342-y>
32. Reners M, Brex M. Stress and periodontal disease. *Int J Dent Hyg* [Internet]. 2007 Nov;5(4):199–204. Available from: <http://doi.wiley.com/10.1111/j.1601-5037.2007.00267.x>
33. Güncü G, Tözüm T, Çaglayan F. Effects of endogenous sex hormones on the periodontium — Review of literature. *Aust Dent J* [Internet]. 2005 Sep;50(3):138–45. Available from: <http://doi.wiley.com/10.1111/j.1834-7819.2005.tb00352.x>
34. Krall EA, Garcia RI, Dawson-Hughes B. Increased risk of tooth loss is related to bone loss at the whole body, hip, and spine. *Calcif Tissue Int* [Internet]. 1996 Dec;59(6):433–7. Available from: <http://link.springer.com/10.1007/BF00369206>
35. Albandar JM. Epidemiology and Risk Factors of Periodontal Diseases. *Dent Clin North Am* [Internet]. 2005 Jul;49(3):517–32. Available from: <https://linkinghub.elsevier.com/retrieve/pii/S0011853205000194>
36. Eke PI, Wei L, Borgnakke WS, Thornton-Evans G, Zhang X, Lu H, et al. Periodontitis prevalence in adults ≥ 65 years of age, in the USA. *Periodontol* 2000 [Internet]. 2016 Oct;72(1):76–95. Available from: <http://doi.wiley.com/10.1111/prd.12145>
37. Hujoel PP, White BA, García RI, Listgarten MA. The dentogingival epithelial surface area revisited. *J Periodontal Res*. 2001;36(1):48–55.
38. Almeida APCPSC, Fagundes NCF, Maia LC, Lima RR. Is there an Association Between Periodontitis and Atherosclerosis in Adults? A Systematic Review. *Curr Vasc Pharmacol* [Internet]. 2018 Sep 10 [cited 2019 Mar 29];16(6):569–82. Available from: <http://www.eurekaselect.com/155333/article>
39. Liccardo D, Cannavo A, Spagnuolo G, Ferrara N, Cittadini A, Rengo C, et al. Periodontal Disease: A Risk Factor for Diabetes and Cardiovascular Disease. *Int J Mol Sci* [Internet]. 2019 Mar 20;20(6):1414. Available from: <https://www.mdpi.com/1422-0067/20/6/1414>

40. Sanz M, Marco del Castillo A, Jepsen S, Gonzalez-Juanatey JR, D'Aiuto F, Bouchard P, et al. Periodontitis and cardiovascular diseases: Consensus report. *J Clin Periodontol* [Internet]. 2020 Mar 3;47(3):268–88. Available from: <https://onlinelibrary.wiley.com/doi/abs/10.1111/jcpe.13189>
41. Tonetti MS, Van Dyke TE. Periodontitis and atherosclerotic cardiovascular disease: consensus report of the Joint EFP/AAP Workshop on Periodontitis and Systemic Diseases. *J Clin Periodontol* [Internet]. 2013 Apr;40(SUPPL. 14):S24–9. Available from: <http://doi.wiley.com/10.1111/jcpe.12089>
42. Potempa J, Mydel P, Koziel J. The case for periodontitis in the pathogenesis of rheumatoid arthritis. *Nat Rev Rheumatol* [Internet]. 2017 Oct 24 [cited 2019 Mar 29];13(10):606–20. Available from: <http://www.nature.com/doi/abs/10.1038/nrrheum.2017.132>
43. Graziani F, Gennai S, Solini A, Petrini M. A systematic review and meta-analysis of epidemiologic observational evidence on the effect of periodontitis on diabetes An update of the EFP-AAP review. *J Clin Periodontol*. 2018;45(2):167–87.
44. Preshaw PM, Taylor JJ, Jaedicke KM, De Jager M, Bikker JW, Selten W, et al. Treatment of periodontitis reduces systemic inflammation in type 2 diabetes. *J Clin Periodontol* [Internet]. 2020;4. Available from: <http://www.ncbi.nlm.nih.gov/pubmed/32106333>
45. Ide M, Harris M, Stevens A, Sussams R, Hopkins V, Culliford D, et al. Periodontitis and Cognitive Decline in Alzheimer's Disease. Garg P, editor. *PLoS One* [Internet]. 2016 Mar 10;11(3):e0151081. Available from: <https://dx.plos.org/10.1371/journal.pone.0151081>
46. Sparks Stein P, Steffen MJ, Smith C, Jicha G, Ebersole JL, Abner E, et al. Serum antibodies to periodontal pathogens are a risk factor for Alzheimer's disease. *Alzheimer's Dement* [Internet]. 2012 May;8(3):196–203. Available from: <http://doi.wiley.com/10.1016/j.jalz.2011.04.006>
47. Holde GE, Jönsson B, Tillberg A, Trovik TA, Oscarson N. Periodontitis Prevalence and Severity in Adults: A Cross-Sectional Study in Norwegian Circumpolar Communities. *J Periodontol*. 2017;88(10):1012–22.
48. Eke PI, Zhang X, Lu H, Wei L, Thornton-Evans G, Greenlund KJ, et al. Predicting Periodontitis at State and Local Levels in the United States. *J Dent Res* [Internet]. 2016 May 4;95(5):515–22. Available from: <http://journals.sagepub.com/doi/10.1177/0022034516629112>
49. Sanz I, Alonso B, Carasol M, Herrera D, Sanz M. Nonsurgical Treatment of Periodontitis. *J Evid Based Dent Pract* [Internet]. 2012 Sep;12(3):76–86. Available from: [http://dx.doi.org/10.1016/S1532-3382\(12\)70019-2](http://dx.doi.org/10.1016/S1532-3382(12)70019-2)
50. Graziani F, Karapetsa D, Alonso B, Herrera D. Nonsurgical and surgical treatment of periodontitis: how many options for one disease? [Internet]. Vol. 75, *Periodontology* 2000. 2017. p. 152–88. Available from: <http://doi.wiley.com/10.1111/prd.12201>
51. Needleman I, Nibali L, Di Iorio A. Professional mechanical plaque removal for prevention of periodontal diseases in adults - systematic review update. *J Clin Periodontol* [Internet]. 2015 Apr;42(S16):S12–35. Available from: <http://doi.wiley.com/10.1111/jcpe.12341>

52. Darcey J, Ashley M. See you in three months! The rationale for the three monthly periodontal recall interval: a risk based approach. *Br Dent J* [Internet]. 2011 Oct 21;211(8):379–85. Available from: <http://dx.doi.org/10.1038/sj.bdj.2011.868>
53. Durstberger G, Bruckmann C, Matejka M. Das Wiener parodontologische Behandlungskonzept, Teil II. Reevaluation – weiterführende Parodontaltherapie (konservativ/chirurgisch) – Recall. *Stomatologie*. 2006;103(2):33–8.
54. Jepsen K, Jepsen S. Antibiotics/antimicrobials: systemic and local administration in the therapy of mild to moderately advanced periodontitis. *Periodontol* 2000 [Internet]. 2016 Jun;71(1):82–112. Available from: <http://doi.wiley.com/10.1111/prd.12121>
55. Goodson JM. Gingival crevice fluid flow. *Periodontol* 2000 [Internet]. 2003 Feb;31:43–54. Available from: <https://doi.org/10.1034/j.1600-0757.2003.03104.x>
56. Litch JM, Encarnacion M, Chen S, Leonard J, Burkoth TL. Use of the polymeric matrix as internal standard for quantitation of in vivo delivery of tetracycline HCl from ActisiteR tetracycline fiber during periodontal treatment. *J Periodontal Res* [Internet]. 1996 Nov;31(8):540–4. Available from: <http://doi.wiley.com/10.1111/j.1600-0765.1996.tb00518.x>
57. Javali MA, Vandana KL. A comparative evaluation of atrigel delivery system (10% doxycycline hyclate) Atridox with scaling and root planing and combination therapy in treatment of periodontitis: A clinical study. *J Indian Soc Periodontol* [Internet]. 2012 Jan [cited 2018 Jun 4];16(1):43–8. Available from: <http://www.ncbi.nlm.nih.gov/pubmed/22628962>
58. Foresight. Periodontitis Treatment. *J Am Dent Assoc* [Internet]. 2001 Jan 1 [cited 2018 May 31];132(1):75. Available from: <http://linkinghub.elsevier.com/retrieve/pii/S0002817714615907>
59. Jouyban A, Fakhree MAA, Shayanfar A. Review of Pharmaceutical Applications of N-Methyl-2-Pyrrolidone. *J Pharm Pharm Sci* [Internet]. 2010 Nov 15;13(4):524. Available from: <https://journals.library.ualberta.ca/jpps/index.php/JPPS/article/view/8257>
60. Holle R, Renggli HH, Böddinghaus B, Bürklin T, Eickholz P, Kim T-S, et al. Non-Surgical Periodontal Therapy With Adjunctive Topical Doxycycline: A Double-Masked, Randomized, Controlled Multicenter Study. II. Microbiological Results. *J Periodontol*. 2005;76(1):66–74.
61. Ligosan Slow Release Produktinformation [Internet]. [cited 2019 Feb 20]. Available from: https://www.kulzer.de/media/webmedia_local/downloads_new/ligosan_4/Ligosan_Produktinformation_DE.pdf
62. Ligosan Slow Release [Internet]. 2017 [cited 2019 Feb 20]. Available from: https://www.kulzer.de/media/webmedia_local/downloads_new/ligosan_4/Fachinfo_Ligosan_Slow_Release_DE.pdf
63. Renvert S, Lessem J, Dahlén G, Lindahl C, Svensson M. Topical minocycline microspheres versus topical chlorhexidine gel as an adjunct to mechanical debridement of incipient peri-implant infections: A randomized clinical trial. *J Clin Periodontol*. 2006;33(5):362–9.
64. OraPharma. ARESTIN Package Insert. OraPharma. 2012;20(2).

65. Stoltze K. Elimination of Elyzol® 25% Dentalgel matrix from periodontal pockets. *J Clin Periodontol*. 1995;22(3):185–7.
66. Fachinformation PerioChip 2,5 mg Insert für Parodontaltaschen [Internet]. 2014 [cited 2018 May 31]. p. 1–3. Available from: http://www.periochip.de/downloads/PerioChip_Fachinformation.pdf
67. Puri K, Dodwad V, Bhat K, Puri N. Effect of controlled-release Periochip™ on clinical and microbiological parameters in patients of chronic periodontitis. *J Indian Soc Periodontol* [Internet]. 2013 Sep [cited 2018 May 31];17(5):605–11. Available from: <http://www.ncbi.nlm.nih.gov/pubmed/24174754>
68. Abrishami M, Iramloo B, Ansari G, Eslami G, Bagheban AA, Anaraki M. The effect of locally delivered xanthan-based CHLO-SITE gel with scaling and root planning in the treatment of chronic periodontitis: microbial findings. *Dent Res J (Isfahan)*. 2009;5(2):47–52.
69. Dinarvand R, Jafarzadeh Kashi T, Eskandarion, Esfandyari-Manesh, Samadi, Atyabi F, et al. Improved drug loading and antibacterial activity of minocycline-loaded PLGA nanoparticles prepared by solid/oil/water ion pairing method. *Int J Nanomedicine* [Internet]. 2012 Jan;7:221. Available from: <http://www.dovepress.com/improved-drug-loading-and-antibacterial-activity-of-minocycline-loaded-peer-reviewed-article-IJN>
70. Mercado N, Bhatt P, Sutariya V, Florez FLE, Pathak Y V. Application of Nanoparticles in Treating Periodontitis: Preclinical and Clinical Overview. In: Pathak Y V, editor. *Surface Modification of Nanoparticles for Targeted Drug Delivery* [Internet]. Cham: Springer International Publishing; 2019. p. 467–80. Available from: https://doi.org/10.1007/978-3-030-06115-9_24
71. Ibrahim AI, Moodley D, Petrik L, Patel N. Use of antibacterial nanoparticles in Endodontics. *South African Dent J*. 2017;72(3):105–12.
72. Akıncıbay H, Şenel S, Yetkin Ay Z. Application of chitosan gel in the treatment of chronic periodontitis. *J Biomed Mater Res Part B Appl Biomater* [Internet]. 2007 Feb;80B(2):290–6. Available from: <http://doi.wiley.com/10.1002/jbm.b.30596>
73. Steenberghe D Van, Rosling B, Söder P., Landry RG, Velden U van der, Timmerman MFT, et al. A 15-Month Evaluation of the Effects of Repeated Subgingival Minocycline in Chronic Adult Periodontitis. *J Periodontol*. 1999;70(6):657–67.
74. Do MP, Neut C, Metz H, Delcourt E, Mäder K, Siepmann J, et al. In-situ forming composite implants for periodontitis treatment: How the formulation determines system performance. *Int J Pharm*. 2015;486(1–2):38–51.
75. Agossa K, Lizambard M, Rongthong T, Delcourt-Debruyne E, Siepmann J, Siepmann F. Physical key properties of antibiotic-free, PLGA/HPMC-based in-situ forming implants for local periodontitis treatment. *Internanational J Pharm*. 2017;521(1–2):282–93.
76. Ma Y, Song J, Almassri HNS, Zhang D, Zhang T, Cheng Y, et al. Minocycline-loaded PLGA electrospun membrane prevents alveolar bone loss in experimental peridontitis. *Drug Deliv* [Internet]. 2020;27(1):151–60. Available from: <https://doi.org/10.1080/10717544.2019.1709921>
77. Griffin MO, Fricovsky E, Ceballos G, Villarreal F. Tetracyclines: a pleiotropic family of compounds with promising therapeutic properties. Review of the

- literature. *Am J Physiol Physiol* [Internet]. 2010 Sep;299(3):C539–48. Available from: <https://www.physiology.org/doi/10.1152/ajpcell.00047.2010>
78. Ian C, Marilyn R. Tetracycline Antibiotics: Mode of Action, Applications, Molecular Biology, and Epidemiology of Bacterial Resistance. *Microbiol Mol Biol Rev.* 2001;65(3):232–60.
79. Dowling AM, Dwyer JO, Adley C. Antibiotics : Mode of action and mechanisms of resistance . Antibiotics : Mode of action and mechanisms of resistance. In: *Antimicrobial Research: Novel bioknowledge and educational programs* [Internet]. 2017. p. 536–45. Available from: <https://www.researchgate.net/publication/317381477%0AAntibiotics>:
80. Chopra I, Hawkey PM, Hinton M. Tetracyclines, molecular and clinical aspects. *J Antimicrob Chemother* [Internet]. 1992;29(3):245–77. Available from: <https://academic.oup.com/jac/article-lookup/doi/10.1093/jac/29.3.245>
81. Garrido-Mesa N, Zarzuelo A, Gálvez J. Minocycline: far beyond an antibiotic. *Br J Pharmacol* [Internet]. 2013 May;169(2):337–52. Available from: <http://doi.wiley.com/10.1111/bph.12139>
82. Agwuh KN, MacGowan A. Pharmacokinetics and pharmacodynamics of the tetracyclines including glycylicyclines. *J Antimicrob Chemother.* 2006;58(2):256–65.
83. Honnorat-Benabbou VC, Lebugle AA, Sallek B, Duffaut-Lagarrigue D. Stability study of tetracyclines with respect to their use in slow release systems. *J Mater Sci Mater Med.* 2001;12(2):107–10.
84. Lauro MF. Metallic soaps. *Oil Fat Ind* [Internet]. 1928 Nov;5(11):329–32. Available from: <http://doi.wiley.com/10.1007/BF02562161>
85. Schmidt PC, Lang S. *Pharmazeutische Hilfsstoffe* [Internet]. Eschborn: Govi-Verlag Pharmazeutischer Verlag; 2013. 258–262 p. Available from: www.govi-verlag.de
86. Makadia HK, Siegel SJ. Poly Lactic-co-Glycolic Acid (PLGA) as Biodegradable Controlled Drug Delivery Carrier. *Polymers (Basel)* [Internet]. 2011 Aug 26;3(3):1377–97. Available from: <http://www.mdpi.com/2073-4360/3/3/1377>
87. Fredenberg S, Wahlgren M, Reslow M, Axelsson A. The mechanisms of drug release in poly(lactic-co-glycolic acid)-based drug delivery systems - A review. *Int J Pharm* [Internet]. 2011;415(1–2):34–52. Available from: <http://dx.doi.org/10.1016/j.ijpharm.2011.05.049>
88. Mäder K. RESOMER® - Biodegradable Polymers for Sutures , Medical Devices , Drug Delivery Systems and Tissue Engineering. 2013;(1):1–5. Available from: <https://www.sigmaaldrich.com/content/dam/sigma-aldrich/articles/material-matters/pdf/resomer-biodegradeable-polymers.pdf>
89. Balouiri M, Sadiki M, Ibsouda SK. Methods for in vitro evaluating antimicrobial activity: A review. *J Pharm Anal* [Internet]. 2016;6(2):71–9. Available from: <http://dx.doi.org/10.1016/j.jpha.2015.11.005>
90. EUCAST EC on AST. Antimicrobial susceptibility testing EUCAST disk diffusion method - Version 7.0. *Eur Soc Clin Microbiol Infect Diseases* [Internet]. 2019;0(January):1–21. Available from: www.eucast.org

91. Holmkvist AD, Friberg A, Nilsson UJ, Schouenborg J. Hydrophobic ion pairing of a minocycline/Ca²⁺/AOT complex for preparation of drug-loaded PLGA nanoparticles with improved sustained release. *Int J Pharm* [Internet]. 2016;499(1–2):351–7. Available from: <http://dx.doi.org/10.1016/j.ijpharm.2016.01.011>
92. Schmid J, Kirchberg M, Sarembe S, Kiesow A, Sculean A, Mäder K, et al. In Vitro Evaluation of Antimicrobial Activity of Minocycline Formulations for Topical Application in Periodontal Therapy. *Pharmaceutics* [Internet]. 2020 Apr 13;12(4):352. Available from: <https://www.mdpi.com/1999-4923/12/4/352>
93. Pirracchio L, Joos A, Luder N, Sculean A, Eick S. Activity of taurolidine gels on ex vivo periodontal biofilm. *Clin Oral Investig*. 2018;22(5):2031–7.
94. Kwasny SM, Opperman TJ. Static biofilm cultures of Gram-positive pathogens grown in a microtiter format used for anti-biofilm drug discovery. *Curr Protoc Pharmacol*. 2010;(SUPPL. 50):1–23.
95. Pettit RK, Weber CA, Kean MJ, Hoffmann H, Pettit GR, Tan R, et al. Microplate Alamar Blue Assay for *Staphylococcus epidermidis* Biofilm Susceptibility Testing Downloaded from <http://aac.asm.org/> on January 29 , 2017 by Cochin University of Science and Technology. *Antimicrob Agents Chemother*. 2005;49(7):2612–7.
96. Kirchberg M, Eick S, Buchholz M, Kiesow A, Sarembe S, Mäder K. Extrudates of lipophilic tetracycline complexes: A new option for periodontitis therapy. *Int J Pharm* [Internet]. 2019 Dec;572(September):118794. Available from: <https://doi.org/10.1016/j.ijpharm.2019.118794>
97. Kiesow A, Buchholz M, Sarembe S, Mäder K, Kirchberg M, Eick S. Tetracycline Complexes With Sustained Activity. WO 2020/089249 A1, 2020.
98. Chow KT, Chan LW, Heng PWS. Formulation of hydrophilic non-aqueous gel: Drug stability in different solvents and rheological behavior of gel matrices. *Pharm Res*. 2008;25(1):207–17.
99. chelation. In: *IUPAC Compendium of Chemical Terminology* [Internet]. Research Triangle Park, NC: IUPAC; 1994. p. 2014. Available from: <http://goldbook.iupac.org/C01012.html>
100. Slater JC. Atomic Radii in Crystals. *J Chem Phys* [Internet]. 1964 Nov 15;41(10):3199–204. Available from: <http://aip.scitation.org/doi/10.1063/1.1725697>
101. Martell AE, Calvin M. *Chemistry of the Metal Chelate Compounds*. Latimer WM, editor. Englewood Cliffs, N.J.: Prentice-Hall, Inc.; 1952. 19–75 p.
102. Zhang Z, Wang Z, Nong J, Nix CA, Ji HF, Zhong Y. Metal ion-assisted self-assembly of complexes for controlled and sustained release of minocycline for biomedical applications. *Biofabrication*. 2015;7(1).
103. Naz S, Khan KA, Zubairi SA. In vitro studies of the loss of antibacterial activity of oxytetracycline in presence of Ca(II) or Mg(II) ions. *Arzneimittelforschung* [Internet]. 1996 Jul [cited 2018 Mar 6];46(7):701–4. Available from: <http://www.ncbi.nlm.nih.gov/pubmed/8842342>
104. Dickert H, Machka K, Braveny I. The uses and limitations of disc diffusion in the antibiotic sensitivity testing of bacteria. *Infection*. 1981;9(1):18–24.

105. Di Caprio R, Lembo S, Di Costanzo L, Balato A, Monfrecola G. Anti-inflammatory properties of low and high doxycycline doses: An in vitro study. *Mediators Inflamm*. 2015;2015.
106. Garrido-Mesa N, Zarzuelo A, Gálvez J. What is behind the non-antibiotic properties of minocycline? *Pharmacol Res* [Internet]. 2013;67(1):18–30. Available from: <http://dx.doi.org/10.1016/j.phrs.2012.10.006>
107. Cunha BA, Baron J, Cunha CB. Similarities and differences between doxycycline and minocycline: clinical and antimicrobial stewardship considerations. *Eur J Clin Microbiol Infect Dis*. 2018;37(1):15–20.
108. Pas T, Bergonzi A, Michiels E, Rousseau F, Schymkowitz J, Koekoekx R, et al. Preparation of Amorphous Solid Dispersions by Cryomilling: Chemical and Physical Concerns Related to Active Pharmaceutical Ingredients and Carriers. *Mol Pharm*. 2020;
109. Adrjanowicz K, Kaminski K, Grzybowska K, Hawelek L, Paluch M, Gruszka I, et al. Effect of cryogrinding on chemical stability of the sparingly water-soluble drug furosemide. *Pharm Res*. 2011;28(12):3220–36.
110. Dooley KJ. (19) United States (12) Patent Application Publication (10) Pub . No . : US 2012 / 0304577 A1 Patent Application Publication. 2012;1(19).
111. Patil H, Tiwari R V., Repka MA. Hot-Melt Extrusion: from Theory to Application in Pharmaceutical Formulation. *AAPS PharmSciTech*. 2016;17(1):20–42.
112. Tiwari R V., Patil H, Repka MA. Contribution of hot-melt extrusion technology to advance drug delivery in the 21st century. *Expert Opin Drug Deliv* [Internet]. 2016;13(3):451–64. Available from: <http://dx.doi.org/10.1517/17425247.2016.1126246>
113. Madan S, Madan S. Hot melt extrusion and its pharmaceutical applications. *Asian J Pharm Sci*. 2012;7(2):123–33.
114. Greenstein G, Tonetti M. The role of controlled drug delivery for periodontitis. The Research, Science and Therapy Committee of the American Academy of Periodontology. *J Periodontol* [Internet]. 2000 Jan;71(1):125–40. Available from: <http://doi.wiley.com/10.1902/jop.2000.71.1.125>
115. Minocycline - DrugBank [Internet]. [cited 2020 Mar 2]. Available from: <https://www.drugbank.ca/drugs/DB01017>
116. Biodegradable Polymers | Sigma-Aldrich [Internet]. [cited 2020 Apr 9]. Available from: <https://www.sigmaaldrich.com/technical-documents/articles/materials-science/polymer-science/resomer.html#products>
117. Zbinovsky V, Chrekian GP. Minocycline. In: *Analytical Profile of Drug Substances* [Internet]. 1977. p. 323–39. Available from: <https://linkinghub.elsevier.com/retrieve/pii/S0099542808603482>
118. Schädlich A, Kempe S, Mäder K. Non-invasive in vivo characterization of microclimate pH inside in situ forming PLGA implants using multispectral fluorescence imaging. *J Control Release* [Internet]. 2014;179(1):52–62. Available from: <http://dx.doi.org/10.1016/j.jconrel.2014.01.024>
119. Jain N, Jain GK, Ahmad FJ, Khar RK. Validated stability-indicating densitometric thin-layer chromatography: Application to stress degradation studies of

- minocycline. *Anal Chim Acta*. 2007;599(2):302–9.
120. Page RC, Offenbacher S, Schroeder HE, Seymour GJ, Kornman KS. Advances in the pathogenesis of periodontitis: Summary of developments, clinical implications and future directions. *Periodontol 2000*. 1997;14(1):216–48.
 121. Greenspan P, Fowler SD. Spectrofluorometric studies of the lipid probe, Nile red. *J Lipid Res*. 1985;26(7):781–9.
 122. Chaudhuri KD. Concentration quenching of fluorescence in solutions. *Zeitschrift für Phys* [Internet]. 1959 Feb;154(1):34–42. Available from: <http://link.springer.com/10.1007/BF01337496>
 123. Hamann S, Kiilgaard JF, Litman T, Alvarez-Leefmans FJ, Winther BR, Zeuthen T. Measurement of Cell Volume Changes by Fluorescence Self-Quenching. *J Fluoresc*. 2002;12(2):139–45.
 124. Roy R, Tiwari M, Donelli G, Tiwari V. Strategies for combating bacterial biofilms: A focus on anti-biofilm agents and their mechanisms of action. *Virulence* [Internet]. 2018 Dec 31;9(1):522–54. Available from: <https://doi.org/10.1080/21505594.2017.1313372>
 125. John MT, Michalowicz BS, Kotsakis GA, Chu H. Network meta-analysis of studies included in the Clinical Practice Guideline on the nonsurgical treatment of chronic periodontitis. *J Clin Periodontol*. 2017;44(6):603–11.
 126. Kassem AA, Ismail FA, Naggar VF, Aboulmagd E. Comparative study to investigate the effect of meloxicam or minocycline HCl in situ gel system on local treatment of periodontal pockets. *AAPS PharmSciTech*. 2014;15(4):1021–8.
 127. Scholz M, Reske T, Böhmer F, Hornung A, Grabow N, Lang H. In vitro chlorhexidine release from alginate based microbeads for periodontal therapy. *PLoS One*. 2017;12(10):1–19.
 128. Tew JG, Marshall DR, Burmeister JA, Ranney RR. Relationship between gingival crevicular fluid and serum antibody titers in young adults with generalized and localized periodontitis. *Infect Immun* [Internet]. 1985;49(3):487–93. Available from: <https://iai.asm.org/content/49/3/487>
 129. Tonetti M, Cugini MA, Goodson JM. Zero-order delivery with periodontal placement of tetracycline-loaded ethylene vinyl acetate fibers. *J Periodontal Res* [Internet]. 1990 Jul;25(4):243–9. Available from: <http://doi.wiley.com/10.1111/j.1600-0765.1990.tb00911.x>
 130. Kim T-S, Klimpel H, Fiehn W, Eickholz P. Comparison of the pharmacokinetic profiles of two locally administered doxycycline gels in crevicular fluid and saliva. *J Clin Periodontol* [Internet]. 2004 Apr;31(4):286–92. Available from: <http://doi.wiley.com/10.1111/j.0303-6979.2004.00494.x>
 131. Sakellari D, Goodson JM, Socransky SS, Kolokotronis A, Konstantinidis A. Concentration of 3 tetracyclines in plasma, gingival crevice fluid and saliva. *J Clin Periodontol* [Internet]. 2000 Jan;27(1):53–60. Available from: <http://doi.wiley.com/10.1034/j.1600-051x.2000.027001053.x>
 132. Brayton JJ, Yang Q, Nakkula RJ, Walters JD. An In Vitro Model of Ciprofloxacin and Minocycline Transport by Oral Epithelial Cells. *J Periodontol* [Internet]. 2002 Nov;73(11):1267–72. Available from: <http://doi.wiley.com/10.1902/jop.2002.73.11.1267>

133. Walters JD, Nakkula RJ, Maney P. Modulation of Gingival Fibroblast Minocycline Accumulation by Biological Mediators. *J Dent Res* [Internet]. 2005 Apr 11;84(4):320–3. Available from: <http://journals.sagepub.com/doi/10.1177/154405910508400405>
134. Gentile P, Frongia ME, Cardellach M, Miller CA, Stafford GP, Leggett GJ, et al. Functionalised nanoscale coatings using layer-by-layer assembly for imparting antibacterial properties to polylactide-co-glycolide surfaces. *Acta Biomater* [Internet]. 2015;21:35–43. Available from: <http://dx.doi.org/10.1016/j.actbio.2015.04.009>
135. Kłodzińska SN, Wan F, Jumaa H, Sternberg C, Rades T, Nielsen HM. Utilizing nanoparticles for improving anti-biofilm effects of azithromycin: A head-to-head comparison of modified hyaluronic acid nanogels and coated poly (lactic-co-glycolic acid) nanoparticles. *J Colloid Interface Sci* [Internet]. 2019 Nov;555:595–606. Available from: <https://linkinghub.elsevier.com/retrieve/pii/S0021979719309051>
136. Han C, Goodwine J, Romero N, Steck KS, Sauer K, Doiron A. Enzyme-encapsulating polymeric nanoparticles: A potential adjunctive therapy in *Pseudomonas aeruginosa* biofilm-associated infection treatment. *Colloids Surfaces B Biointerfaces* [Internet]. 2019;184(March):110512. Available from: <https://doi.org/10.1016/j.colsurfb.2019.110512>
137. Gao Z, Song M, Liu RL, Shen Y, Ward L, Cole I, et al. Improving in vitro and in vivo antibacterial functionality of Mg alloys through micro-alloying with Sr and Ga. *Mater Sci Eng C* [Internet]. 2019;104(March):109926. Available from: <https://doi.org/10.1016/j.msec.2019.109926>
138. Nguyen NYT, Grelling N, Wetteland CL, Rosario R, Liu H. Antimicrobial Activities and Mechanisms of Magnesium Oxide Nanoparticles (nMgO) against Pathogenic Bacteria, Yeasts, and Biofilms. *Sci Rep*. 2018;8(1):1–23.
139. Kirchberg M, Eick S, Buchholz M, Rosche F, Kiesow A, Sarembe S, et al. Controlled release minocycline-lipid-complex extrudates for the therapy of periodontitis with enhanced flexibility. *Int J Pharm* [Internet]. 2020 Aug 30 [cited 2020 Jul 2];586:119578. Available from: <https://linkinghub.elsevier.com/retrieve/pii/S0378517320305627>
140. Desai D, Sandhu H, Shah N, Malick W, Zia H, Phuapradit W, et al. Selection of Solid-State Plasticizers as Processing Aids for Hot-Melt Extrusion. *J Pharm Sci* [Internet]. 2018;107(1):372–9. Available from: <https://doi.org/10.1016/j.xphs.2017.09.004>
141. Lehner E, Gündel D, Liebau A, Plontke S, Mäder K. Intracochlear PLGA based implants for dexamethasone release: Challenges and solutions. *Int J Pharm X* [Internet]. 2019 Dec;1(May):100015. Available from: <https://doi.org/10.1016/j.ijpx.2019.100015>
142. Witt C, Mäder K, Kissel T. The degradation, swelling and erosion properties of biodegradable implants prepared by extrusion or compression moulding of poly(lactide-co-glycolide) and ABA triblock copolymers. *Biomaterials*. 2000;21(9).
143. PLA & PLGA Biodegradable Polymers [Internet]. 2018 [cited 2019 Dec 9]. Available from: <https://www.sigmaaldrich.com/safc/actives-formulations/pla-plga.html>

144. Swaminathan V, Kildsig DO. An examination of the moisture sorption characteristics of commercial magnesium stearate. *AAPS PharmSciTech*. 2001;2(4).
145. Reddy MJ, Kumar JS, Subba Rao U V., Chu PP. Structural and ionic conductivity of PEO blend PEG solid polymer electrolyte. *Solid State Ionics*. 2006;
146. Northcutt LA, Orski S V., Migler KB, Kotula AP. Effect of processing conditions on crystallization kinetics during materials extrusion additive manufacturing. *Polym (United Kingdom)* [Internet]. 2018;154(September):182–7. Available from: <https://doi.org/10.1016/j.polymer.2018.09.018>
147. Crowley MM, Zhang F, Repka MA, Thumma S, Upadhye SB, Kumar Battu S, et al. Pharmaceutical Applications of Hot-Melt Extrusion: Part I. *Drug Dev Ind Pharm* [Internet]. 2007 Jan 26;33(9):909–26. Available from: <http://www.tandfonline.com/doi/full/10.1080/03639040701498759>
148. Shawe J, Riesen R, Widmann J, Schubnell M. UserCom - Information for users of METTLER TOLEDO thermal analysis systems. Mettler Toledo. 2000. p. 1–28.
149. Imming C. Minocyclin [Internet]. Böckler F, Dill B, Dingerdissen U, Eisenbrand G, Faupel F, Fugmann B, et al., editors. Thieme Gruppe PP - Stuttgart; 2007. Available from: <https://roempp.thieme.de/lexicon/RD-13-02563>
150. Dubinskaya VA, Polyakov NA, Suponitskii YL, Dement'Eva NN, Bykov VA. Studies of moisture exchange between stearic acid, calcium stearate, and magnesium stearate. *Pharm Chem J*. 2010;44(2):89–93.
151. Wootton M, MacGowan AP, Howe RA. Towards better antimicrobial susceptibility testing: impact of the Journal of Antimicrobial Chemotherapy. *J Antimicrob Chemother* [Internet]. 2017 Feb 23;72(2):323–9. Available from: <https://academic.oup.com/jac/article-lookup/doi/10.1093/jac/dkw494>
152. Bloomfield SF, Looney E. Evaluation of the repeatability and reproducibility of European suspension test methods for antimicrobial activity of disinfectants and antiseptics. *J Appl Bacteriol* [Internet]. 1992 Jul;73(1):87–93. Available from: <http://doi.wiley.com/10.1111/j.1365-2672.1992.tb04975.x>
153. Smita M, Ramandeep D, Mukund K. A Review Of Denture Adhesives Used In The Dental Profession. *Ann Essences Dent*. 2010;2(3):129–33.
154. Yoncheva K, Gómez S, Campanero MA, Gamazo C, Irache JM. Bioadhesive properties of pegylated nanoparticles. *Expert Opin Drug Deliv*. 2005;2(2):205–18.
155. Wang Q, Li C, Ren T, Chen S, Ye X, Guo H, et al. Poly(vinyl methyl ether/maleic anhydride)-Doped PEG-PLA Nanoparticles for Oral Paclitaxel Delivery to Improve Bioadhesive Efficiency. *Mol Pharm*. 2017;14(10):3598–608.
156. León-Rodríguez L, Leiro-Vidal J, Blanco-Méndez J, Luzardo-Álvarez A. Incorporation of PVMMA to PLGA MS enhances lectin grafting and their in vitro activity in macrophages. *Int J Pharm*. 2010;402(1–2):165–74.
157. Burnett CL, Bergfeld WF, Belsito D V., Hill RA, Klaassen CD, Liebler DC, et al. Final report of the Amended Safety Assessment of PVM/MA copolymer and its related salts and esters as used in cosmetics. *Int J Toxicol*. 2011;30(5 Suppl).

158. Yoncheva K, Lizarraga E, Irache JM. Pegylated nanoparticles based on poly(methyl vinyl ether-co-maleic anhydride): Preparation and evaluation of their bioadhesive properties. *Eur J Pharm Sci.* 2005;24(5):411–9.
159. Elizondo E, Sala S, Imbuluzqueta E, González D, Blanco-Prieto MJ, Gamazo C, et al. High Loading of Gentamicin in Bioadhesive PVM/MA Nanostructured Microparticles Using Compressed Carbon-Dioxide. *Pharm Res* [Internet]. 2011 Feb 2;28(2):309–21. Available from: <http://link.springer.com/10.1007/s11095-010-0248-x>
160. Duque L, Körber M, Bodmeier R. Impact of change of matrix crystallinity and polymorphism on ovalbumin release from lipid-based implants. *Eur J Pharm Sci* [Internet]. 2018;117(2017):128–37. Available from: <https://doi.org/10.1016/j.ejps.2018.02.019>
161. Thirion-Delalande C, Gervais F, Fisch C, Cuiné J, Baron-Bodo V, Moingeon P, et al. Comparative analysis of the oral mucosae from rodents and non-rodents: Application to the nonclinical evaluation of sublingual immunotherapy products. Ryffel B, editor. *PLoS One* [Internet]. 2017 Sep 8;12(9):e0183398. Available from: <https://dx.plos.org/10.1371/journal.pone.0183398>

DEUTSCHE ZUSAMMENFASSUNG

In der vorliegenden Arbeit wurden neue Tetracyclinderivat-Komplexe mit anhaltender Aktivität erforscht und nachfolgend in hochflexible Extrudate als Drug Delivery System zur lokalen Behandlung von Parodontitis eingearbeitet. Während der Entwicklung dieser Komplexe wurden Oxytetracyclin, Minocyclin und Doxycyclin hinsichtlich ihrer Fähigkeit zur Komplexbildung mit den Fettsäuresalzen Magnesium- und Calciumstearat untersucht.

Der Zweck dieses Unterfangens war die Stabilisierung der Arzneistoffe, da sie in ihrer komplexierten Chelat-Form weniger anfällig für Abbau und Epimerisierung sind. Die Bildung dieser lipophilen Komplexe wurde mittels UV/Vis-, IR-Spektroskopie und Mikroskopie charakterisiert. Dabei zeigten sich erhebliche Unterschiede in der Neigung der Tetracycline, Komplexe zu bilden. Minocyclin und Doxycyclin zeigten ähnliches Potential in Hinblick auf die Komplexbildung. Im Gegensatz dazu war Oxytetracyclin weniger in der Lage Komplexe zu bilden, besonders mit steigendem Fettsäureanteil. Diesem Umstand liegt wahrscheinlich die hydrophilere Natur dieses Tetracyclinderivats zugrunde. Generell bildeten sich Komplexe mit Magnesiumstearat verlässlicher. Der Grund dafür lag in Magnesiums geringerem Atomradius im Vergleich zu Calcium. Dieser kleinere Atomradius vereinfachte die Interaktion des divalenten Kations mit den chelatisierenden funktionellen Gruppen. Weiterhin war die Komplexbildung abhängig vom molaren Verhältnis der beiden Komponenten. Die molaren Verhältnisse von 2:1, 1:1 und 1:2 (Tetracyclinderivat : Fettsäuresalz) wurden näher betrachtet. Dabei erwiesen sich die 1:2 Verhältnisse als vorteilhaft, da sie nach der Trocknung homogene, amorphe Strukturen aufwiesen. Interaktionen zwischen Tetracyclinen und polyvalenten Kationen sind auch als ein Faktor bekannt, der zu einer Reduktion der antimikrobiellen Aktivität führen kann. Aufgrund dessen wurde ein Disc Diffusion Test durchgeführt, der die Aktivität der Tetracycline auch nach der Interaktion mit den Fettsäuresalzen sicherstellen sollte.

Nachdem diese Vorarbeiten abgeschlossen wurden, konnte das Hauptziel der Arbeit verfolgt werden. Dies umfasste die Produktion eines lokal applizierbaren, bioabbaubaren Drug Delivery Systems, das über mehrere Wochen kontrolliert freisetzt. Idealerweise sollte die Applikationsform einfach in der Handhabung, mechanisch belastbar und unkompliziert zu produzieren sein. Für die Verwirklichung dieser ambitionierten Ziele wurde die Schmelzextrusion als Produktionsverfahren ausgewählt.

Für die Schmelzextrusion waren sowohl die Minocyclin- als auch die Doxycyclin-Komplexe im 1:2 Verhältnis vielversprechende Kandidaten. Aber die Wahl fiel

schließlich auf die Minocyclin-Komplexe aufgrund ihres breiteren Wirksamkeitsspektrums und der überlegenen Gewebepenetration. Die ersten Prototypen mit einem Durchmesser von 600 µm wurden mit PLGA als freisetzungskontrollierendes Polymer produziert. Damit wurde die Basis für die Implementierung weiterer Eigenschaften geschaffen. Jedoch wurden diese ersten Extrudate zunächst hinsichtlich ihrer mechanischen Stabilität und ihres Freisetzungsverhaltens untersucht. Mit einer Pinzette waren sie einfach zu handhaben, aber sie hielten mechanischer Beanspruchung nicht ausreichend stand. Frühzeitiger Materialbruch war der größte Nachteil dieser Extrudate. Jedoch entsprach ihr Freisetzungsverhalten grundsätzlich dem angestrebten Zeitfenster. Die Minocyclin-Lipid-Komplex (MLC) – PLGA Extrudate boten eine kontrollierte Freisetzung über 42 Tage, was bisher kein anderes Drug Delivery System erreicht hatte. Weiterhin wurde der MLC auf seine Stabilität in wässriger Umgebung überprüft. Dieses Experiment demonstrierte eine verbesserte Stabilität des MLC im Vergleich zum reinen Arzneistoff gegenüber Degradation und somit eine längere Haltbarkeit. Zusätzlich wurden diese Extrudate mit dem Fluoreszenzfarbstoff Nilrot beladen, um die Penetration von Wasser in die Prototypen zu überwachen. Die Ergebnisse wiesen auf eine vollständige Permeation von Wasser in die Matrix innerhalb einer Woche hin. Um diesen ersten Entwicklungszyklus abzuschließen, wurden die Extrudate im Vergleich mit Arestin® Mikropartikeln in mikrobiologischen Assays getestet, um ihre antimikrobielle *in vitro*-Aktivität zu bewerten. Die Extrudate stellten sich als gleichwertig effektiv gegen sich neu bildende Biofilme heraus und zusätzlich hielt ihre Aktivität länger an.

Die meisten der bisher zusammengefassten Resultate sind Inhalt der zwei ersten im Peer-Review begutachteten Artikel, die im „International Journal of Pharmaceutics“ und in „Pharmaceutics“ publiziert wurden. Weiterhin ist das Konzept der lipophilen Tetracyclin Komplexe mit anhaltender Aktivität durch ein Patent geschützt.

Von hier an wurde PEG-PLGA als Matrix-Polymer untersucht, um das Freisetzungsprofil auf eine höhere Initialfreisetzung anzupassen. Ebenso wurden zwei Weichmacher (GMS und PEG) eingearbeitet, um die mechanischen Eigenschaften zu verbessern. Der zweite Entwicklungszyklus gipfelte in hochflexiblen Extrudaten mit exzellenten mechanischen Eigenschaften und der gewünschten Freisetzungsrate von 42 Tagen. Ihre innere Zusammensetzung wurde mittels XRPD und DSC-Analyse detailliert aufgeschlüsselt. MLC-PEG-PLGA Extrudate, bestehend aus Expansorb DLG 50 – 6P mit Zusatz von 10% PEG 1500, erwiesen sich als der Prototyp mit den geeignetsten Eigenschaften. Zusätzlich wurden 300 µm Extrudate mit fadenartigen

Eigenschaften erfolgreich produziert und charakterisiert. Diese Resultate sind ebenfalls im „International Journal of Pharmaceutics“ publiziert. Nach der Publikation wurde das antimikrobielle Potential dieser Prototypen ebenfalls noch in gleicher Weise untersucht, wie es mit den Extrudaten der ersten Generation geschah. Sie zeigten eine gleichwertig zufriedenstellende Leistung, aber waren den MLC-PLGA-Extrudaten in dieser Hinsicht nicht überlegen.

An diesem Punkt erfüllten die Extrudate bereits die angestrebten Anforderungen der vorgetragenen, idealen, lokalen Applikationsform zur Behandlung von Parodontitis:

- Der Arzneistoff ist durch Komplexierung mit Magnesiumstearat erfolgreich stabilisiert
- Die Extrudate bieten eine kontrollierte Freisetzung über einen Zeitraum von mindestens 42 Tagen
- Sie bestehen aus einer bioabbaubaren Matrix
- Die Produktion mittels Schmelzextrusion ist umweltfreundlich, kontinuierlich, bietet Potential für Up-Scaling und ist frei von toxischen Lösungsmitteln
- Die Extrudate sind hochflexibel, biegsam und mechanisch widerstandsfähig
- Die mechanischen Eigenschaften ermöglichen eine unkomplizierte Handhabung für den Zahnarzt und vereinfachen die Applikation

Wie gerade aufgeführt vereinigen die Extrudate einige vorteilhafte Eigenschaften und umgehen die Nachteile mehrerer (früher verwendeter,) kommerzieller Systeme. Um einige von Ihnen wieder ins Gedächtnis zu rufen: fehlende Bioabbaubarkeit, kurze Aktivitätszeiten und komplizierte Applikation waren Gründe, die zur Marktrücknahme in der Vergangenheit führten.

Nichtsdestotrotz wurde die weitere Verbesserung der Extrudate durch die Implementation eines zusätzlichen Polymers angestrebt. PVM/MA wurde als mukoadhäsiver Zusatz ausgewählt, um die Platzierung im gingivalen Sulcus nach der Applikation sicherzustellen. Leider beeinflusste PVM/MA das Freisetzungsprofil negativ und hatte ebenfalls einen ungewollten Einfluss auf das mechanische Verhalten. Daher wurde PVM/MA als potentiell mucoadhäsives Polymer ausgeschlossen und die MLC-PEG-PLGA Extrudate mit 10% PEG-Zusatz blieben die finalen Prototypen.

Künftig sollten noch andere mukoadhäsive Stoffe getestet werden, sofern diese Eigenschaft in die Extrudate noch implementiert werden soll. Dabei sollte das Augenmerk auf den Erhalt des Freisetzungsprofils sowie der flexiblen Eigenschaften gelegt werden. Um die vorgetragene Erklärung für die PEG-PLGA – PVM/MA

Interaktionen zu untermauern, könnte die Durchführung von Gel-Permeations-Chromatographie – Experimenten nützlich sein. Veränderungen im Molekulargewicht, speziell nach Extrusion und nachfolgender Inkubation im Freisetzungsmedium, könnten einen Einblick in die ablaufenden, chemischen Reaktionen geben. Weiterhin könnten die PEG 1500 Konzentration und die Extrusionsparameter für eine fortgeschrittene Feinabstimmung variiert werden. Ebenso bietet die Untersuchung der Kompatibilität der lipophilen Tetracyclinderivat-Komplexe mit anderen Polymeren mögliche Forschungsthemen. Bezüglich der Komplexe in Verbindung mit (PEG-)PLGA ist eine Vielfalt an Applikationsfeldern abseits der Parodontitis-Therapie vorstellbar. Zum Beispiel steht Minocyclin zur Debatte für die Anwendung in der Neurologie aufgrund seiner pleiotropen Effekte. Dafür könnten die Komplexe in geeignete Drug Delivery Systeme eingearbeitet werden, wie beispielsweise Nanopartikel oder in elektrogesponnene Vliese. Vorversuche während der frühen Phase dieser Arbeit zeigten, dass der MLC auch in andere Applikationsformen inkorporiert werden kann. Exemplarisch stellte sich bei diesen hier nicht präsentierten Ergebnissen heraus, dass die Produktion von MLC-PLGA Mikropartikeln mittels Lösungsmittel-Verdampfungs-Methode möglich ist.

Diese Arbeit entstand aus einem kooperativen Projekt zwischen der Martin-Luther-Universität Halle-Wittenberg, dem Fraunhofer-Institut für Zelltherapie und Immunologie IZI (Halle), dem Fraunhofer-Institut für Mikrostruktur von Werkstoffen und Systemen IMWS (Halle) und der Universität Bern. In diesem Projekt wurde ein potentes Drug Delivery System zur lokalen Behandlung von Parodontitis konzeptualisiert und realisiert. Aktuell schafft diese Kooperation die Umgebung, um diese vielversprechenden Drug Delivery Systeme zur klinischen Anwendung zu führen. Daher könnten diese Extrudate schon in der nahen Zukunft Zahnärzten und Patienten zur Verfügung gestellt werden.

DANKSAGUNG

Allen voran möchte ich meinem Doktorvater und Betreuer Prof. Dr. Karsten Mäder von ganzem Herzen danken. Ich danke ihm für das entgegengebrachte, uneingeschränkte Vertrauen und die fortwährende Unterstützung während meiner Promotionszeit. Seine unkomplizierte und angenehme Art Probleme anzugehen und die Arbeitsgruppe zu leiten, schufen stets eine Atmosphäre des Vertrauens und Respekts. Deshalb war ich wirklich gerne Teil seiner Arbeitsgruppe.

Im Zuge des kooperativen Projekts mit den Fraunhofer Instituten und der Universität Bern möchte ich allen Beteiligten danken:

- Ich danke Prof. Dr. Sigrun Eick von der Universität Bern für die Konzeptualisierung und Durchführung der mikrobiologischen Untersuchungen
- Dr. Mirko Buchholz möchte ich für die gute Zusammenarbeit und die Beschaffung von Arbeitsmitteln danken
- Dr. Andreas Kiesow möchte ich ebenso für die angenehme Zusammenarbeit danken und speziell für die gemeinsame Vorstellung unseres Projekts vor der Jury des Hugo Junkers Preises 2019
- Dr. Sandra Sarembe danke ich ebenfalls für die Mitwirkung am Projekt und den wertvollen Beitrag bei den gemeinschaftlichen Projekttreffen

Weiterhin möchte ich Dr. Martin Kleinschmidt und Dr. Fred Rosche vom Fraunhofer Institut für die Entwicklung und Messung mit der LC-MS/MS-Methode danken. Dabei möchte ich auch noch dem Hochleistungszentrum „Chemie- und Biosystemtechnik“ danken. Diese von der Fraunhofer Gesellschaft initiierte Plattform hat diese Arbeit mit einem Projekt des Landes Sachsen-Anhalt (1604/00078) mit Unterstützung von EFRE Fonds der europäischen Union gefördert. Die Möglichkeit an diesem Projekt mitzuwirken, war für mich eine großartige Erfahrung.

Natürlich möchte ich auch der ganzen Arbeitsgruppe für Pharmazeutische Technologie danken. Dr. Henrike Lucas danke ich für Ihre angenehme Art, Ihr Organisationstalent, den hilfreichen Input bei Problemstellungen und die wunderbare Zusammenarbeit in den Praktika. Ich danke Frau Manuela Woigk, die ich zeitweise mit Proben für die HPLC-Messungen überflutet habe. Frau Kerstin Schwarz möchte ich für die DSC-Messungen danken. Heike Rudolf danke ich für die ATR-FTIR-Messungen. Dr. Christoph Wagner vom Institut für Chemie danke ich für die Ermöglichung der Röntgendiffraktometrie-Messungen. Eric Lehner und Dr. Tom Wersig danke ich für die tolle Zeit im Studium und auch für das Wegweisen zu Beginn meiner Promotion. Eike Folker Busmann und Jonas Steiner möchte ich für die entspannte Atmosphäre im

Büro und für ihre Freundschaft danken. Ebenso möchte ich Johannes Albrecht, Benedikt Göttel, Anastasios Nalbadis, Johanna Zech, Anne Dümichen, Miriam Klein und Dr. Marie-Luise Trutschel für die schöne Zeit als Arbeitsgruppe, auch abseits der Universität, danken.

Einen ganz besonderen Dank möchte ich an Dr. Thomas Wetzlar für seine Freundschaft, seine Volleyball-Expertise, das immer offene Ohr und die Suche nach grammatikalischen Fehlern in dieser Arbeit richten. Genauso möchte ich Lisa Joachimi für das Korrekturlesen und Ihre langjährige Freundschaft danken. Elisabeth danke ich für die gemeinsame und vor allem schöne Zeit im Homeoffice.

Dem gesamten Team der Kohlschütter-Apotheke unter Leitung von Cornelia Krüger möchte ich für das freundliche Miteinander und das angenehme Arbeitsklima danken.

Unabhängig vom aktiven Beitrag zur Fertigstellung dieser Arbeit möchte ich allen danken, die mich auf meinem Weg bis hierher begleitet und unterstützt haben. Dabei möchte ich mich ausdrücklich bedanken bei:

- Mathias Freier für seine Freundschaft und, dass er stets für mich da war
- Tobias und Melissa Heusel für ihre Freundschaft und die Unterstützung in allen Lebenslagen
- Felix Naundorf für seine Freundschaft und das immer offene Ohr
- Dr. Fabian Lentz und Luise Lentz für die langjährige Freundschaft
- Minh Duc Nguyen für seine unverkennbare Art, seine Freundschaft und die tolle Zeit als Mitbewohner
- Michael Gäbe für seine menschliche Größe und seine Freundschaft
- Martin Hanke und Dr. Claudia Krähe für ihre Freundschaft und die eine oder andere Hilfestellung in Hinsicht auf die englische Grammatik
- Nils und Anne Dittmann für ihre Herzlichkeit und ihre Freundschaft
- Melanie Pietsch, Gesine Schilken, Anika Dammann, Carolin Tell, Annika Wittenbecher, Sandra Kendzia, Juliane Wernert, Georg Thum, Nico Kwapis und Christian Gebhardt für ihre Freundschaft

Abschließend möchte ich meiner Familie von ganzem Herzen danken. Ausdrücklicher Dank gilt meiner Mutter Kathrin und meiner Schwester Sydney, die immer an mich geglaubt haben. Genauso besonders danke ich meinem Vater Christian, seiner Frau Stefanie und meinem Bruder Tom, die mir stets mit Rat und Tat zur Seite standen. Meinem Großvater Hans, Ute, „Tante“ Carola und Oma Erika, die mich ebenso in all meinen Vorhaben unterstützt haben, möchte ich hiermit auch für Alles danken.

LEBENS LAUF

PERSÖNLICHE DATEN

Name: Martin Kirchberg

Geburtsdatum: 29.06.1990

Geburtsort: Bernburg (Saale), Deutschland

AUSBILDUNG UND BERUFLICHE ENTWICKLUNG

06/2017 – Heute Martin-Luther-Universität Halle-Wittenberg, Halle (Saale)
Wissenschaftlicher Mitarbeiter/Doktorand
in der Arbeitsgruppe für Pharmazeutische Technologie und Biopharmazie unter Leitung von Prof. Dr. Karsten Mäder

06/2017 – Heute Kohlschütter-Apotheke, Steinweg 25, 06110 Halle
Apotheker (Mini-Job)

02/2015 – 05/2017 Kohlschütter-Apotheke, Steinweg 25, 06110 Halle
Apotheker

11/2013 – 01/2015 Kohlschütter-Apotheke, Steinweg 25, 06110 Halle
Pharmazeut im praktischen Jahr

10/2009 – 10/2013 Martin-Luther-Universität Halle-Wittenberg, Halle (Saale)
Studierender der Pharmazie

10/2008 – 09/2009 Klinikum Bernburg, Kustrenaer Straße 98, 06406 Bernburg
Zivildienstleistender

07/2008 Abitur am Gymnasium Carolinum Bernburg, 06406 Bernburg

PUBLIKATIONSLISTE UND AUSZEICHNUNGEN

Patent

A. Kiesow, M. Buchholz, S. Sarembe, K. Mäder, M. Kirchberg, S. Eick; Tetracycline complexes with sustained activity: WIPO/PCT (International Publication Number WO 2020/089249 A1) datiert auf den 07.05.2020 als gemeinschaftliche Erfindung des Fraunhofer-Instituts, der Martin-Luther-Universität Halle-Wittenberg und der Universität Bern.

Publikationen

Kirchberg M, Eick S, Buchholz M, Kiesow A, Sarembe S, Mäder K. Extrudates of lipophilic tetracycline complexes: A new option for periodontitis therapy. Int J Pharm [Internet]. 2019 Dec;572(September):118794. Available from: <https://doi.org/10.1016/j.ijpharm.2019.118794>

Schmid J, Kirchberg M, Sarembe S, Kiesow A, Sculean A, Mäder K, et al. In Vitro Evaluation of Antimicrobial Activity of Minocycline Formulations for Topical Application in Periodontal Therapy. Pharmaceutics [Internet]. 2020 Apr 13;12(4):352. Available from: <https://www.mdpi.com/1999-4923/12/4/352>

Kirchberg M, Eick S, Buchholz M, Rosche F, Kiesow A, Sarembe S, et al. Controlled release minocycline-lipid-complex extrudates for the therapy of periodontitis with enhanced flexibility. Int J Pharm [Internet]. 2020 Aug 30 [cited 2020 Jul 2];586:119578. Available from: <https://linkinghub.elsevier.com/retrieve/pii/S0378517320305627>

Konferenzbeiträge

M. Kirchberg, B. Göttel, A. Schädlich, S. Kempe, H. Metz, K. Mäder; Microenvironmental investigations of degrading PLGA implants; CRS Germany Local Chapter 22nd annual meeting, March 01 – 02, 2018, Halle (Saale), Germany (Abstract & Poster)

M. Kirchberg, B. Göttel, A. Schädlich, S. Kempe, H. Metz, K. Mäder; Noninvasive characterization of the microenvironment inside degrading PLGA polymers; 11th World Meeting on pharmaceuticals, Biopharmaceutics and Pharmaceutical Technology, March 19 – 22, Granda, Spain (Abstract & Poster)

M. Kirchberg, S. Eick, M. Buchholz, A. Kiesow, S. Sarembe, K. Mäder; Minocycline extrudates for periodontitis therapy; CRS Germany Local Chapter 23rd annual meeting, March 07 – 08, 2019, Leipzig, Germany (Abstract & Poster)

S. Eick, M. Kirchberg, A. Kiesow, A. Sculean, K. Mäder, M. Buchholz; In-vitro-activity of tetracycline formulations for topical application in periodontal therapy, June 19 – 22, 2019, Vancouver, Canada (Co-Author (not present at the congress) Abstract & Poster)

M. Kirchberg, S. Eick, M. Buchholz, A. Kiesow, S. Sarembe, K. Mäder; Controlled releasing minocycline extrudates for the treatment of periodontitis; CRS Annual Meeting & Exposition, 2019 July 21 – 24, Valencia, Spain (Abstract & Poster)

Auszeichnung

Hugo Junkers Preis 2019 – 3. Platz im Bereich „Innovativste Projekte der angewandten Forschung“ mit „PARODEX – Extrudate zur Parodontitisbehandlung“

(Am Projekt beteiligte Personen: Prof. Dr. Karsten Mäder, Apotheker Martin Kirchberg, Dr.-Ing. Andreas Kiesow, Dr.-Ing. Sandra Sarembe, Dr. Mirko Buchholz, Prof. Dr. Sigrun Eick) <https://www.hugo-junkers-preis.de/preistraeger/preistraeger-2019>

SELBSTSTÄNDIGKEITSERKLÄRUNG

Hiermit erkläre ich an Eides statt, dass ich die vorliegende Arbeit selbstständig und ohne fremde Hilfe angefertigt und keine anderen als die angegebenen Quellen und Hilfsmittel benutzt sowie die den verwendeten Werken wörtlich oder inhaltlich entnommenen Stellen als solche kenntlich gemacht habe.

Ferner erkläre ich, dass ich mich mit dieser Dissertation erstmals um die Erlangung eines Doktorgrads bewerbe. Die vorliegende Arbeit ist weder im Inland noch im Ausland in gleicher oder ähnlicher Form einer anderen Prüfungsbehörde zum Zweck einer Promotion oder eines anderen Prüfungsverfahrens vorgelegt worden.

Halle, den 02.09.2020


Martin Kirchberg